

Role of Secretory Processes in Cardiac Fibroblasts in Heart Failure Development and Progression

Doctoral Thesis

In partial fulfillment of the requirements for the degree

“Doctor of Philosophy (Ph.D.)”

in the Molecular Medicine Study Program

at the Georg-August University Göttingen

Submitted by

Naim Kittana

Born in

Nablus, Palestine

Göttingen, September 2014

Members of the Thesis Committee:

Supervisor

Prof. Dr. Susanne Lutz
Institute of Pharmacology
University Medical Center Göttingen
Georg-August-University Göttingen

Second member of the thesis committee

Prof. Dr. Dörthe M. Katschinski
Department of Cardiovascular Physiology
University Medical Center Göttingen
Georg-August-University Göttingen

Third member of the thesis committee

Prof. Dr. Blanche Schwappach
Department of Molecular Biology
University Medical Center Göttingen
Georg-August-University Göttingen

Date of Disputation:

AFFIDAVIT

Here I declare that my doctoral thesis entitled "**Role of Secretory Processes in Cardiac Fibroblasts in Heart Failure Development and Progression**" has been written independently with no other sources and aids than quoted.

Naim Kittana
Göttingen, September 2014

Dedication

*This thesis is dedicated to my deceased father
who left me memories that will long be treasured*

*It is also dedicated to
my beloved mother, wife, daughters and siblings*

Acknowledgement

I would like to express my deepest gratitude to my supervisor Professor Dr. Susanne Lutz for the unlimited support and encouragement starting from preparing the proposal of my project until the very last days of my PhD. During my work with Susanne I acquired from her lots of experiences and valuable knowledge, not only in designing and performing experiments in a good quality, but also in evaluating, interpreting and understanding the data, and how to link different things together to come up with conclusions and new hypotheses. I also learned from her how to express my findings in a precise and clear way. I learned from Susanne how to organize the working environment, how to be an efficient member in a teamwork and how to lead a scientific project. Susanne was not only a wonderful supervisor, but also a great and cheerful friend.

I would like also to thank very much my thesis committee members, Prof. Dr. Dörthe Katschinski and Prof. Dr. Blanche Schwappach for following the progress of my project and for providing me with valuable suggestions, excellent ideas and useful criticism, which were indeed indispensable.

Many thanks for Prof. Dr. Wolfram Zimmermann for giving me the opportunity to join the institute of pharmacology, and for his great support and valuable comments and suggestions, he always made during our regular weekly meetings.

Very special thanks for our kind technical assistant Mrs. Beate Ramba, who trained me on several techniques and was always supportive and helpful, especially during the tough times. Beate was also a close friend, she helped me improve my German language, and I always enjoyed chatting and exchanging ideas with her not only about science, but also about different aspects of life. I would like also to express my gratitude to my colleagues and friends Aline, Anita, Sebastian, Svenja, Kerstin, Wiebke and to all other members in the institute of pharmacology for the joyful time and fruitful collaboration.

I will never forget to express my greatest appreciation and thankfulness to my beloved wife Duaa and my little daughters Leen and Sara, who accompanied me in this challenging journey, inspired me to overcome the difficulties and tolerated my long absence from home. I am also very thankful to my beloved mother, who was always with me to provide me with courage and support.

I am also very thankful to the German Academic Exchange Service (DAAD) for offering me a PhD scholarship and for the great support they provided me during my stay in Germany.

Table of contents

| | |
|-------------------------------------------------------------------------------|------|
| Table of contents..... | I |
| List of Abbreviation..... | V |
| Symbols and units..... | VIII |
| List of Figures..... | IX |
| List of tables..... | XI |
| 1. Summary..... | 1 |
| 2. Introduction..... | 2 |
| 2.1. Heart failure..... | 2 |
| 2.2. Cardiac fibrosis..... | 4 |
| 2.3. Contribution of CF to cardiac remodeling..... | 4 |
| 2.3.1. CF and myocardium homeostasis..... | 4 |
| 2.3.2. Differentiation of CF into myofibroblasts..... | 5 |
| 2.4. Role of Ang II in the pathogenesis of cardiac fibrosis..... | 7 |
| 2.4.1. Ang II-induced reactive oxygen species production in CF..... | 8 |
| 2.4.2. Regulation of TGF- β by Ang II signaling..... | 11 |
| 2.5. Regulation of calcium in CF..... | 11 |
| 2.5.1. Ang II-dependent calcium (Ca ²⁺) signaling..... | 11 |
| 2.5.1.1.1. PKC signaling..... | 12 |
| 2.5.1.1.2. Calcineurin signaling..... | 13 |
| 2.5.1.1.3. Transient receptor potential channels..... | 13 |
| 2.5.2. Ca ²⁺ oscillation in CF..... | 14 |
| 2.6. Regulation of bioactive molecules expression and secretion..... | 15 |
| 2.6.1. Regulation of secretory processes by Ca ²⁺ | 15 |
| 2.6.2. Regulation of gene expression by actin filaments and microtubules..... | 16 |
| 2.7. Connective tissue growth factor..... | 18 |
| 2.7.1. Protein structure of CTGF..... | 18 |
| 2.7.2. Physiological functions of CTGF..... | 20 |
| 2.7.3. Role of CTGF in fibrotic heart disease..... | 20 |
| 2.7.4. Regulation of CTGF in CF..... | 21 |
| 2.8. Aim of the project..... | 22 |

| | | |
|------------|----------------------------------------------------------------------------------------------------------------|----|
| 3. | Materials and methods | 23 |
| 3.1. | Materials..... | 23 |
| 3.1.1. | Chemicals, reagents and consumables | 23 |
| 3.1.2. | Restriction enzymes and related supplements | 26 |
| 3.1.3. | Kits | 26 |
| 3.1.4. | Cells and viruses | 27 |
| 3.1.5. | Antibodies..... | 27 |
| 3.1.6. | Chemicals used for cell organelle fluorescence staining | 29 |
| 3.1.7. | Oligonucleotides, primers and plasmids..... | 29 |
| 3.1.8. | Buffers, solutions and media..... | 31 |
| 3.1.9. | Inhibitors | 37 |
| 3.1.10. | Devices and softwares..... | 37 |
| 3.2. | Methods..... | 39 |
| 3.2.1. | Isolation, maintenance and passaging of primary neonatal rat cardiac fibroblasts | 39 |
| 3.2.2. | Culturing, maintenance and passaging of primary normal human ventricular cardiac fibroblasts (NHCF-V) | 41 |
| 3.2.3. | Culturing, passaging and maintenance of HEK293A cells..... | 42 |
| 3.2.4. | Live cell calcium imaging and time lapse analysis..... | 42 |
| 3.2.5. | Fluorescence staining for cell microscopy..... | 43 |
| 3.2.6. | Sirius red-based colorimetric microassay for collagen..... | 43 |
| 3.2.7. | Protein biochemical analysis..... | 44 |
| 3.2.7.1. | Preparation of samples for immunoblotting | 44 |
| 3.2.7.2. | Protein separation, by sodium dodecyl sulfate polyacrylamide gel electrophoresis (SDS-PAGE), and blotting..... | 45 |
| 3.2.7.3. | Exchanging antibodies from nitrocellulose membranes..... | 45 |
| 3.2.8. | Molecular biology..... | 46 |
| 3.2.8.1. | Determination of relative change in gene expression | 46 |
| 3.2.8.1.1. | RNA isolation | 46 |
| 3.2.8.1.2. | RNA analysis by formaldehyde (FA) agarose gel-electrophoresis . | 46 |
| 3.2.8.1.3. | RNA reverse transcription into cDNA..... | 47 |
| 3.2.8.1.4. | Quantitative polymerase chain reaction (qPCR) | 47 |
| 3.2.8.2. | RT-PCR for verification of gene expression | 48 |

| | | |
|-------------|----------------------------------------------------------------------------------------------------------------------------------------------------|----|
| 3.2.8.3. | Construction of an adenovirus for overexpression of tetracysteine (TC) tagged CTGF | 49 |
| 3.2.8.3.1. | Restriction digestion | 49 |
| 3.2.8.3.2. | DNA agarose gel electrophoresis | 49 |
| 3.2.8.3.3. | Purification of DNA from agarose gel..... | 49 |
| 3.2.8.3.4. | Amplification of CTGF gene from cDNA by PCR | 49 |
| 3.2.8.3.5. | Addition of KpnI and XhoI restriction sites to CTGF gene by PCR | 50 |
| 3.2.8.3.6. | Hybridization of TC-tag oligonucleotides..... | 51 |
| 3.2.8.3.7. | DNA ligation | 51 |
| 3.2.8.3.8. | Transformation of DH10B bacteria by heat shock protocol | 52 |
| 3.2.8.3.9. | Transformation of AdEasier cells by Inoue protocol | 52 |
| 3.2.8.3.10. | Isopropanol precipitation of DNA | 53 |
| 3.2.8.3.11. | Transfection of HEK293A cells by recombinant adenovirus plasmid | 53 |
| 3.2.8.3.12. | Amplification of recombinant adenovirus by HEK293A cells | 53 |
| 3.2.8.3.13. | Purification of recombinant adenovirus | 54 |
| 3.2.8.3.14. | Cloning strategy | 54 |
| 3.2.9. | Statistical analysis | 56 |
| 4. | Results | 57 |
| 4.1. | Role of Ca ²⁺ in the regulation of CTGF | 57 |
| 4.1.1. | Characterization of Ang II-induced Ca ²⁺ transient in CF | 57 |
| 4.1.1.1. | Ang II induces Ca ²⁺ transient in both NRCF and NHCF-V | 57 |
| 4.1.1.2. | Ca ²⁺ handling in NRCF is independent of the differentiation state | 59 |
| 4.1.1.3. | AT1 receptor -PLC-β signaling cascade mediates the Ang II-CaT..... | 60 |
| 4.1.1.4. | Intracellular Ca ²⁺ stores are the major sources for the Ang II-CaT..... | 62 |
| 4.1.1.5. | Blockade of TRPC3 channels enhances the ΔRFU _{Max} of the Ang II-CaT | 64 |
| 4.1.1.6. | TRPC3 channels and the intracellular Ca ²⁺ stores play a role in the regulation of the Ang II-induced-Ca ²⁺ oscillation..... | 66 |
| 4.1.1.7. | The NADPH oxidases (NOXs) and Rac1 GTPases are regulators of the Ang II-CaT in NRCF | 68 |
| 4.1.2. | Ca ²⁺ controls the expression and secretion of CTGF | 72 |
| 4.1.2.1. | Chelation of intracellular Ca ²⁺ by BAPTA-AM affects the basal and induced levels of CTGF expression and secretion | 72 |

| | | |
|----------|-----------------------------------------------------------------------------------------------------------------------------------------------------------------|-----|
| 4.1.2.2. | Depletion of intracellular Ca ²⁺ by TGN affects mainly CTGF secretion | 77 |
| 4.1.2.3. | Blockade of IP3Rs by XeC inhibits CTGF secretion | 79 |
| 4.1.2.4. | Blockade of TRPC3 channels induces CTGF secretion, without influencing the expression..... | 82 |
| 4.1.2.5. | Inhibition of NOX2 subunits assembly has no impact on the regulation of CTGF | 85 |
| 4.1.3. | Determination of downstream targets for Ca ²⁺ that mediate CTGF regulation..... | 86 |
| 4.1.3.1. | Calcineurin and PKC oppositely regulate CTGF expression..... | 86 |
| 4.1.3.2. | Ca ²⁺ regulates CTGF independently of ERK1/2 or Ca ²⁺ /calmodulin-dependent protein kinase II δ (CaMKII δ) signaling | 92 |
| 4.1.3.3. | Ca ²⁺ , PKC and Rac1 are involved in CTGF regulation in NHCF-V | 94 |
| 4.2. | Role of the cytoskeleton in CTGF regulation..... | 95 |
| 4.2.1. | Role of the actin filaments in CTGF regulation | 95 |
| 4.2.2. | Role of the microtubules in the regulation of CTGF..... | 98 |
| 4.3. | Prospects for studying CTGF by live cell imaging using Ad.TC-CTGF | 101 |
| 5. | Discussion | 104 |
| 5.1. | Regulation of the Ca ²⁺ transient in CF | 104 |
| 5.2. | Regulation of the Ca ²⁺ oscillation in CF..... | 106 |
| 5.3. | Influence of ROS-regulating mediators on the Ca ²⁺ handling in CF | 106 |
| 5.4. | Mechanism of CTGF regulation by cytoskeleton-dependent and Ca ²⁺ -dependent signaling pathways..... | 108 |
| 5.4.1. | Role of ROS in the regulation of CTGF | 112 |
| 5.4.2. | Ca ²⁺ is involved in the regulation of CTGF in human cardiac fibroblasts . | 112 |
| 6. | Bibliography..... | 113 |
| | Curriculum Vitae..... | 125 |

List of Abbreviation

| | |
|-----------------|-------------------------------------------------------------------------------------------|
| 122 | U73122 |
| 343 | U73343 |
| ACE | Angiotensin converting enzyme |
| Ad.EGFP | Adenovirus encoding EGFP |
| Ad.HA-CTGF | Adenovirus encoding HA-CTGF |
| Ad.TC-CTGF | Adenovirus encoding TC-CTGF |
| ADP | Adenosine diphosphate |
| Ang II | Angiotensin II |
| Ang II-CaT | Ang II-induced Ca ²⁺ transient |
| APS | Ammonium persulfate |
| Arp2/3 | Actin related proteins |
| AT1-R | Ang II type1 receptor |
| ATP | Adenosine triphosphate |
| AUC | Area under the curve |
| BAPTA-AM | 1,2-bis(2-aminophenoxy)ethane-N,N,N',N'-tetraacetic acid tetrakis(acetoxymethyl ester) |
| BMP-4 | Bone morphogenetic proteins-4 |
| CaMKII δ | Calcium/calmodulin-dependent protein kinase II δ |
| CBFHH | Calcium- and bicarbonate- free Hanks with HEPES |
| cDNA | Complementary DNA |
| CDX | Methyl-beta-cyclodextrin |
| CF | Cardiac fibroblasts |
| CR | Cysteine-rich |
| CsA | Cyclosporin A |
| CT | Carboxy-terminal |
| CTGF | Connective tissue growth factor |
| DAG | Diacylglycerol |
| DAPI | 4',6-diamidino-2-phenylindole |
| DMSO | Dimethylsulfoxide |
| DNA | Deoxyribonucleic acid |
| ECM | Extracellular matrix |
| EMT | Epithelial-mesenchymal transition |
| ER | Endoplasmic reticulum |
| ERK1/2 | Extracellular signal-regulated kinases 1/2 |
| ET | Endothelin-1 |
| FA | Formaldehyde |
| FAK | Focal adhesion kinase |
| FCS | Fetal calf serum |

| | |
|-------------------------------|----------------------------------------------------|
| FGM | Fibroblasts growth medium |
| G-actin | Globular actin |
| GDP | Guanosine diphosphate |
| GEFs | Guanine nucleotide exchange factors |
| GPCR | G-protein coupled receptor |
| GTP | Guanosine triphosphate |
| H ₂ O ₂ | Hydrogen peroxide |
| HA | Hemagglutinin |
| HEPES | 4-(2-hydroxyethyl)-1-piperazineethanesulfonic acid |
| HF | Heart failure |
| HRP | Horseradish peroxidase |
| IF | Immunofluorescence |
| IGF | Insulin-like growth factor |
| IGFBP | Insulin-like growth factor binding protein |
| IL-1 β | Interleukin-1 β |
| IL-6 | Interleukin-6 |
| IP3 | Inositol triphosphate |
| IP3R | IP3 receptors |
| JAK | Janus kinase |
| LAT-A | Latrunculin A |
| LM | Low medium |
| MAM | Mitochondria-associated ER membranes |
| MAP | Mitogen activated protein |
| MI | Myocardial infarctions |
| MMPs | Matrix metalloproteinases |
| MOPS | 3-N-morpholino-propanesulfonic-acid |
| MRTFs | Myocardin-related transcription factors |
| MyoF | Myofibroblasts |
| NCX3 | Na ⁺ -Ca ²⁺ -exchanger 3 |
| NEAA | Non-essential amino acids |
| NFAT | Nuclear factor of activated T cells |
| NHCF-V | Normal human ventricular cardiac fibroblasts |
| NKM | Non-cardiomyocyte medium |
| NOXs | NADPH oxidases |
| NRCF | Neonatal rat cardiac fibroblasts |
| O ₂ | Oxygen molecule |
| O ₂ ⁻ | Superoxide |
| OD | Optical density |
| P/S | Penicillin/streptomycin |
| P0 | Passage 0 |
| P1 | Passage 1 |

| | |
|---------------|-----------------------------------------------------------|
| PBGD | Porphobilinogen deaminase |
| PBS | Phosphate-buffered saline |
| PDGF | Platelet derived growth factor |
| PFA | Paraformaldehyde |
| PI3K | Phosphatidylinositol 3-kinase |
| PIP2 | Phosphatidylinositol 4,5-bisphosphate |
| PIPES | Piperazine-N,N'-bis(2-ethanesulfonic acid) |
| PKC | Protein kinase C |
| PLC- β | Phospholipase C- β |
| PLD2 | Phospholipase D2 |
| Pyr3 | Pyrazole 3 |
| qPCR | Quantitative polymerase chain reaction |
| RAAS | Renin-Ang II-aldosterone system |
| RFU | Relative fluorescence unit |
| RNA | Ribonucleic acid |
| ROCE | Receptor-operated Ca^{2+} entry |
| ROCK | Rho-kinases |
| ROS | Reactive oxygen species |
| RT-PCR | Reverse transcription polymerase chain reaction |
| SEM | Standard error mean |
| Scr | Scrambled |
| SDS | Sodium dodecyl sulfate |
| SDS-PAGE | Sodium dodecyl sulfate polyacrylamide gel electrophoresis |
| sm-actin | α -smooth muscle-actin |
| SOCE | Store-operated Ca^{2+} entry |
| SRF | Serum response factor |
| STIM1 | Stromal interaction molecule 1 |
| TC | Tetracysteine |
| TEMED | Tetramethylethylenediamine |
| TGF- β | Transforming growth factor-beta |
| TGN | Thapsigargin |
| TIMPs | Tissue inhibitors of metalloproteinases |
| TN-C | Tenascin-C |
| TNF- α | Tumor necrosis factor-alpha |
| TNS | Trypsin neutralizing solution |
| TRP | Transient receptor potential |
| TRPA | Transient receptor potential ankyrin |
| TRPC | Transient receptor potential canonical |
| TRPM | Transient receptor potential melastatin |
| TRPML | Transient receptor potential mucolipin |

| | |
|-----------------------------|----------------------------------------------|
| TRPP | Transient receptor potential polycystin |
| TRPV | Transient receptor potential vanilloid |
| TSP | Thrombospondin |
| VEGF | Vascular endothelial growth factor |
| VSB | Virus storage buffer |
| VWF-C | Von Willebrand factor type C |
| WGA | Wheat germ agglutinin |
| XeC | Xestospongin C |
| Δ RFU | Change in fluorescence intensity |
| Δ RFU _{Max} | Change in the maximal fluorescence intensity |

Symbols and units

| | |
|--------------------|----------------|
| α | Alpha |
| β | Beta |
| γ | Gamma |
| δ | Delta |
| ϵ | Epsilon |
| ζ | Zeta |
| η | Eta |
| θ | Theta |
| ι | Iota |
| μ | Mu |
| ν | Nu |
| $^{\circ}\text{C}$ | Degree Celsius |
| sec | Second |
| min | Minute |
| hr | Hour |
| ng | Nanogram |
| μg | Microgram |
| mg | Mg |
| g | Gram |
| μl | Microliter |
| ml | Milliliter |
| l | Liter |
| nM | Nanomolar |
| μM | Micromolar |
| M | Molar |
| cm | Centimeter |
| % | Percent |

List of Figures

| | |
|--------------------------------------------------------------------------------------------------------------------------|----|
| Figure 1: Vicious circle of heart failure..... | 4 |
| Figure 2: Role of cardiac fibroblasts in cardiac remodeling..... | 6 |
| Figure 3: Mechanism of NOX1/2 activation by Ang II..... | 10 |
| Figure 4: Protein structure of CTGF | 19 |
| Figure 5: Induction of Ca ²⁺ transients in NRCF and NHCF-V by different concentrations of Ang II..... | 59 |
| Figure 6: Comparison of the Ang II-CaT in P0 and P1 NRCF..... | 60 |
| Figure 7: Signaling cascade underlying the Ang II-CaT | 61 |
| Figure 8: Contribution of the intracellular Ca ²⁺ stores to the Ang II-CaT | 63 |
| Figure 9: Contribution of TRPC3 channels to the Ang II-CaT in NRCF..... | 65 |
| Figure 10: Investigation of Ca ²⁺ oscillation in cardiac fibroblasts..... | 67 |
| Figure 11: Investigation of the role of Rac1 in Ca ²⁺ handling | 70 |
| Figure 12: Investigation of the role of NOX2 in Ca ²⁺ handling..... | 72 |
| Figure 13: Investigation of the general role of Ca ²⁺ in the regulation of CTGF expression and secretion..... | 73 |
| Figure 14: Fluorescence microscopy of NRCF treated for 24 hr with BAPTA-AM..... | 75 |
| Figure 15: Fluorescence microscopy of NRCF treated for 3 hr with BAPTA-AM..... | 76 |
| Figure 16: Investigating the effect of intracellular Ca ²⁺ depletion by TGN on CTGF regulation | 77 |
| Figure 17: Fluorescence microscopy of TGN-treated NRCF..... | 79 |
| Figure 18: Evaluating the effect of IP3R blockade by XeC on CTGF regulation..... | 80 |
| Figure 19: Fluorescence microscopy of XeC-treated NRCF | 81 |
| Figure 20: Investigating the effect of TRPC3 blockade on CTGF regulation | 83 |
| Figure 21: Fluorescence microscopy for NRCF treated with Pyr3..... | 84 |
| Figure 22: Evaluation of the the effect of NOX2 inhibition by gp91-ds-tat on CTGF regulation | 85 |
| Figure 23: Investigating the role of PKC and calcineurin in CTGF regulation..... | 87 |
| Figure 24: Fluorescence microscopy for NRCF treated for 24 hr with Go 6983 | 89 |
| Figure 25: Fluorescence microscopy for NRCF treated for 3 hr with Go 6983 | 90 |
| Figure 26: Fluorescence microscopy for CsA-treated NRCF | 92 |

| | |
|--------------------------------------------------------------------------------------------------------------------|-----|
| Figure 27: Verification of the role of ERK1/2 and CaMKII in the Ca ²⁺ -dependent Ang II signaling | 93 |
| Figure 28: Validating the role of Ca ²⁺ , PKC and Rac1 in the regulation of CTGF in NHCF-V | 94 |
| Figure 29: Fluorescence microscopy of NRCF treated with LAT-A..... | 95 |
| Figure 30: Fluorescence microscopy of the effect of LAT-A on microtubules..... | 96 |
| Figure 31: Investigating the effects of the actin filaments disruption on CTGF regulation | 97 |
| Figure 32: Fluorescence microscopy for NRCF treated with colchicine | 99 |
| Figure 33: Disruption of microtubules by colchicine significantly induces CTGF expression and secretion..... | 100 |
| Figure 34: Evaluation of the Ad.TC-CTGF in NRCF | 103 |

List of tables

| | |
|-----------------------------------------------------------------------------------------------------------|----|
| Table 1: Chemicals and reagents | 25 |
| Table 2: Consumables | 25 |
| Table 3: Restriction enzymes | 26 |
| Table 4: Kits | 26 |
| Table 5: Bacterial and mammalian cells | 27 |
| Table 6: Adenoviruses..... | 27 |
| Table 7: Primary antibodies..... | 28 |
| Table 8: Horseradish peroxidase (HRP)-conjugated secondary antibodies for western blotting..... | 28 |
| Table 9: Fluorophore-conjugated secondary antibodies for immunofluorescence..... | 29 |
| Table 10: Chemicals used for cell organelle/actin fluorescence staining..... | 29 |
| Table 11: TC-tag oligonucleotides | 29 |
| Table 12: Primers used for cloning of CTGF gene..... | 29 |
| Table 13: Primers used for qPCR and RT-PCR..... | 30 |
| Table 14: Plasmids used for the construction of TC-CTGF overexpressing recombinant adenovirus..... | 30 |
| Table 15: Composition of the used buffers, solutions and media | 36 |
| Table 16: End concentration in cell culture for each of the used inhibitors | 37 |
| Table 17: Devices | 39 |
| Table 18: Softwares | 39 |
| Table 19: Mix for a single replicate | 47 |
| Table 20: General qPCR program | 48 |
| Table 21: Reaction mixture for the PCR step..... | 48 |
| Table 22: General program for the PCR step | 48 |
| Table 23: Reaction mixture for CTGF gene amplification from cDNA | 50 |
| Table 24: PCR program for CTGF gene amplification from cDNA | 50 |
| Table 25: PCR reaction mixture for the addition of restriction sites to the ends of CTGF gene by PCR..... | 50 |
| Table 26: PCR program for the addition of restriction sites to the ends of CTGF gene | 51 |
| Table 27: Hybridization reaction for TC-tag oligonucleotides | 51 |

1. Summary

Cardiac fibroblasts play a major role in fibrogenesis associated with heart failure, since they produce ECM components and secrete important fibrosis-associated mediators, such as connective tissue growth factor (CTGF). CTGF expression and secretion can be induced by the angiotensin II (Ang II) type1 receptor (AT1-R) activation. Within this thesis, the role of the Ca^{2+} - and cytoskeleton-dependent signaling pathways elicited by Ang II on the regulation of CTGF were investigated in neonatal rat cardiac fibroblasts (NRCF). Ang II was shown to induce a Ca^{2+} transient via the PLC- β canonical pathway with an EC_{50} in a physiological range. This transient was detectable in the absence of extracellular Ca^{2+} and in accordance, the depletion of intracellular Ca^{2+} by thapsigargin (TGN) completely suppressed it. Interestingly, the blockade of the transmembrane TRPC3 channels by pyrazole 3 increased this transient and strongly inhibited the Ang II-induced Ca^{2+} oscillations. In addition, the Ca^{2+} oscillation could be also blocked by TGN. Moreover, the NADPH oxidase and its accessory activator Rac1 were found to be involved in the regulation of the induced Ca^{2+} transient in the cytosol and in mitochondria. In the next step, the impact of Ca^{2+} and its effector proteins were studied on CTGF expression and secretion. First, to demonstrate the overall outcome of Ca^{2+} on the regulation of CTGF, BAPTA-AM was used and showed that the chelation of intracellular Ca^{2+} resulted in the inhibition of CTGF expression and secretion. Second, with help of the inhibitor Go 6983 the involvement of protein kinase C (PKC) as a downstream mediator could be established. Third, in contrast to the downregulation of CTGF expression by PKC inhibition, an increase in CTGF expression was found in response to calcineurin inhibition by cyclosporin A (CsA). Next, the role of the actin cytoskeleton and of microtubules were studied. Actin filament disruption by latrunculin A (LAT-A) led to a similar decrease in CTGF expression as BAPTA-AM, which also had an actin depolymerizing effect. Similar, PKC inhibition was found to disrupt the actin cytoskeleton. All three interventions led in addition to major morphological changes of the Golgi apparatus, which is the major storage place of CTGF. In contrast to the actin cytoskeleton, the integrity of the microtubules was not affected under most conditions. To finally determine the role of these thick filaments in CTGF regulation, the microtubules depolymerizing drug colchicine was applied, which dispersed the Golgi apparatus, increased the CTGF expression and uncoupled it from the AT1R signaling

cascade. In summary, CTGF is regulated by a crosstalk of Ca^{2+} -dependent signaling, involving PKC and calcineurin, and cytoskeleton-dependent pathways involving actin filaments and microtubules.

2. Introduction

Heart diseases are the most common death causes not only in industrial societies, but also in low- and middle-income countries. During the last decades, huge efforts have been made to understand the molecular mechanisms involved in the dysregulation of cardiac function in order to improve the pharmacological therapy. Despite the intervention with several classes of modern therapeutics has clearly reduced the mortality of cardiac diseases, it is still not possible to reverse the diseased cardiac phenotype, this is most likely due to our limited knowledge of the detailed underlying molecular pathomechanisms. One reason for this might be attributed to the strong research focus on the malfunction of cardiomyocytes, disregarding the complex cellular composition of the cardiac tissue, where non-cardiomyocytes compose a major cell population [1]. It can be assumed that these cells, including cardiac fibroblasts, endothelial cells, pericytes, smooth muscle cells and immune cells, communicate with each other as well as with the cardiomyocytes and are therefore similarly affected by the neurohumoral changes occurring in heart diseases [2, 3]. Moreover, it is highly possible that non-cardiomyocytes expedite the progression of the cardiac remodelling as occurring in heart diseases [4].

2.1. Heart failure

Heart failure (HF) is a common cause for disability and death worldwide. According to a global epidemiological study in the year 2012, the prevalence of HF was over 23 million worldwide, with a lifetime risk of developing the disease to be one in five, and a five-year mortality rate that is higher than in many types of cancer [5].

HF is a progressive chronic disease that is generally characterized by imbalance between cardiac output and the metabolic demand of the body. It usually results from diminished contractility of the myocardium (systolic dysfunction), inadequate filling of the

heart (diastolic dysfunction), or more often a combination of both dysfunctions. Several underlying disease conditions have long been identified to stand behind cardiac dysfunctions, including myocardial infarctions (MI), chronic ischemia, dilated cardiomyopathy, ventricular hypertrophy (which results from chronic pressure overload or volume overload), cardiac valves stenosis and pericardial diseases. Any of these diseases can weaken cardiac contractility and so can reduce cardiac output, leading to a reduction in renal blood perfusion, which in turn activates the renin-angiotensin II (Ang II)-aldosterone system (RAAS), resulting in increased Ang II generation and aldosterone secretion, which mediate several events that are associated with cardiac remodeling, such as hypertrophy and fibrosis. On the other hand, the reduction in the cardiac output results in the activation of the sympathetic nervous system, due to a decline in carotid sinus firing. The persistent activation of the sympathetic nervous system on one side contributes to the myocardial remodeling, and on the other side causes desensitization of the β -adrenergic receptors. Together, cardiac remodeling and β -adrenergic receptors desensitization further exacerbate the dysfunction of cardiac contractility and cardiac output, and by that a vicious cycle is initiated, which persists along the progression of the disease (Fig. 1) [6]. It is worthy to mention that in the early stage of HF development, the activation of the RAAS as well as the sympathetic activation improve cardiac function, but the chronic activation of these two systems leads to the detrimental, irreversible and progressive cardiac remodeling [7].

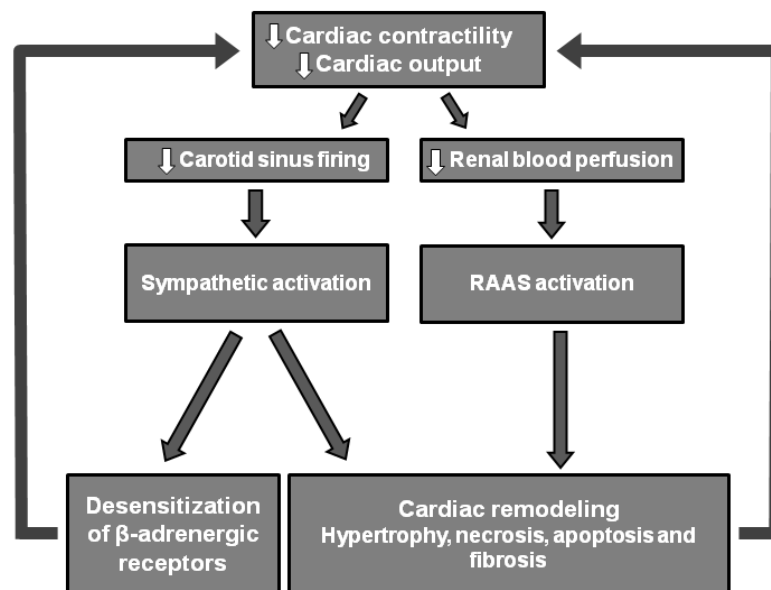


Figure 1: Vicious circle of heart failure

The reduction of the cardiac output, due to several underlying etiologies, induces the activation of the sympathetic nervous system and RAAS, which eventually results in the desensitization of the β -adrenergic receptors and in cardiac remodeling, and consequently in further reduction of the cardiac output. Modified from Maack and coworkers [8].

2.2. Cardiac fibrosis

Cardiac fibrosis is a feature of cardiac remodeling that occurs along the course of HF development. It is characterized by increased deposition of extracellular matrix (ECM) proteins, mainly by activated cardiac fibroblasts (CF) as well as by vascular smooth muscle cells [9]. There are two types of fibrosis: reparative fibrosis, which is secondary to cardiac cell necrosis as in the case of ischemia and aging, where the dead tissue is replaced by a scar. The second type of fibrosis is the reactive fibrosis, which results from persistent stimulation of CF, but without direct tissue injury as in the case of chronic hypertension [10]. With time, reactive fibrosis causes necrosis and apoptosis of cardiomyocytes, resulting in reparative fibrosis. Cardiac fibrosis increases the stiffness of the myocardium, thus impairs cardiac filling and contraction of the myocardium [9].

2.3. Contribution of CF to cardiac remodeling

2.3.1. CF and myocardium homeostasis

The CF numerically comprise a major cell population of the myocardium [11]. Normally they produce and deposit ECM proteins, including collagen types I, III, V and VI, laminin, elastin, proteoglycans and glycosaminoglycan. In the same time they secrete different kinds of matrix metalloproteinases (MMPs) which degrade ECM as well as tissue inhibitors of metalloproteinases (TIMPs) [12]. Under healthy conditions, the balance between synthesis and turnover of ECM by CF is tightly regulated, so that CF can build up a 3D network of connective tissue, where myocytes, fibroblasts and ECM interact with each other in a way that ensures structural integrity of the heart, proper distribution of contraction force and proper electromechanical function of the myocardium [4]. *In vitro* studies have shown that

CF can couple to cardiomyocytes via connexin 43, and that this coupling allows synchronization of spontaneous beating of distant cardiomyocytes, which suggests a potential role in the regulation of electrophysiology of the heart [13]. In addition, the connective tissue that is synthesized by CF acts as a natural electrical insulator, which allows gradual distribution of electrical impulse throughout the cardiac tissue being important for the orderly contraction of the different parts of the heart [14]. Moreover, CF secrete a plethora of bioactive molecules, such as connective tissue growth factor (CTGF), transforming growth factor-beta (TGF- β), tumor necrosis factor-alpha (TNF- α), interleukin 1beta (IL-1 β), interleukin-6 (IL-6), endothelin-1 (ET), natriuretic peptides and vascular endothelial growth factor (VEGF). These mediators generally function in an autocrine and paracrine fashion to regulate proliferation, migration, differentiation, gene expression and secretion of mediators by CF and other cells. Interestingly, it was also found that CF can secrete all components of the RAAS system including angiotensinogen, renin and the angiotensin converting enzyme (ACE), which allows local generation of Ang II in the microenvironment of CF and cardiomyocytes. This might play a central role in myocardial homeostasis as well as in the pathogenesis of HF [15] as will be explained in more details below.

2.3.2. Differentiation of CF into myofibroblasts

Under stress conditions, like cardiac injury and chronic hypertension, CF tend to differentiate into myofibroblasts (MyoF), which are disease-affected CF [16] and normally not present in a healthy myocardium [4]. MyoF acquire the ability to express α -smooth muscle-actin (sm-actin), allowing the contraction of ECM fibers, they also acquire greater capacity to secrete bioactive molecules, ECM proteins, MMPs and TIMPs, which help MyoF in scar formation (Fig. 2) [15, 17, 18]. Usually after successful wound closure the MyoF e.g. in the skin undergo apoptosis [19], but the scenario that occurs in the infarct heart is somewhat different. For so far unclear reasons, following “healing” and scar formation, MyoF in the mature infarct scar persist for a long time, months or years [20], and play a key role in excessive scarring and fibrosis. Eventually, they participate in the pathogenesis of cardiac remodeling and HF [21].

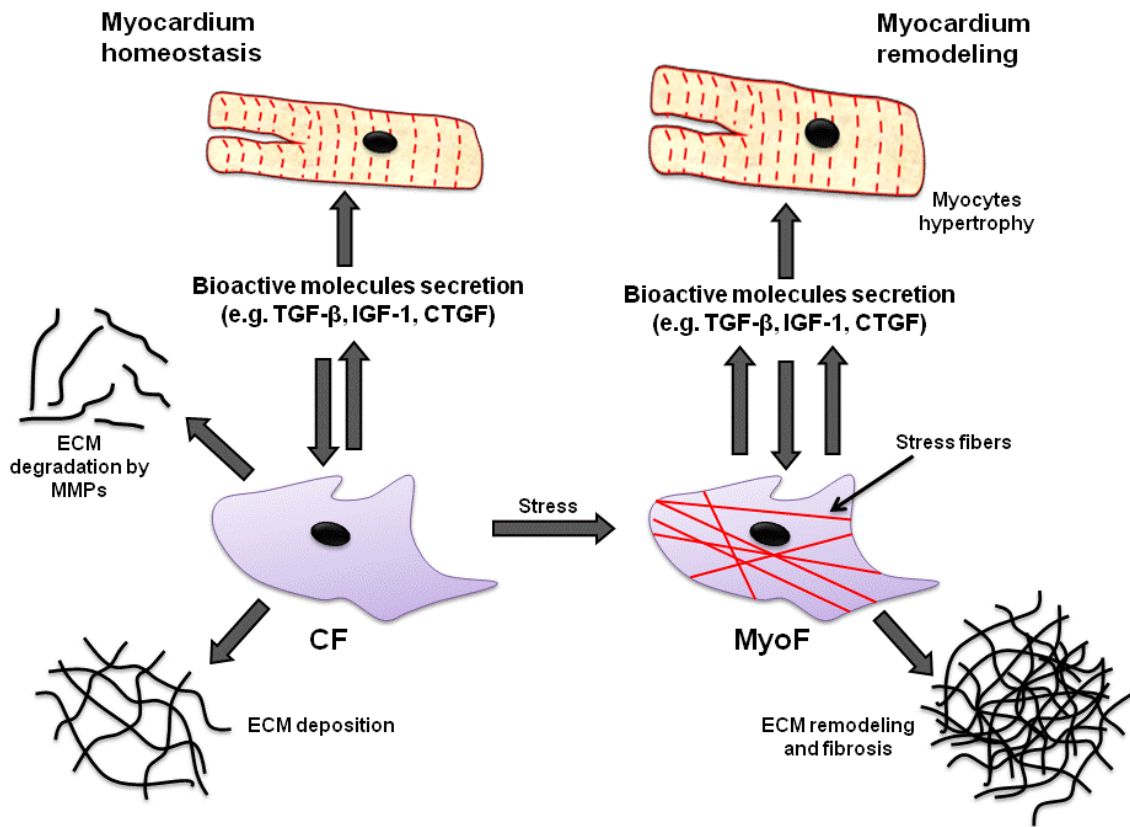


Figure 2: Role of CF in cardiac remodeling

The different biological activities of CF are essential for the maintenance of the myocardium homeostasis. Under stress conditions, CF differentiate into MyoF, which have enhanced biological activities that are in favor of supporting myocytes hypertrophy and the increased deposition and turnover of the ECM, which contributes to the myocardium remodeling.

Experimentally it is difficult to analyze the distinct functions of CF and MyoF, as maintaining the CF phenotype in culture is challenging. Whenever these cells are seeded on plastic cell culture plates/dishes, they spontaneously start to differentiate into MyoF, which can be detected by an increased expression of α -sma. In this case, CF differentiate into MyoF because plastic surfaces are generally stiffer than healthy cardiac tissue [22]. Therefore, most of the current publications about fibroblasts are actually showing data on

the pathobiology of MyoF, and consequently there is a lack of information on precise differences between CF and MyoF. In addition, the more these cells are passaged, the more they express α -sma, i.e. the more they acquire the myofibroblastic phenotype [16]. Several other factors have been indentified so far which shift CF characteristics into more myofibroblastic phenotype including the presence of serum, glucose level in the culture medium, the addition of certain bioactive molecules like TGF- β and the electrical and mechanical stimulation [23-26].

2.4. Role of Ang II in the pathogenesis of cardiac fibrosis

In patients with HF, the levels of Ang II in the circulation, myocardium and the central nervous system are increased [27, 28]. Beside the fact that Ang II induces hypertrophy in cardiomyocytes [29], Ang II also induces the differentiation of CF into MyoF [30], and it stimulates these cells to deposit ECM proteins [31] and to secret profibrotic mediators such as TGF- β and CTGF [32, 33].

Ang II is the active end product of the RAAS, where angiotensinogen is converted by renin into angiotensin I, which is then cleaved by the angiotensin converting enzyme (ACE) into Ang II. Two isotypes of Ang II receptors have been identified both belong to the G-protein coupled receptor (GPCR) superfamily and are named as AT1 and AT2 receptors. In healthy adult individuals, Ang II exerts its biological functions mainly via activation of the AT1 receptors [34]. In the adult heart, AT1 receptors are expressed in different cardiac cell types including CF [35], cardiomyocytes [36] and vascular smooth muscle cells [37]. They are able to couple to different isoforms of G-proteins at the same time, and therefore, they can simultaneously initiate different signal transduction pathways depending on the activated G-protein. Each of the activated G-proteins can in turn activate several signaling cascades, which crosstalk with each other and regulate each other. Therefore, the activation of AT1 receptors initiates a highly complex regulated signal transduction network resulting in an array of physio-pathophysiological effects.

2.4.1. Ang II-induced reactive oxygen species production in CF

In general, reactive oxygen species (ROS) are highly reactive oxygen derivatives, such as hydrogen peroxide (H_2O_2) and superoxide ($\text{O}_2^{\cdot-}$), which have a great capacity to interact with and oxidize various cellular macromolecules resulting in modifications that influence the functionality and activity of the affected molecules. The role of ROS in the physiology of immune cells was identified as early as in the 1960s, when it was found that ROS generation is crucial for the elimination of phagocytized pathogens by immune cells [38, 39]. Later ROS generation was detected in various non-immune tissues, which was perceived as an unfavourable and inevitable event that accompanies the normal catalytic activities of enzymes, which can participate under certain circumstances in the pathogenesis of several diseases including heart failure [40, 41]. However, the intensive investigations for the biology of ROS over the last few decades expanded our understanding of ROS biology to include, beside pathological effects, vital contributions to cellular physiology [42].

The generation of ROS is usually performed by the multi-subunit NADPH oxidases (NOXs), which are localized to various subcellular microdomains such as caveolae, mitochondria, the nucleus, and endosomes, and therefore the generation of ROS is thought to be highly compartmentalized, which allows specific targeting of certain signaling cascade molecules [43, 44]. The NOX family consists of several isozymes: NOX1-5 and 2 related enzymes (DUOX1, DUOX2). These enzymes catalyze the transfer of one electron from NADH or NADPH to an oxygen molecule (O_2) converting it into superoxide ($\text{O}_2^{\cdot-}$), which can be converted into H_2O_2 by superoxide dismutase [45]. NOXs are generally known to be differentially expressed in different cardiac cell types. In CF several publications have shown that NOX2 and NOX4 are expressed, but the expression of other NOXs cannot be excluded. NOX2 is composed of two membrane-spanning subunits, which are an oxidizing subunit (gp91phox also called NOX2) and a complex stabilizing subunit (p22phox), besides the three cytoplasmic components Rac1/2, p40phox, p67phox and p47-phox. Likewise, NOX4 also has two membrane-spanning subunits; the complex stabilizing p22phox subunit and the oxidizing NOX4 subunit. The involvement of cytoplasmic subunits in NOX4 activation is still unclear; some publications reported an association with Poldip2 [46], others suggested a Rac1-

mediated activation [47], and some suggested that NOX4 is constitutively active and does not require additional regulatory subunits [48-50].

ROS has been also shown to be involved in the fibrogenesis of several organs including heart, lung, liver and kidney [51]. In the heart, ROS generation is acutely upregulated in response to ischemia/reperfusion of the myocardium that occurs during MI [52], and is also chronically generated in the myocardium of patients with heart failure in response to chronic Ang II and TGF- β stimulation [53]. Ang II-induced NOX activation in CF has been shown to mediate several fibrogenic effects such as the induction of fibroblasts proliferation and differentiation into MyoF, the deposition and organization ECM proteins [51, 54], the epithelial-mesenchymal transformation [55], as well as the induction of several pro-fibrotic genes including endothelin-1 [56], TGF- β [57], MMPs [58] and CTGF [59].

It has been reported that among the different signaling pathways initiated by AT1 receptors, only G-proteins are important for NOX activation. G α_q and G $\beta\gamma$ subunits activates PLC- β , which mediates the increase in cytosolic Ca²⁺ concentration along with the generation of DAG, both of which work together to activate protein kinase C (PKC), which in turn phosphorylates p47phox, causing the translocation of the p47phox-p67phox complex from the cytosol to the Nox2-p22phox trans-membrane complex. In the same time, G $\beta\gamma$ subunit activates phosphatidylinositol 3-kinase (PI3K), which activates Rac1 protein causing it to translocate from the cytosol to join the Nox2-p22phox trans-membrane complex. By that, NOX2 complex is complete and is able to produce ROS. On the other hand, PKC causes by unknown mechanism the association of NOXA1 and NOXO1 to the NOX1-p22phox trans-membrane complex. Also activated Rac1 associates with NOX1 complex and contributes to its activity. Phospholipase D2 (PLD2) is activated by DAG and is thought to be important to replenish the precursors of DAG (Fig. 3) [60].

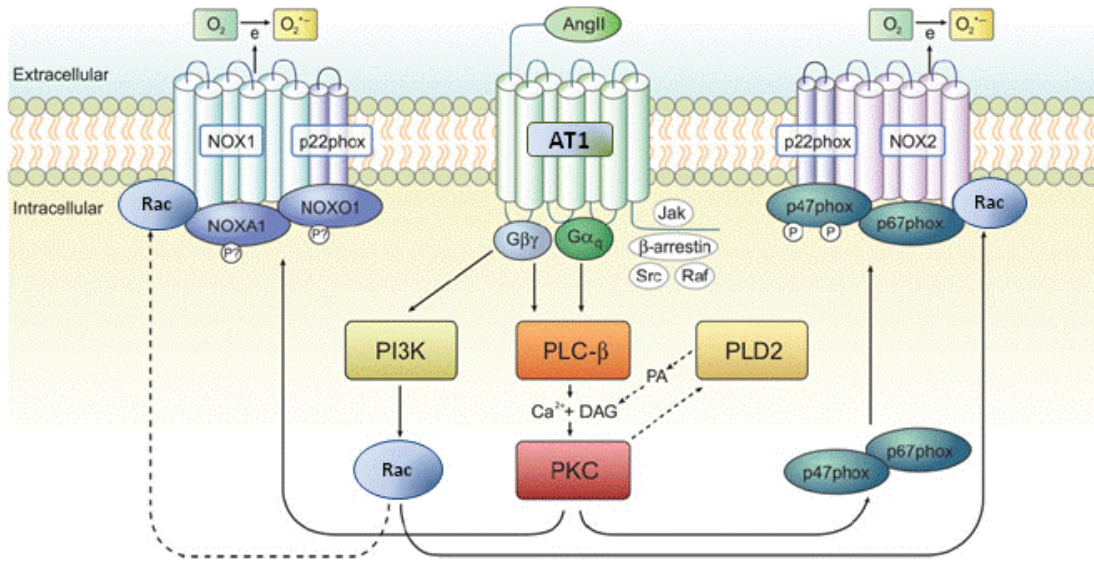


Figure 3: Mechanism of NOX1/2 activation by Ang II

Ang II can induce the assembly of the subunits of NOX1/2 via PLC-β-PKC signaling pathway, which is activated by $G\alpha_q$ and $G\beta\gamma$ subunits of G-protein. In the same time, $G\beta\gamma$ subunit mediates PI3K-dependent activation of Rac1, a necessary step to allow the association of Rac1 with NOX1/2 complexes. The scheme was adopted from Choi and coworkers [60].

Moreover, it has been shown that when the AT1 receptors are activated, they translocate to cholesterol rich rafts in the cell membranes called caveolae, which are associated with caveolin-1 and hold several signaling molecules, including NOXs [61-63]. Interestingly, Ang II-induced Rac1 activation and ROS generation can be inhibited when the integrity of the caveolae was disrupted [63, 64]. In addition, Ang II was found to induce the expression of p67phox and p22phox subunits in adventitial and CF [65, 66]. Another Ang II-dependent signaling pathway for the activation of NOX has been reported in CF through the activation of $G\alpha_{12/13}$ and Rac1, which was shown to be important for Ang II-induced nuclear factor of activated T cells (NFAT) activation [67].

2.4.2. Regulation of TGF- β by Ang II signaling

TGF- β is elevated in the circulation and myocardium of patients with HF [68] and in the myocardium of patients with MI [69]. Also it has been shown that cultured human CF and neonatal rat CF can secrete this cytokine. TGF- β induces the differentiation of CF into MyoF, an action that is thought to be mediated by the generation of ROS [70, 71], and it stimulates these cells to deposit ECM proteins [25, 32] and to secrete the profibrotic CTGF protein [72]. Different stimuli can upregulate TGF- β , such as Ang II and ROS generation [15]. It has been shown that Ang II can induce TGF- β expression via a NOX-dependent signaling pathway, which involves PKC-dependent p38-mitogen activated protein (MAP) kinase activation that in turn activates the transcription factor AP-1, a step that is necessary for the induction of TGF- β gene transcription [73, 74]. Other proposed Ang II-mediated signaling pathways for the induction of TGF- β could involve the Ang II-induced expression of Egr-1 and c-Fos transcription factors [75], which were shown to induce TGF- β gene transcription [76, 77].

2.5. Regulation of calcium in CF

2.5.1. Ang II-dependent calcium (Ca²⁺) signaling

AT1 receptors couple besides others (see section 1.4.1) to G $\alpha_{q/11}$ proteins, through which they can activate phospholipase C- β (PLC- β) resulting in the release of intracellular Ca²⁺ from the endoplasmic reticulum (ER). This action is mediated via generation of the second messenger inositol triphosphate (IP3) from phosphatidylinositol 4,5-bisphosphate (PIP2) by the PLC- β . Once IP3 is generated, it is released in the cytosol, where it activates the IP3 receptors (IP3R) that are located in the membranes of the ER. The IP3R are Ca²⁺ channels, which open due to the allosteric changes that occur in response to IP3 binding resulting in a release of Ca²⁺ from the ER [78-80]. This pathway was shown in several publications to be involved in Ang II-induced contraction of vascular smooth muscle cells and in cardiomyocytes [81, 82]. Besides IP3, the hydrolysis of PIP2 generates diacylglycerol (DAG), which remains anchored to the cell membrane. The Ca²⁺ which is released by IP3 causes the translocation of protein kinase C (PKC) isozymes to the plasma membrane, where they get activated by DAG [79, 83] and hence initiate signaling cascades which is involved in regulation of the expression of

several genes [84, 85]. Besides, DAG is known to activate the transient receptor potential canonical (TRPC) channels, which are Ca^{2+} permeable cation channels [86, 87].

The targets of Ca^{2+} , which are located in the cytosol and different cellular organelles, sense the change in the intracellular Ca^{2+} concentration either directly by interacting with Ca^{2+} ions or indirectly via scaffolding proteins like calmodulin, which when activated can interact with different Ca^{2+} -dependent enzymes, such as kinases and phosphatases [88], through which different physiological functions of Ca^{2+} , such as the regulation of gene expression and vesicular secretion, can be mediated.

2.5.1.1.1. *PKC signaling*

PKC constitute an extended family of several isozymes of serine/threonine kinases that are known to be activated by phospholipase associated receptors. They vary mainly based on the composition of the regulatory domain at the N-terminus, PKC isozymes can be classified into three categories with various sensitivities to Ca^{2+} and DAG. Conventional PKC isozymes, such as PKC α , β I, β II, γ , require both Ca^{2+} and DAG for activation. Novel PKC isozymes, such as PKC δ , ϵ , η , θ , require only DAG. Atypical PKC isozymes, such as PKC ζ , ι , μ , ν , and these isozymes are completely insensitive to Ca^{2+} or DAG [89-92].

PKC α , β I, β II, δ , ϵ , and ζ are expressed in adult and neonatal CF [93]. Several studies have identified PKC as potential therapeutic targets for cardiac fibrosis associated with heart failure. The inhibition of PKC α and β was shown to suppress cardiac fibrosis in a rat post-myocardial infarction model [94]. In addition, the selective over-expression of PKC β II in the myocardium resulted in severe cardiac fibrosis [95]. On the other hand, the knockout of PKC ϵ enhanced the interstitial cardiac fibrosis in a mouse model of pressure overload [96].

It has been reported that PKC ϵ mediate the Ang II-induced adhesion of fibroblasts to the ECM via a mechanism involving β I-integrins. In addition, it has been found that PKC δ and PKC ζ oppositely regulate TGF- β I-induced proliferation of neonatal rat CF [93, 97].

Moreover, PKCs were found to be involved in the regulation of Ang II-induced CTGF expression in an isozyme-dependent manner. The blockade of PKC α , ζ , or ϵ inhibited the Ang II-induced CTGF expression, whereas the knockdown of PKC δ significantly enhanced the Ang II-induced CTGF expression [98].

2.5.1.1.2. *Calcineurin signaling*

Calcineurin is a Ca²⁺ and calmodulin-dependent protein phosphatase IIB. It is composed of two subunits, calcineurin A, which is the catalytic subunit, and calcineurin B, which is the regulatory subunit [99]. Under resting conditions, calcineurin is inactive due to the low cytoplasmic Ca²⁺ concentration, but upon the activation of the GPCR-PLC- β/γ -IP3 pathway, the cytoplasmic Ca²⁺ concentration is elevated, so that Ca²⁺ binds calmodulin causing conformational changes that allow binding to calcineurin to activate its phosphatase activity. Ca²⁺ can also directly interact with the regulatory subunit of calcineurin [100]. The classical targets for activated calcineurin are the members of the nuclear factor of activated T cells (NFAT), which are transcription factors localized mainly to the cytosol when they are in the inactive phosphorylated state. Active calcineurin is necessary to dephosphorylate NFAT proteins, a step that is indispensable to allow NFAT proteins to cross the nuclear envelope, so that they can function as transcription factors [101].

Calcineurin-NFAT signaling is known to be vital for normal homeostasis as well as in the pathogenesis of different diseases, including cardiovascular diseases [102]. Over-expression of calcineurin was reported to induce cardiac hypertrophy and heart failure, which could be prevented by inhibiting calcineurin by cyclosporin A (CsA) [103]. Moreover, it was reported that calcineurin mediates the Ang II-induced cardiomyocytes hypertrophy and CF hyperplasia [104].

2.5.1.1.3. *Transient receptor potential channels*

Transient receptor potential (TRP) channels form a superfamily of 6 related subfamilies: TRPC (canonical), TRPV (vanilloid), TRPM (melastatin), TRPA (ankyrin), TRPP (polycystin) and TRPML (mucolipin). All TRP channels are composed of 6-

transmembrane domains that are arranged to form cation-permeable pores. Generally, these channels are nonselective cation channels with most of them showing a Ca^{2+} to Na^+ permeation ratio of less than 1:10 [105-107].

The TRPC channel subfamily consists of seven isoforms, numbered from 1-7. Several studies provided evidences that these channels can contribute to store-operated Ca^{2+} entry (SOCE) [108, 109], nevertheless, it is still controversial whether they are instead a specialized receptor-operated Ca^{2+} entry (ROCE) mediators, that replenish the intracellular Ca^{2+} stores following IP₃-mediated Ca^{2+} release, as in the case of TRPC3/6/7 [86, 107]. Some TRPC channels have been reported to act as mechanosensitive channels [110, 111]. However, the mechanism of TRPC channel activation is still highly unclear, and the data available show lots of controversial findings, since so many factors are involved in the regulation of the activity of these channels, including the cell type, the level of expression, the cellular localization and the availability of interaction partners [107].

Several isoforms of TRPC channels, such as TRPC1/3/5/6 were shown to be upregulated and involved in the pathogenesis of heart failure in several animal models, where calcineurin-NFAT signaling was frequently involved, which mediates the expression of several hypertrophic genes. Moreover, TRPC1/3 were found to be upregulated in cardiomyocytes in response to Ang II, endothelin-1 and phenylephrine treatment [112-116].

2.5.2. Ca^{2+} oscillation in CF

Ca^{2+} oscillation is a repetitive cyclical change in the cytoplasmic Ca^{2+} concentration observed in different types of cells, especially the non-excitable ones, in response to different physiological stimuli. There are evidences that the amplitude, frequency and duration of these signals actually play a major role in the regulation of different cellular processes such as, proliferation, contraction and secretion [117-119].

It has been shown that GPCR activation results in cyclic generation of IP₃ that was consistently parallel with the cyclic change in the cytoplasmic Ca^{2+} levels [120-122]. In the same time, Bird and Putney, 2005 reported that the intracellular Ca^{2+} stores are the

major source of the oscillating Ca^{2+} supported by an Ca^{2+} influx through store-operated Ca^{2+} channels (SOC), such as Orai1 channels [117]. During Ca^{2+} oscillation the reduction of the Ca^{2+} concentration in the endoplasmic reticulum, is sensed by the stromal interaction molecule 1 (STIM1), which in turn causes the plasma membrane Orai1 channels to open: This mechanism is important to maintain the filling of the endoplasmic Ca^{2+} stores [123]. Moreover, it was reported that TRPC3 channels can mediate agonist-activated Ca^{2+} oscillation via non-capacitative calcium entry [117, 124], besides several other publications that reported direct and indirect coupling between the IP3Rs and the TRPC3 channels [125-127]. Therefore, it can be hypothesized that TRPC3 channels play a role in Ca^{2+} oscillation via regulating the activity of the IP3Rs. Recent studies in MyoF have reported a correlation between the frequency of Ca^{2+} oscillation and the cycles of MyoF contractions, which was dependent on the elastic modulus of the cell culture surface as well as on the intracellular mechanical stress that is transduced by actin filaments [128]. Ca^{2+} oscillation was found to be synchronized between physically contacting MyoF, which is mediated by adherens junctions, suggesting that the mechanosensitive ion channels could be involved [129].

2.6. Regulation of bioactive molecules expression and secretion

Several studies have shown that actin filaments and microtubules function is not limited to the provision of physical support to the cells, but rather extend to include the regulation of various cellular processes, such as the regulation of gene expression and vesicular secretion. Actin filaments and microtubules were reported to function as tracks along which the secretory vesicles travel towards the cell membrane. In addition, they can regulate the kinetics of some transcription factors, and also transduce physical signals from the outer environment to the nucleus, whereby they can regulate the expression of different genes [130].

2.6.1. Regulation of secretory processes by Ca^{2+}

The role of Ca^{2+} in the mechanism of neurotransmitters and hormones secretion has been recognized and well characterized over the last few decades. The release of the neurotransmitters is normally triggered in response to the influx of Ca^{2+} through voltage-

gated Ca^{2+} channels, which are activated by action potentials. Whereas, the secretion of hormones is usually triggered by intracellular Ca^{2+} release that is mediated by GPCR-PLC- β -IP3 signaling pathway. Ca^{2+} is known to be involved in the mechanism of intracellular secretory vesicle trafficking [131] and fusion of the secretory vesicles with the target cell membrane, which involves interaction with the Ca^{2+} sensor synaptotagmin-1 protein [132]. Synaptotagmin is located on the membrane of the secretory vesicles and has two C2 domains (C2A and C2B) that are homologous to the Ca^{2+} -binding domain of PKC. The C2A domain binds syntaxin SNAP-25 proteins (the cell membrane components of the SNARE complex) and phospholipids on the cell membrane in a Ca^{2+} dependent manner, which is important to tether the secretory vesicles to the plasma membrane and facilitate membrane fusion and exocytosis [133].

2.6.2. Regulation of gene expression by actin filaments and microtubules

Actin filaments, also called microfilaments, are polymers of globular actin (G-actin) that forms flexible double-stranded helix fibers of several micrometers in length and up to 7 nm in diameter. They form higher order structures of bundles and networks. Actin polymerization is a reversible spontaneous process that can be facilitated by the hydrolysis of the ATP bound to G-actin to ADP. The rate of actin polymerization is proportional to the concentration of the G-actin, and normally there is equilibrium between actin polymerization and dissociation. Several actin-binding proteins regulate the assembly and disassembly of the actin filaments, such as cofilin that enhances the rate of actin filaments depolymerization, profilin that antagonizes the function of cofilin by enhancing the exchange of ADP for ATP on G-actin, and the actin related proteins (Arp2/3) proteins, which functions as a nucleation point for the polymerization of a new actin filaments [134, 135]. RhoA GTPase is also a major promoter for actin filaments polymerization. It functions mainly via two downstream signaling pathways: one that is mediated through the Rho-kinases (ROCK) that activate LIM kinase-mediated phosphorylation of cofilin, which inactivates cofilin, resulting in the stabilization of the actin filaments [136]. The other pathway involves the activation of the formins (mDia1 and mDia2), which are a potent nucleator and polymerization factor for actin filaments [137].

Several extracellular stimuli, such as GPCRs (coupled to $G\alpha_{q/11}$ and $G\alpha_{12/13}$), TGF- β receptors and integrins, can modulate the activity of the RhoGTPases through Rho guanine nucleotide exchange factors (GEFs), which influences the rate of actin filaments organization, and thereby the concentration of cytoplasmic free G-actin. High cytoplasmic free G-actin is known to bind myocardin-related transcription factors (MRTFs), preventing them from entering the nucleus and therefore interacting with the serum response factor (SRF), as a result SRF cannot induce gene expression. Therefore, the equilibrium between the polymerized and free actin can regulate the expression of certain gene expression [138].

Microtubules are composed of a polymer of α -tubulin and β -tubulin monomers that are alternatively linked together to form protofilaments, each 13 protofilaments associate laterally to form a hollow cylindrical polymer of 25 nm in diameter. γ -tubulin are specially located in the microtubule organizing centers, from which the microtubules polymerization originates, so that the α -tubulin subunit is exposed at the beginning of the protofilament (-) end and the β -tubulin subunit exposed at the opposite end (+) end, at which the elongation of the microtubule usually occurs [139]. Microtubules need GTP for polymerization and stability, and the status of the microtubules oscillate between regular growing phase and rapid disassembly phase (catastrophe). The loss of the GTP-bound tubulin from the (+) end of growing protofilaments is believed to result in the instability of the microtubule protofilaments, causing them to shift to the catastrophe phase [140].

The disruption of microtubules has been shown by different studies to change the expression of different genes. It has been shown by Cho and coworkers that treatment with Nocadazole, an effective microtubules disrupting drug, was associated with the modulation of gene expression of 50 genes [141]. Moreover, it was shown that microtubules sequester Smad2 transcription factors, making them less available to activation by TGF- β receptors [142]. Several other transcription factors, such as MIZ-1 and Egr3 were found to associate with the microtubules, so that their activity was assumed to be regulated by the polymerization state of the microtubules [143, 144].

2.7. Connective tissue growth factor

The connective tissue growth factor (CTGF), also known as CCN2, was first identified as a platelet derived growth factor (PDGF)-related mitogen that is secreted by human vascular endothelial cells [145-147]. Later, it was shown that CTGF is highly expressed during embryonic development and re-expressed in almost all fibrotic tissues including the fibrotic heart. With this respect, it has been demonstrated that MyoF but also other cardiac cells are substantial sources of CTGF.

2.7.1. Protein structure of CTGF

The analysis of its protein structure revealed that it is a 38-kDa cysteine-rich protein that is composed of four modules: I) insulin-like growth factor binding protein module (IGFBP) for the binding of insulin-like growth factor (IGF), II) von Willebrand factor type C (VWF-C) module for the binding of TGF- β and bone morphogenetic proteins-4 (BMP-4), III) thrombospondin (TSP)-type I homology module for the binding of vascular endothelial growth factors (VEGF) and various isoforms of integrins and some cell surface receptors like LRP-1. This module has a cysteine-rich (CR) region. And finally, IV) the carboxy-terminal (CT) cysteine knot motif and heparin-binding module for the binding of proteoglycan sulphate proteoglycans, which allows the binding and interaction with the ECM proteins. This complex structure combining growth factor binding and ECM binding modules defines CTGF as a matricellular protein [145].

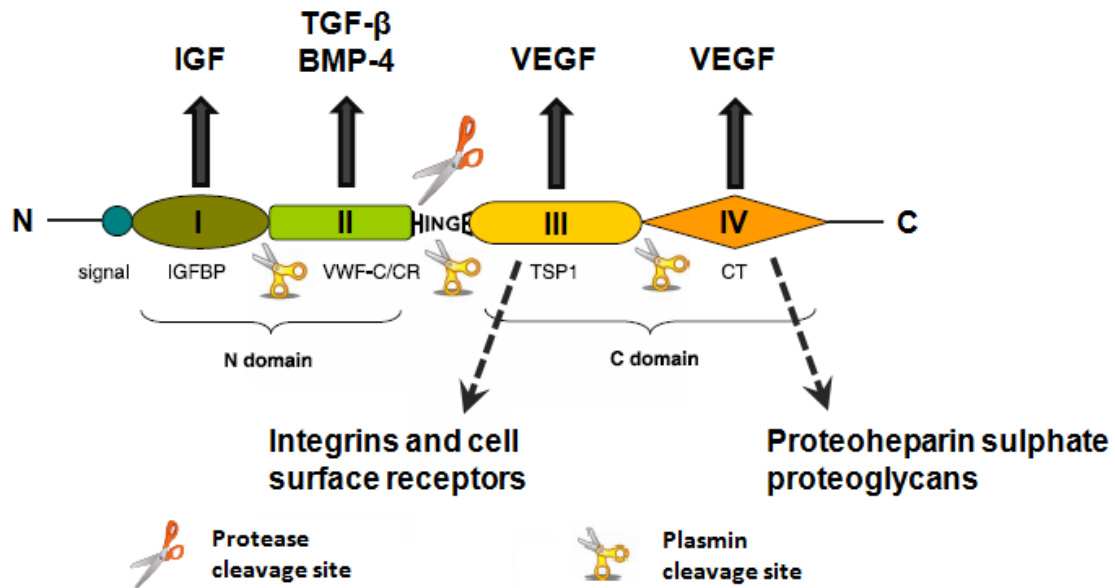


Figure 4: Protein structure of CTGF

The scheme shows the 4 modules of CTGF and their interactions with different growth factors, cell surface and ECM proteins. It also shows the cleavage sites for proteases and plasmin. The scheme was adapted with modifications from de Winter and coworkers and Gressner and Gressner [145, 148].

In addition to its 4 modules, CTGF contains a hinge region with a protease cleavage site that is sensitive to most proteases including elastases, matrix metalloproteinases (MMPs) and plasmin. The cleavage of the hinge region separates the N-domain from the C-domain resulting in two fragments of similar molecular weight. Plasmin, as well as chymotrypsin can also cleave module I and IV. Therefore, four different fragments of CTGF, in addition to the full-length protein, can be found in body fluids and in the supernatant of CTGF-producing cells (Fig. 4). It is postulated that these different fragments can fulfill different physiological functions [145, 148, 149]. The full length and C-terminus CTGF were reported to stimulate cell proliferation and collagen synthesis in different cells including fibroblasts. Also full length CTGF and module III were found to induce fibronectin synthesis and to mediate interaction with integrins, which is important for cell adhesion. They were also reported to induce the phosphorylation of extracellular signal-regulated kinases 1/2 (ERK1/2), which drive a signaling cascade that activates

collagen synthesis and induces fibrosis [150-152]. However, the induction of collagen synthesis by CTGF was found to be dependent on the presence of other factors like insulin and IGF, and is also tissue specific [148].

2.7.2. Physiological functions of CTGF

CTGF is known to play a vital role during the embryogenesis stage, since its absence was associated with malformation of cartilages, bones and blood vessels. However, CTGF expression and secretion continues during the adulthood [153, 154]. The structure of CTGF protein gives it the capacity to interact with several growth factors as well as cell surface and ECM proteins, allowing CTGF to function as a modulator for several cellular processes including cell migration, proliferation and differentiation, besides ECM synthesis and the cell-ECM interaction [155-157]. In addition, it was reported that CTGF mediates the deposition of fibronectin in response to TGF- β through upregulation of the active $\alpha 5\beta 1$ integrin [158]. Based on the ability of CTGF to bind fibronectin and integrin on one hand, the ability to enhance the binding of fibronectin to fibrin on the other hand, it was proposed that CTGF promotes fiber-fiber, fiber-matrix and matrix-matrix interactions through direct interaction with ECM proteins [145].

2.7.3. Role of CTGF in fibrotic heart disease

CTGF and TGF- β are both upregulated in the myocardium of patients with HF, and are thought to play an important role in the pathogenesis of the disease, especially in the development of fibrosis [72]. Several publications have reported that CTGF mediates several functions of TGF- β . However, it was found that different CTGF fragments actually mediate different functions, that is, the N-terminal domain of CTGF mediates MyoF differentiation and collagen synthesis, while the C-terminal domain mediates the proliferation of fibroblasts [159]. Moreover, CTGF was shown to enhance the fibrotic process associated with HF, which was mainly dependent on its CT domain [160]. In addition, CTGF synergizes the ability of TGF- β to induce epithelial-mesenchymal transition (EMT), which is a known mechanism for the accumulation of fibroblasts in the site of injury and the later scar formation. Several mechanisms have been proposed with this respect, for example, it was shown that CTGF inhibits Smad7 phosphorylation,

which is a counter-regulatory mechanism for the activation of Smad2/3, the main second messengers for TGF- β signaling. Also it was found that CTGF enhances the binding of TGF- β to its own receptor and besides this there were some reports that CTGF induces the expression of the EMT marker tenascin-C (TN-C) [145, 161]. Moreover, it was found that CTGF is important for the expression of the stretched-induced fibrillary collagen α -1(III), MMPs and Ccl2/7/8 chemokines in primary CF, which are involved in fibrogenesis associated with cardiomyopathies [162].

In contrast to the concept of the profibrotic role of CTGF, there are several recent publications reporting that CTGF has cardioprotective effects. Gravning and coworkers published two papers in the year 2011 and 2012 reporting that the over-expression of CTGF resulted in a diminished infarct size, but without a remarkable effect on the collagen content [163, 164]. Moreover, another two publications from the same lab in the year 2013 reported that CTGF overexpression has cardioprotective effects via attenuating the cardiac hypertrophy in response to chronic pressure-overload by either abdominal aortic banding or to chronic exposure to isoproterenol [165, 166]. A report from another lab in the year 2013 confirmed the cardioprotective effects of CTGF, and proposed that it increases the tolerance of cardiomyocytes towards hypoxia and oxidative stress via PI3-kinase (PI3K)-dependent Akt/GSK-3 β signaling [167].

2.7.4. Regulation of CTGF in CF

CTGF is complexly regulated by different factors, including mechanical signaling, which can be transduced to the nucleus via certain cytoskeleton-dependent signaling involving integrins, and biochemical activation by autocrine and paracrine factors, like Ang II and TGF- β . In addition, functional Golgi apparatus was also found to play a role with this respect. Muehlich and coworkers reported a direct relationship between the formation of stress fibers and the expression of CTGF, which reflected an inverse relationship between the level of the monomeric G-actin and the level of CTGF expression. In addition, the overexpression of constitutively active RhoA, which is in favor of actin filaments formation, significantly enhanced the expression of CTGF. A similar induction of CTGF expression was also obtained with overexpression of the serum response factor (SRF) [168]. Several other reports demonstrated a regulatory role for the actin filaments on CTGF expression via mediating shear-stress signals to the nucleus and the

regulation of SRF [168, 169]. Moreover, as mentioned in section 1.6.2, the function of SRF requires the translocation of MRTF from the cytosol to the nucleus, where it complexes with SRF to function as transcription factor. However, it was also found that the monomeric G-actin binds MRTF in the cytosol, thus preventing it from translocation to the nucleus, and that the interaction between the monomeric G-actin and MRTF is dependent on the level of the monomeric G-actin in the cytosol, which is inversely related to the polymerization of actin filaments [138]. Taking these findings together, it can be concluded that for the induction of CTGF expression, actin polymerization is required, so that less G-actin is available in the cytosol in order to allow MRTF-SRF complex to form in the nucleus. In addition, it has been found that CTGF expression can be induced by a mechanism involving the activation of focal adhesion kinase (FAK), Src-family of tyrosine kinases and PI3K, which translate the mechanical signaling by integrin and cytoskeleton into a change in CTGF expression [170].

2.8. Aim of the project

Cardiac fibrosis occurs a one major process in cardiac remodeling during heart disease. Within this process the numerical highly abundant CF secrete excessive amounts of extracellular matrix proteins as well as fibrosis-associated growth factors, cytokines and so called matricellular proteins. The connective tissue growth factor (CTGF) belongs to the latter protein family and has been shown to be strongly increased in its expression during cardiac fibrosis. The aim of this project was to unravel mechanisms, which are involved in the control of the expression and secretion of this protein in CF with a strong focus on calcium- and cytoskeleton-dependent mechanisms. In the detail, the angiotensin II-dependent regulation of the calcium handling in neonatal rat CF was studied, downstream mechanisms leading to a change in the regulation of CTGF were analyzed, and the impact of changes in the actin cytoskeleton as well as in microtubules was determined.

3. Materials and methods

3.1. Materials

3.1.1. Chemicals, reagents and consumables

| Chemicals and reagents | Company |
|---------------------------------------------------------------------------------------------------|-------------------|
| 1,2-bis(2-aminophenoxy)ethane-N,N,N',N'-tetraacetic acid tetrakis(acetoxymethyl ester) (BAPTA-AM) | AAT Bioquest |
| 3-N-morpholino-propanesulfonic-acid (MOPS) | AppliChem |
| 4-(2-hydroxyethyl)-1-piperazineethanesulfonic acid (HEPES) | Carl Roth |
| 4',6-diamidino-2-phenylindole (DAPI) | Roche |
| Acetic acid (100%) | Carl Roth |
| Acrylamide rotiphorese gel 30 solution (30 % acrylamide/bisacrylamide, mixing ratio 37.5:1) | Carl Roth |
| Agar | Peqlab |
| Agarose | AppliChem |
| Ammonium persulfate (APS) | AppliChem |
| Angiotensin II, human (Ang II) | Sigma-Aldrich |
| Aqua B. Braun | Braun |
| Ascorbic acid | AppliChem |
| Bromophenol blue | AppliChem |
| Calcium chloride hexahydrate (CaCl ₂ .6H ₂ O) | AppliChem |
| Carbenicillin | Applichem |
| Cesium chloride (CsCl) | Biomol |
| Colchicine | Cayman Chemicals |
| Cyclosporin A (CsA) | Tocris |
| Dimethylsulfoxide (DMSO) | Sigma-Aldrich |
| DMEM Glutamax, 1 g/l glucose, pyruvate | Life Technologies |
| DMEM Glutamax, 4.5 g/l glucose | Life Technologies |
| DNA loading buffer (6x) | Thermo-Scientific |
| DNase I type V | Merck |
| Ethanol, absolute | J.T. Baker |
| Ethidium bromide | Sigma-Aldrich |
| Fetal calf serum (FCS) | Life Technologies |
| FITC-phalloidin | Sigma-Aldrich |
| Formaldehyde (37%) | Merck |
| Formamide | Sigma-Aldrich |
| GeneRuler 1 Kb DNA ladder | Thermo-Scientific |
| GeneRuler 1 Kb plus DNA ladder | Thermo-Scientific |

| | |
|-------------------------------------------------------------------------------------------|-------------------|
| Glucose | AppliChem |
| Glycerol | AppliChem |
| Glycine | AppliChem |
| Go 6983 | Tocris |
| gp91-ds-tat | Mo BioTec |
| gp91-ds-tat; sgp91 ds-tat, scrambled (Scr) | Mo BioTec |
| HEPES-buffered saline solution | Lonza |
| Igepal CA-630 | Sigma-Aldrich |
| Isopropanol | Carl Roth |
| Kanamycin | Sigma-Aldrich |
| Kn-92 | Calbiochem |
| Kn-93 | Calbiochem |
| Latrunculin-A (LAT-A) | Cayman Chemicals |
| Magnesium chloride (MgCl ₂) | AppliChem |
| Magnesium sulphate monohydrate (MgSO ₄ .H ₂ O) | AppliChem |
| Manganese(II) chloride tetrahydrate (MnCl ₂ .4H ₂ O) | AppliChem |
| Methanol | Carl Roth |
| Methyl-beta-cyclodextrin (CDX) | Sigma-Aldrich |
| Non-essential amino acids (NEAA) (100x) | Life Technologies |
| NSC 23766 | Tocris |
| Paraformaldehyde (PFA) | Sigma-Aldrich |
| Penicillin/streptomycin (P/S) (100x) | Life Technologies |
| Phosphate-buffered saline (PBS) without Ca ²⁺ | Life Technologies |
| Picric acid | Sigma-Aldrich |
| Piperazine-N,N'-bis(2-ethanesulfonic acid) (PIPES) | Carl Roth |
| Polyfect | Qiagen |
| Ponceau S | Sigma-Aldrich |
| Potassium chloride (KCl) | AppliChem |
| Potassium dihydrogen phosphate (KH ₂ PO ₄) | AppliChem |
| Pyrazol 3 (Pyr3) | Sigma-Aldrich |
| Roti-block (10x) | Carl Roth |
| Roti-immunoblock (10x) | Carl Roth |
| Roti-mark standard, protein molecular weight marker | Carl Roth |
| Sodium acetate (CH ₃ COONa) | AppliChem |
| Sodium bicarbonate (NaHCO ₃) | Roth |
| Sodium chloride (NaCl) | AppliChem |
| Sodium dihydrogen phosphate (NaH ₂ PO ₄) | AppliChem |
| Sodium dodecyl sulfate (SDS) | AppliChem |
| Sodium hydrogen phosphate dihydrate (Na ₂ HPO ₄ .2H ₂ O) | AppliChem |
| Sodium hydroxide (NaOH) | AppliChem |
| β-Mercaptoethanol | AppliChem |
| Tetramethylethylenediamine (TEMED) | Merck |
| Thapsigargin (TGN) | Calbiochem |

| | |
|--------------------------------------------------------|-------------------|
| Tris ultrapure (Tris base) | AppliChem |
| TRITC-phalloidin | Sigma-Aldrich |
| Triton X-100 | Carl Roth |
| Trypan blue | Fluka |
| Trypsin | BD Biosciences |
| Trypsin-EDTA 0.05% | Life Technologies |
| Trypsin neutralizing solution (TNS) | Lonza |
| Tryptone | AppliChem |
| Tween 20 | Carl Roth |
| U73122 (122) | Tocris |
| U73343 (343) | Tocris |
| Valsartan | Sigma-Aldrich |
| Wheat germ agglutinin (WGA), Alexa-fluor 488 conjugate | Life Technologies |
| Yeast extract | AppliChem |
| Xestospongin C (XeC) | Cayman Chemicals |

Table 1: Chemicals and reagents

| Article | Specification | Source |
|-------------------------------------------|------------------------------|--------------------|
| Cell culture dishes | 6, 10, 15 cm | Greiner Bio One |
| Cell scrapers | 1.7 cm blade | Sarstedt |
| Centrifuge tubes | Polyallomer (16 x 102 mm) | Beckman |
| Dialysis device | Float-A-lyzer G2, MWCO 20 KD | Spectrum Labs |
| Filter syringes | Non pyrogenic, 0.2 µM | Sarstedt |
| Filtration sets | 250, 500, 1000 ml, 0.22 µM | Corning |
| Flexitip pipette tips | 0.5-200 µl | Peqlab |
| Micro-Amp optical adhesive films | PCR compatible | Applied Biosystems |
| Micro-Amp optical reaction plates | 384-well | Applied Biosystems |
| Multi-well cell culture plates | 6, 12, 24, 96-well | Greiner Bio One |
| Nitrocellulose membrane, Whatman, Protran | Pore size 0.2 µM | GE Healthcare |
| PCR reaction tubes | 0.2 ml | Sarstedt |
| Pipette tips | 10, 100, 200 1000 µl | Sarstedt |
| Pipette tips with filters | 10, 100, 200 1000 µl | 4titude |
| Reaction and centrifuge tubes | 15, 50 ml | Greiner Bio One |
| Reaction tubes | 0.5, 1.5, 2 ml | Sarstedt |
| Serological pipettes | 1, 2, 5, 10, 25 ml | Sarstedt |
| Wide opening, serological pipettes | 10 ml | Falcon |

Table 2: Consumables

3.1.2. Restriction enzymes and related supplements

| Restriction enzymes | Buffer | Company |
|---------------------|-------------------------|---------------------|
| AfIII | 10x NEB buffer 2 | New England Biolabs |
| EcoRV | 10x NEB buffer 3 | |
| KpnI | 10x NEB buffer 2 | |
| PacI | 10x NEB buffer 4 | |
| PmeI | 10x NEB buffer 4 | |
| PstI | 10x NEB buffer 3 | |
| XhoI | 10x NEB buffer 2 | |
| SmaI | 10x Tango yellow buffer | Thermo-Scientific |

Table 3: Restriction enzymes

3.1.3. Kits

| Kit | Application | Company |
|-------------------------------------------------------|----------------------------------------------|---------------------|
| 5x HOT FIREPOL EvaGreen qPCR Mix Plus | qPCR | Solis Biodyne |
| Exprep plasmid SV midi | Midiprep plasmid purification from bacteria | GeneAll |
| Exprep plasmid SV mini | Miniprep plasmid purification from bacteria | GeneAll |
| FGM-3 Bullet kit | Culturing and maintenance of NHCF-V | Lonza |
| GoTaq green master mix | PCR | Promega |
| High pure PCR product purification kit | PCR product purification | Roche |
| Lumi-light western blotting substrate | Chemiluminescence protein blot visualization | Roche |
| PrimeSTAR HS DNA polymerase | Gene amplification by PCR | TAKARA |
| Quick ligation kit | DNA ligation | New England Biolabs |
| Revert Aid First Strand cDNA Synthesis Kit | RNA reverse transcription into cDNA | Thermo-Scientific |
| RNeasy | Total RNA isolation | Qiagen |
| Screen Quest Fluo-8 No Wash | Live cell Ca ²⁺ imaging | AAT Bioquest |
| Super signal west femto maximum sensitivity substrate | Chemiluminescence protein blot visualization | Thermo-Scientific |

Table 4: Kits

3.1.4. Cells and viruses

| Cells | Descriptions |
|---------------------------------------------------------------|-------------------------------------------------------------------------------------------------------------|
| DH10B bacteria | High-efficiency chemically competent cells for transformation |
| AdEasier bacteria | BJ5183 bacteria transformed with adenoviral backbone plasmid pAdEasy-1 |
| HEK293A | Immortalized human embryonic kidney cell line |
| Tsa201 | Transformed HEK293 stably expressing SV40 temperature-sensitive T antigen |
| Primary neonatal rat cardiac fibroblasts (NRCF) | Isolated weekly from neonatal Wistar rats (1-3 days old) |
| Primary normal human ventricular cardiac fibroblasts (NHCF-V) | Purchased from Lonza (catalogue No. CC-2904, Lot No. 351481), isolated from healthy 50 year old male donor. |

Table 5: Bacterial and mammalian cells

| Adenovirus | Source |
|------------|--------------------------------------------------------------------------------------|
| Ad.EGFP | Susanne Lutz, Mannheim |
| Ad.HA-CTGF | Department of Life Science, Gwangju Institute of Science and Technology, South Korea |

Table 6: Adenoviruses

3.1.5. Antibodies

| Primary antibody against | Dilution | | Source | Type/ Clone | Catalogue No. | Company |
|-------------------------------------------|----------|----------|--------|--------------------|---------------|----------------|
| | WB | IF | | | | |
| Acetylated tubulin | 1:2000 | 1:500 | Mouse | Monoclonal/6-11B-1 | T6793 | Sigma-Aldrich |
| CaM kinase II δ (CaMKII δ) | 1:5000 | Not used | Mouse | Monoclonal/438422 | MAB4176 | R&D Systems |
| Caveolin-1 | 1:200 | Not used | Mouse | Monoclonal/7C8 | sc-53564 | Santa Cruz |
| CTGF | 1:200 | 1:50 | Goat | Polyclonal/L-20 | sc-14939 | Santa Cruz |
| ERK1/2 | 1:1000 | Not used | Rabbit | Polyclonal | 9102S | Cell Signaling |

| | | | | | | |
|---------------------------------------|----------|----------|--------|---------------------|---------|-------------------|
| PathScan Multiplex Western Cocktail I | 1:200 | Not used | Rabbit | mixed antibodies | 5301 | Cell Signaling |
| Phospho-CaMKII | 1:5000 | Not used | Mouse | Monoclonal/22B1 | MA1-047 | Thermo-Scientific |
| Phospho-ERK1/2 | 1:1000 | Not used | Rabbit | Polyclonal | 9101S | Cell Signaling |
| Polyglutamylated tubulin | 1:2000 | 1:500 | Mouse | Monoclonal/B3 | T9822 | Sigma-Aldrich |
| TRPC3 | Not used | 1:100 | Rabbit | Polyclonal | ACC-016 | Alomona Labs |
| Tyrosin-tubulin | 1:800 | 1:200 | Mouse | Monoclonal/TU B-1A2 | T9028 | Sigma-Aldrich |
| Vimentin | Not used | 1:500 | Mouse | Monoclonal/ V9 | V6630 | Sigma-Aldrich |
| sm-actin | 1:2500 | Not used | Mouse | Monoclonal 1A4 | A5228 | Sigma-Aldrich |
| α -tubulin | 1:2000 | 1:500 | Mouse | Monoclonal/B-5-1-2 | T5168 | Sigma-Aldrich |
| β -actin | 1:5000 | 1:1250 | Mouse | Monoclonal/ AC-74 | A2228 | Sigma-Aldrich |

Table 7: Primary antibodies

| Secondary antibody against | Dilution | Source | Catalogue No. | Company |
|----------------------------|----------|--------|---------------|---------------|
| Goat | 1:10000 | Donkey | sc-2020 | Santa Cruz |
| Mouse | 1:10000 | Rabbit | A9044 | Sigma-Aldrich |
| Rabbit | 1:40000 | Goat | A9169 | Sigma-Aldrich |

Table 8: Horseradish peroxidase (HRP)-conjugated secondary antibodies for western blotting

| Secondary antibody against | Dilution | Fluorophore | Source | Catalogue No. | Company |
|----------------------------|----------|-----------------|--------|---------------|-------------------------|
| Goat | 1:300 | Cy3 | Rabbit | 305-165-003 | Jackson Immuno Research |
| Goat | 1:100 | FITC | Rabbit | 305-095-003 | Jackson Immuno Research |
| Goat | 1:300 | Alexa-fluor 680 | Donkey | 705-625-147 | Jackson Immuno Research |

| | | | | | |
|--------|-------|-----------------|------|-------------|-------------------------|
| Mouse | 1:300 | Alexa-fluor 488 | Goat | 115-545-003 | Jackson Immuno Research |
| Mouse | 1:300 | Cy3 | Goat | 115-165-068 | Jackson Immuno Research |
| Rabbit | 1:100 | Alexa-fluor 594 | Goat | 111-585-003 | Jackson Immuno Research |

Table 9: Fluorophore-conjugated secondary antibodies for immunofluorescence

3.1.6. Chemicals used for cell organelle fluorescence staining

| Chemical | Stock concentration | Dilution |
|--------------------------------------------------------|---------------------|----------|
| DAPI | 1 mg/ml | 1:1000 |
| FITC-phalloidin | 0.5 mg/ml | 1:300 |
| TRITC-phalloidin | 0.5 mg/ml | 1:500 |
| Wheat germ agglutinin (WGA), Alexa-fluor 488 conjugate | 1 mg/ml | 1:200 |

Table 10: Chemicals used for cell organelle/actin fluorescence staining

3.1.7. Oligonucleotides, primers and plasmids

| Oligonucleotide | Strand | Sequence (5' → 3') |
|-----------------------------------------|---------|------------------------------------------------------------|
| Tetracysteine (TC)-tag oligonucleotides | Forward | TTAAGCCGCCATGTTCTTGAAGTGTGGCC- GGGCTGCTGTATGGAGCCTGGTAC |
| | Reverse | CAGGCTCCATACAGCAGCCCGGGCAACAGT- TCAAGAACATGGCGGC |

Table 11: TC-tag oligonucleotides

| Gene | Primer | Sequence (5' → 3') |
|---------------------------------------------------------------------------------|---------|------------------------------|
| Amplification of CTGF gene without overhang | Forward | CTCTCCAAGAAGACTCAG C |
| | Reverse | GCAGTTAGG AACCCAGATTTA |
| Amplification of CTGF gene with the addition of KpnI and XhoI restriction sites | Forward | CCTGGTACCCTCGCCTCCGTCGCG |
| | Reverse | AGACTCGAGGTCCCTTACTCCCTGGCTT |

Table 12: Primers used for cloning of CTGF gene

| Gene | Primer | Sequence (5' → 3') | Annealing temperature |
|-----------------------------|---------|--------------------------|-----------------------|
| CTGF | Forward | CCGGGTTACCAATGACAATA | 58°C |
| | Reverse | CACACCCCACAGAACTTAGC | |
| PBGD (housekeeping gene) | Forward | CCTGAAACTCTGCTTCGCTG | 55, 57 or 58°C |
| | Reverse | CTGGACCATCTTCTTGCTGAA | |
| IP3R1 (variants 1, 2 and 3) | Forward | AGCACCTTGGGCTTGGTTGATGA | 57°C |
| | Reverse | CCGTCCCCAGCAATTCCTGTT | |
| IP3R2 | Forward | CAACGTCGGCCACTAGCTCTAAA | 57°C |
| | Reverse | AAGCTCCCCGTCTCTCACAGTTT | |
| IP3R3 | Forward | AGCAATGGGGATAACGTGGTTGTG | 57°C |
| | Reverse | GTCACAGGTCAGGAACTTCTCCT | |
| TRPC3 | Forward | ACTGGGCATGGGTA ACTCAA | 53°C |
| | Reverse | TTCAGTTCACCTTCGTTACCT | |

Table 13: Primers used for qPCR and RT-PCR

| Plasmid | Description |
|---------------------|------------------------------------------------------------------------------------------------------------------------------|
| pcDNA 3.1/Zeo(+) | Mammalian expression vector, allows high level of constitutive gene expression in mammalian cells |
| pShuttle-CMV vector | Facilitates the transfer of the gene of interest to AdEasier bacteria, where it can be recombined with the pAdEasy-1 plasmid |
| pAdEasy-1 | E1 and E3 double deletion adenoviral backbone vector |

Table 14: Plasmids used for the construction of TC-CTGF overexpressing recombinant adenovirus

3.1.8. Buffers, solutions and media

| Immunoblotting | |
|------------------------------------------------------------|----------------------------------------------------------------------------------------------------------------------------------------------------------------------|
| GST-fish buffer (500 ml) | 25 ml 1 M Tris (pH 7.4 with HCl) 75 ml 1 M NaCl 2 ml 1 M MgCl ₂ 50 ml glycerol 5 ml Igepal CA-630 up to 500 ml distilled water |
| 4x SDS-PAGE sample loading buffer without glycerol (50 ml) | 5 ml β-mercaptoethanol 3.25 g SDS 15 ml 300 mM Tris (pH 6.8 with HCl) 0.125 g bromophenol blue up to 50 ml distilled water |
| 4x SDS-PAGE sample loading buffer with glycerol (50 ml) | 25 ml glycerol 5 ml β-mercaptoethanol 3.25 g SDS 15 ml 300 mM Tris (pH 6.8 with HCl) 0.125 g bromophenol blue up to 50 ml distilled water |
| 10x TBS buffer (1000 ml) | 12.12 g Tris 87.65 g NaCl up to 1000 ml distilled water pH 7.4 with HCl |
| TBS-T buffer (1000 ml) | 1000 ml 10x TBS 1 ml tween 20 |
| 5x SDS-PAGE electrophoresis buffer (1000 ml) | 15.1 g Tris 94 g glycine 5 g SDS up to 1000 ml distilled water pH 8.3 with KOH |
| Blotting buffer (1000 ml) | 3.02 g Tris 14.4 g glycine 200 ml methanol up to 1000 ml distilled water |
| 12 % SDS-polyacrylamide gel (50 ml) | 16.5 ml distilled water 20 ml acrylamide rotiphorese gel 30 solution 12.5 ml 1.5 M Tris (pH 8.8 with HCl) 0.5 ml 10% SDS 0.5 ml 10% APS 0.02 ml TEMED |

| | |
|------------------------------------|----------------------------------------------------------------------------------------------------------------------------------------------------------------------|
| 15% SDS-polyacrylamide gel (50 ml) | 11.5 ml distilled water 25 ml acrylamide rotiphorese gel 30 solution 12.5 ml 1.5 M Tris (pH 8.8 with HCl) 0.5 ml 10% SDS 0.5 ml 10% APS 0.02 ml TEMED |
| 5% SDS-polyacrylamide gel (20 ml) | 13.6 ml distilled water 3.4 ml acrylamide rotiphorese gel 30 solution 2.5 ml 1 M Tris (pH 6.8 with HCl) 0.2 ml 10% SDS 0.2 ml 10% APS 0.02 ml TEMED |
| 10% SDS (100 ml) | 10 g SDS up to 100 ml distilled water |
| 10% APS (10 ml) | 1 g APS up to 10 ml distilled water |
| Ponceau S stain (100 ml) | 5 ml glacial acetic acid 0.2 g Ponceau S powder up to 100 ml distilled water |
| Stripping buffer (500 ml) | 3.79 g Tris 3.9 ml β -mercaptoethanol 10 g SDS up to 500 ml distilled water pH 6.7 with HCl |
| Immunofluorescence (IF) | |
| 4% paraformaldehyde (PFA) (250 ml) | 10 g paraformaldehyde 50 μ l 10 N NaOH 25 ml 10x PBS up to 250 ml distilled water pH adjusted to 7.0 with HCl |
| 0.05% Triton (50 ml) | 250 μ l 10x Triton up to 50 ml PBS |
| 1x Roti-immunoblock (50 ml) | 5 ml 10x Roti-immunoblock up to 50 ml distilled water |

| Formaldehyde (FA) agarose gel electrophoresis | |
|------------------------------------------------------|-----------------------------------------------------------------------------------------------------------------------------------------------------------------------------------------------------------------|
| 10x FA gel buffer (1000 ml) | 41.46 g MOPS 6.8 g sodium acetate 2.9 g EDTA up to 1000 ml distilled water pH 7.0 with NaOH |
| 1x FA gel running buffer (1000 ml) | 100 ml 10x FA gel buffer 20 ml 37% FA up to 1000 ml RNase-free water |
| 1.2% FA gel (100 ml) | 1.2 g agarose 10 ml 10x FA gel buffer up to 100 ml RNase-free water heat with mixing, cool to 65°C, add 1.8 ml 37% FA and 3 µl ethidium bromide (10 mg/ml) then cast |
| 5x RNA loading buffer (10 ml) | 16 µl saturated aqueous bromophenol blue solution 80 µl 500 mM EDTA (pH 8.0 NaOH) 720 µl 37% FA 2 ml glycerol anhydrous 3.084 ml formamide 4 ml FA gel buffer up to 10 ml RNase-free water |
| DNA agarose gel electrophoresis | |
| 1% DNA agarose gel (50 ml) | 0.5 g agarose powder 50 ml 1x TAE buffer 2 µl ethidium bromide (10 mg/ml) |
| 50x TAE buffer (1000 ml) | 242.28 g Tris 57.1 ml glacial acetic acid 200 ml 0.25 M EDTA (pH 8.0 with NaOH) up to 1000 ml distilled water |
| Bacterial culture media and plates | |
| LB medium (1000 ml) | 10 g tryptone 5 g yeast extract 10 g NaCl up to 1000 ml distilled water pH 7.0 autoclave |

| | |
|---------------------------------------------|------------------------------------------------------------------------------------------------------------------------------------------------------------------------------------------------------------------------------------------------------------------|
| LB agar plates with carbenicillin (1000 ml) | <p>10 g tryptone 5 g yeast extract 10 g NaCl 15 g agar up to 1000 ml distilled water pH 7.0 with NaOH autoclave let cool to about 50°C, then add 1 ml carbenicillin stock (50 mg/ml), then cast as 20 ml/10 cm petri dish</p> |
| LB agar plates with kanamycin (1000 ml) | <p>10 g tryptone 5 g yeast extract 10 g NaCl 15 g agar up to 1000 ml distilled water, pH 7.0 autoclave let cool to about 50°C, then add 1 ml kanamycin stock (33 mg/ml), then cast as 20 ml/10 cm petri dish</p> |
| SOB medium (1000 ml) | <p>20 g tryptone 5 g yeast extract 0.5 g NaCl 10 ml 25 mM KCl up to 1000 ml distilled water pH 7.4 autoclave 5 ml autoclaved 2 M MgCl₂</p> |
| SOC medium (100 ml) | <p>1 ml filter-sterilized 2 M glucose up to 100 ml SOB medium</p> |
| 0.5 M PIPES buffer (20 ml) | <p>3.02 g PIPES up to 20 ml distilled water pH 6.7 with NaOH</p> |
| Inoue buffer (10 ml) | <p>108.8 g MnCl₂·4H₂O 22 mg CaCl₂·6H₂O 186 mg KCl 200 µl 0.5 M PIPES up to 10 ml distilled water</p> |

| Cell isolation | |
|-------------------------------------------------------------------|--------------------------------------------------------------------------------------------------------------------------------------------------------------------------------------------------------------------------------------------------------------------------------------------------------------------------------------------------------------------------------------|
| Calcium- and bicarbonate- free Hanks with HEPES (CBFHH) (1000 ml) | 40 ml NaCl stock (200 g/l) 10 ml MgSO ₄ .H ₂ O stock (20 g/l) 10 ml KH ₂ PO ₄ stock (6 g/l) 10 ml Na ₂ HPO ₄ .2H ₂ O stock (5.97 g/l) 10 ml glucose dihydrate stock (100 g/l) 100 ml HEPES stock (47.66 g/l) up to 1000 ml distilled water, sterile by filtration pH 7.4 with NaOH |
| 50x trypsin stock solution (10 ml) | 1 g trypsin/10 ml CBFHH, dissolved overnight at 4°C with continuous rotation, sterilized by filter syringe (0.2 µM) |
| DNase I stock solution (100 ml) | 100 mg DNase I type V/100 ml distilled water |
| Heat inactivated FCS (50 ml) | 50 ml FCS was incubated in a water bath adjusted to 56°C for 30 min, during which it was shaken gently every 5 min. |
| Non-cardiomyocyte medium (NKM) | 500 ml DMEM GlutaMax 1 g/l glucose 50 ml heat-inactivated FCS 5 ml P/S (100x) |
| Trypsin working solution (50 ml) | 0.5 ml P/S (100x) 1.3 ml trypsin stock 0.2 ml DNase I stock up to 50 ml CBFHH |
| DNase-working solution (50 ml) | 0.5 ml P/S (100x) 1.7 ml FCS 0.2 ml DNase I stock up to 50 ml CBFHH |
| 0.4% Trypan blue (100 ml) | 0.4 mg trypan blue 100 ml distilled water |
| NRCF culture media | |
| Fibroblasts growth medium (FGM) | 500 ml DMEM GlutaMAX 4.5 g/l glucose 50 ml FCS 5 ml P/S (100x) 5 ml NEAA (100x) |

| | |
|--------------------------------------------------------------|--------------------------------------------------------------------------------------------------------------------------------------------------------------------------------------------------------------------------------------------------------------------------------------|
| Low medium (LM) | 500 ml DMEM GlutaMax 1 g/l glucose 5 ml P/S (100x) |
| HEK293A culture media | |
| HEK293A growth medium | 500 ml DMEM GlutaMAX 4.5 g/l glucose 50 ml heat-inactivated FCS 5 ml P/S (100x) |
| HEK293A low serum medium | 500 ml DMEM GlutaMAX 4.5 g/l glucose 2.5 ml heat-inactivated FCS 5 ml P/S (100x) |
| Buffers for adenovirus purification | |
| 10x Virus storage buffer (VSB) (1000 ml) | 100 ml 1 M Tris, (pH 7.4 with HCl) 80 g NaCl 50 ml 1 M KCl 10 ml 1 M MgCl ₂ up to 1000 ml distilled water |
| Light cesium chloride (CsCl) (1.209 g/ml) | 11.02 g CsCl, fill up to 50 g 1x VSB |
| Heavy cesium chloride (CsCl) (1.459 g/ml) | 21.10 g CsCl, fill up to 50 g 1x VSB |
| Sirius red-based colorimetric microassay for collagen | |
| Sirius red solution (100 ml) | 100 mg siruis red dye powder 100 ml saturated aqueous picric acid |
| Bouin's solution (16 ml) | 15 ml saturated aqueous picric acid 5 ml 35% formaldehyde 1 ml 100% acetic acid |
| Other buffers and solution | |
| Calcium-free Tyrode's solution (500 ml) | 20 ml stock I (175 g NaCl, 10 g KCl, 25 ml MgCl ₂ , up to 1000 ml distilled water) 19 ml stock II (50 g/l NaHCO ₃) 10 ml stock III (5.8 g/l NaH ₂ PO ₄) 0.5 g glucose 50 mg ascorbic acid up to 500 ml distilled water |
| 3 M Sodium acetate (1000 ml) | 246 g sodium acetate up to 1000 ml distilled water pH 5.2 with acetic acid |

Table 15: Composition of the used buffers, solutions and media

3.1.9. Inhibitors

| Inhibitor | Stock solutions | Solvent | End concentration in cell culture | Control condition |
|--------------------------------------|------------------|-------------------|-----------------------------------|-------------------|
| BAPTA-AM | 13.1 mM | DMSO | 7 μ M | DMSO |
| Colchicine | 2.5 mg/ml | Water | 1.3, 5 μ g/ml | Water |
| Cyclosporin A (CsA) | 40 mM | DMSO | 20 nM | DMSO |
| Go 6983 | 50 mM | DMSO | 6 μ M | DMSO |
| gp91 ds-tat | 50 mM | Water | 5 μ M | Water |
| gp91 ds-tat; sgp91 ds-tat, scrambled | 50 mM | Water | 5 μ M | Water |
| Kn-92 | 1 mM | Water | 2 μ M | Water |
| Kn-93 | 1 mM | DMSO | 2 μ M | DMSO |
| Latrunculin-A (LAT-A) | 100 μ g/ml | Ethanol, absolute | 5.5, 7, 8.5 ng/ml | Ethanol, absolute |
| Methyl-beta-cyclodextrin (CDX) | Freshly prepared | Water | 2.5 mM | Water |
| NSC 23766 | 50 mM | Water | 50 μ M | Water |
| Pyrazol 3 (Pyr3) | 10.95 mM | DMSO | 3 μ M | DMSO |
| Thapsigargin (TGN) | 1 mM | DMSO | 3 μ M | DMSO |
| U73122 (122) | 5 mM | DMSO | 1.5 μ M | DMSO |
| U73343 (343) | 5 mM | DMSO | 1.5 μ M | DMSO |
| Valsartan | 2.3 mM | DMSO | 15 nM | DMSO |
| Xestospongine C (XeC) | 5.6 mM | Ethanol, absolute | 1.4, 100 μ M | Ethanol, absolute |

Table 16: End concentration in cell culture for each of the used inhibitors

3.1.10. Devices and softwares

| Device | Model | Company |
|------------------------|----------------------------------------------------------------------|---------------------|
| Autoclave | VX-150 | Systec |
| Cell counter | Casy | Roche |
| Cell counting chamber | Fuchs-Rosenthal bright-line | Marienfeld-Superior |
| Cell culture incubator | Steri-cult 200 Incubator | Forma Scientific |
| Cell culture incubator | Labotect Incubator C 200 | Labotect |
| Cell sieve | Cell dissociation sieve - tissue grinder kit (250 μ m pore size) | Sigma-Aldrich |
| Centrifuge bench top | Centrifuge 5804 R | Eppendorf |

| | | |
|-------------------------------------------------------|-----------------------------------------|--------------------------|
| Centrifuge bench top | Sigma 3K30 | Sigma |
| Centrifuge table top | Tabletop centrifuge 5415 D | Eppendorf |
| Centrifuge table top | Combi-spin FVL-2400N | Biosan |
| Centrifuge table top | Centrifuge 5417 R | Eppendorf |
| Chemiluminescence imaging system | Versa doc MP | Bio-Rad |
| Double distilled water system | Milli-Q | Millipore |
| Electric power supply and control | Powerpac | Bio-Rad |
| Heating block | Thermo mixer compact | Eppendorf |
| Horizontal system for submerged gel electrophoresis | H5 | BRL |
| Horizontal system for submerged gel electrophoresis | Mini-sub cell GT | Bio-Rad |
| Incubator | CFC-free | Sanyo |
| Inverted fluorescence microscope | Axiovert 200 | Zeiss |
| Inverted fluorescence microscope with climate chamber | Olympus IX 81 | Olympus |
| Inverted microscope | Axiovert S100 TV | Zeiss |
| Microscope camera | CAM-XM10-T-Camera | Olympus |
| Microscope filter Cy5 | BP 635/40 | Olympus |
| Microscope filter DAPI | BP 403/12 | Olympus |
| Microscope filter EGFP | BP 470/20 | Olympus |
| Microscope filter FITC | BP492/18 | Olympus |
| Microscope filter Texas Red | BP 572/23 | Olympus |
| Microscope objective 20x | LUCPLFLN20xPH 0.45 | Olympus |
| Microscope objective 40x | LUCPLFLN40xPH 0.60 | Olympus |
| Microscope objective 60x | PlanApo N60x/1.42 oil | Olympus |
| pH meter | WTW | Inolab |
| Pipettes | Pipetman | Gilson |
| Plate reader | FlexStation3 | Molecular Devices |
| Pump | ME2 | Vacuubrand |
| Real-Time-PCR-System | TaqMan 7900HT Fast Real-Time-PCR System | Applied Biosystems |
| Rocker | Diomax 1030 | Heidolph |
| Rotation shaker | Reax 3 | Heidolph |
| Scale | Portable | Sartorius |
| Shaker | GFL 3016 | GLF |
| Shaker | Vibramax 100 | Heidolph |
| Shaking incubator | Innova 4300 | New Baunswick Scientific |
| Sonicator | Sonifier B-12 | Branson Sonic Power |
| Spectrophotometer | Nanodrop 1000 | Peqlab |

| | | |
|--------------------------------------------------------------|--------------------------------------|-------------------------------------|
| Temperature control chamber | Certomat | B. Braun |
| Thermocycler | Mastercycler gradient | Eppendorf |
| Ultracentrifuge | L8-70M | Beckman |
| Ultracentrifuge rotor | SW-27 | Beckman |
| UV agarose gel imaging system | Gel doc XR | Bio-Rad |
| UV lamb plate | TI 1 | Biometra |
| Vortexer | VF 2 Vortexer | Janke u. Kunkel IKA Labortechnik |
| Water bath | 2764 | Eppendorf |
| Western blot gel electrophoresis and protein blotting system | Mini-protean tetra cell 4-gel system | Bio-Rad |

Table 17: Devices

| Software | Use | Company |
|----------------------------------------------------|--------------------------------------------------------------------------------|------------------------------------|
| GraphPad prism 5.0 | Statistical calculations and graphs drawing | GraphPad |
| Image J 1.60_20, time series analyzer V2.0 plug-in | Evaluation of fluorescence intensity | National Institutes of Health, USA |
| Quantity One 4.6.5 | Operating the Versa doc MP system and for semi-quantification of western blots | Bio-Rad |
| SDS 2.4 | Operating the TaqMan 7900HT Fast Real-Time-PCR System, and its data analysis | Applied Biosystems |
| Xcellence pro | Operating the Olympus microscopy system for cell imaging | Olympus |

Table 18: Softwares

3.2. Methods

3.2.1. Isolation, maintenance and passaging of primary neonatal rat cardiac fibroblasts

Neonatal rat cardiac fibroblasts (NRCF) were isolated from neonatal rats (1-3 days old) according to a modified protocol by Simpson and Savion, 1982 [171]. Briefly, the animals were decapitated, the thoracic cavity was quickly opened and the hearts were removed.

The pedicles and the atria were removed, and the ventricles were cut into small pieces (about 1-2 mm size). After that, the cardiac cells were released from the ventricular tissues by repeated digestion cycles. To do so, the ventricular tissues were incubated with trypsin working solution with mild rocking at room temperature until it started to become cloudy (1-4 min), at this point, the supernatant solution was transferred into a collecting tube containing fetal calf serum (FCS), and DNase I working solution was added to the tissues. The tissues were triturated several times to physically release the loosened cells. Then, the supernatant was transferred into the collecting tube, and a new digestion cycle was started. The digestion cycles continued until no more cells were released. After that, the collecting tubes were centrifuged at 60 g, 4°C for 15 min, the supernatant was aspirated, the pellets were resuspended in non-cardiomyocyte medium (NKM), and the cells from different collecting tubes were pooled together. Next, the cells were strained through a pre-wetted cell sieve (250 µm pore size), and were collected in a new 50 ml reaction tube. After that, a sample from the cell suspension was mixed with 0.4% trypan blue as 1:1, and the mixture was then transferred into Fuchs-Rosenthal bright-line cell counting chamber to determine the number and viability of the yielded cells. Finally, NRCF were isolated from cell suspension by making use of their ability to adhere much faster to plastic cell culture surfaces comparing to cardiomyocytes and other cell types. To do so, the cell suspension was diluted with an appropriate volume of NKM, and the cells were seeded on 15 cm cell culture dishes as 10 million cells/dish. The cells were incubated at 37°C, 5% CO₂, 99% humidity for 1 hr, after which the medium containing the non-adherent cells was changed for fibroblasts growth medium (FGM). By this, most of the adherent cells are NRCF, and these cells are considered passage 0 (P0). The cells were maintained in FGM until the desired confluency had been reached.

Confluent NRCF culture plates were washed twice with pre-warmed PBS, after that, they were incubated with pre-warmed 0.05% trypsin-EDTA (7 ml/15 cm dish) until the cells started to round up and detach, at this point 20 ml/15 cm dish FGM was added, and the cells were collected in 50 ml reaction tube, diluted further with FGM, triturated well and seeded in new cell culture dishes and plates, so that the splitting ratio was 1:4 with respect to culturing surface area. Passage one (P1) was always used unless otherwise indicated.

Usually 24 hr before running any experiment, the cells were washed twice with PBS, and the FGM was exchanged by low medium (LM). This step was referred to as starvation.

3.2.2. Culturing, maintenance and passaging of primary normal human ventricular cardiac fibroblasts (NHCF-V)

Handling of NHCF-V cells was according to the instructions of the supplier company, using the media and solutions supplied with the cells. To do so, the frozen components of the FGM-3Bullet kit (FCS, recombinant human insulin, recombinant human fibroblast growth factor, and gentamycin/amphotericin) were thawed on ice and combined with the supplied basal medium.

FGM-3Bullet medium was added first into the culture vessels as 1 ml/5 cm², and was allowed to equilibrate in the cell culture incubator for at least 30 min. After that, the cryovial of the NHCF-V cells was quickly thawed in a water bath set to 37°C, the cells were resuspended in the cryovial and dispensed into the equilibrated cell culture vessels.

The cells were passaged when they had already reached 70-80% confluency. FGM-3Bullet medium was added first into the culture vessels as 1 ml/5 cm², as was allowed to equilibrate in the cell culture incubator for at least 30 min. The medium on the cells was removed and the cells were washed two times with room temperature HEPES-buffered saline solution. After that, trypsin-EDTA was added only enough to cover the cell culture surface, and the cells were incubated at room temperature until most of the cells had already detached from the vessel. At this point, room temperature trypsin neutralizing solution (TNS) was added in a volume equivalent to two times that of the already added trypsin-EDTA. The cell suspension was collected and diluted with the appropriate volume of FGM-3Bullet medium, before the cells were seeded in new cell culture vessels.

3.2.3. Culturing, passaging and maintenance of HEK293A cells

The cryovials of HEK293A cells were thawed quickly in 37°C water bath, and were directly diluted with an appropriate volume of HEK293A growth medium. After that, the cells were seeded in 15 cm dishes, and the medium was exchanged every other day. When the cells were 70-80% confluent, they were passaged. To do so, the cells were washed twice with pre-warmed PBS, after that, they were incubated with pre-warmed 7ml 0.05% trypsin-EDTA until the cells started to round up and detach, at this point HEK293A growth medium was added, the cell suspension was collected in 50 ml reaction tube and diluted with the appropriate volume of HEK293A growth medium. The cell suspension was triturated well, and was then dispensed in new cell culture dishes and plates according to the desired splitting ratio.

In case of passaging HEK293A cells for transfection, a serial dilution from the cell suspension was performed and seeded in cell culture plates so that on the next day, the plates with the appropriate cell confluency could be used.

3.2.4. Live cell calcium imaging and time lapse analysis

Generally, experiments were performed in 12-well plates. The cells were initially incubated separately with 570 μ l medium containing the experimental conditions for 1 hr, unless otherwise indicated. After that, 60 μ l/well of the Ca^{2+} sensitive fluorescent dye solution was added, and the cells were incubated with the dye for 25-30 min in the climate chamber of the inverse fluorescence microscope (Olympus), where the conditions were adjusted to 37°C, 5% CO_2 , 57.37% lamp intensity and the exposure time to 290 millisecond. The 20x objective and the GFP filter were used to visualize the cells. Time-lapse recording was programmed as one frame every 5 sec for a duration of 5 min, with the first frame taken at 0 second. Ang II (100 nM) was added at the 20th second (after the first five frames), unless otherwise indicated. The change in fluorescence intensity for individual cells, which correlates to the change in cytoplasmic Ca^{2+} level, was analyzed with the help of Image J, using time series analyzer version 2 plug-in. For each experiment, several fields from different wells were analyzed with at least 70 cells per field. For all of the Ca^{2+} transient assays, the baseline fluorescence (first 5 frames

before the addition of Ang II) was subtracted from the graph to normalize the background fluorescence, unless otherwise indicated. The change in the maximal fluorescence intensity ($\Delta\text{RFU}_{\text{Max}}$) was used to compare the effect of different conditions on the intensity of the Ca^{2+} transient. The percentages of the Ca^{2+} oscillating cells and the cell with mitochondrial Ca^{2+} loading were determined by manual counting.

3.2.5. Fluorescence staining for cell microscopy

After cells were incubated overnight with the treatment conditions, the medium was aspirated and the cells were fixed with 4% paraformaldehyde (PFA) for 15 min at room temperature. After that, they were washed three times with PBS, and incubated for 5 min with 0.05% Triton solution to permeabilize the cellular membranes, this was followed by washing three times with PBS and incubation with 1x Roti-immunoblock for 1 hr at room temperature. Then, the cells were incubated with PBS containing the antibody against the protein(s) of interest (using the dilutions shown in table 7), DAPI to stain the nuclei, and when needed fluorophore-conjugated-phalloidin to stain actin and fluorophore-conjugated WGA to stain the cellular membranous structures including the Golgi apparatus (using the dilutions shown in table 10). The cells were incubated with this solution overnight at 4°C shuttle shaking and protected from light. On the next day, the cells were washed three times with PBS, and were incubated with the appropriate fluorophore-conjugated secondary antibodies (using the dilutions shown in table 9) for 1 hr at room temperature while shaking and protected from light. At the end, the cells were washed three times with PBS and were imaged by inverse fluorescence microscopy (Olympus).

3.2.6. Sirius red-based colorimetric microassay for collagen

The assay was performed using 12-well plates of confluent NRCF according to the protocol described by Tullberg-Reinert and Jundt [172]. Following cell treatment, the medium was removed and the cells were washed three times with PBS followed by 1 hr incubation at room temperature with Bouin's solution for fixation (1 ml/well). After that, Bouin's solution was removed and the plates were washed with running tap water for

15 min, followed by air drying. When the plates were completely dry, 1 ml/well of sirius stain solution was added and the cells were stained for 1 hr under mild shaking. After that, the dye was removed and the cells were washed extensively with 0.01 N HCl to remove the excess dye. Then, each well received 0.4 ml of 0.1 N NaOH, and the plate was placed on a shaker for 30 min at room temperature to dissolve the dye. Finally, the dissolved dye was transferred into a 96-well plate, and the absorbance was measured at 550 nm wave length against 0.1 N NaOH using FlexStation 3 plate reader.

3.2.7. Protein biochemical analysis

3.2.7.1. *Preparation of samples for immunoblotting*

Generally, NRCF were initially incubated with the inhibitor in question (according to the concentrations shown in table 16) or the corresponding control condition for 1 hr, before Ang II (100 nM) was added. After about 24 hr, the conditioned medium was collected and kept on ice, and ice-cold GST-fish lysis buffer was used to lyse the cells with the help of cell scrapers. Then, the scraped cells were centrifuged at 13000 g for 5 min to remove cell debris, and the supernatant was mixed as 1:4 with the 4x sample loading buffer without glycerol. Medium samples were mixed as 1:4 with the 4x sample loading buffer containing glycerol. After that, the samples were incubated at 95°C for 5 min on a heating block, then on ice for few minutes, and finally they were centrifuged briefly and kept cooled until use.

In case of checking protein phosphorylation, the cell lysates were quickly collected 5 min after Ang II treatment, using 1x SDS sample loading buffer containing glycerol, because SDS instantly denature proteins, thus blocking the activity of phosphatases. Since the 1x SDS sample loading buffer can also disrupt the nuclear envelope resulting in the release of DNA, which makes the samples very viscous, the samples were exposed to three cycles of sonication on ice each lasted for 15 sec, with the output knob adjusted to 4. After that, the samples were incubated at 95°C for 5 min on a heating block, then on ice for few minutes, and finally they were centrifuged briefly and kept cooled until use.

3.2.7.2. Protein separation, by sodium dodecyl sulfate polyacrylamide gel electrophoresis (SDS-PAGE), and blotting

Protein samples mixed with loading buffer were loaded on 15% or 12% SDS-polyacrylamide gels (table 15), depending on the molecular weight of the investigated proteins. The electrophoresis was performed with 200 volts for 70 min. After that, the proteins were blotted onto nitrocellulose membranes for 1 hr under cooled conditions with 100 volts. Then, the nitrocellulose membranes were incubated for 5 min in Ponceau S stain at room temperature to stain the proteins on the membrane and to visualize the protein marker. The excess dye was washed off several times with distilled water, and when necessary the membranes were cut according to the protein marker to allow the incubation with different primary antibodies. The membranes were destained by washing several times with TBS-T, followed by incubation with 1x Roti-block for 1 hr at room temperature. After that, they were washed three times with TBS-T, each for 5 min followed by overnight incubation with the appropriate primary antibodies (diluted with TBS-T as shown in table 7) at 4°C with shaking. On the next day, the membranes were washed three times with TBS-T each for 5 min, and then, they were incubated with the appropriate HRP-conjugated secondary antibodies (diluted with TBS-T as shown in table 8) for 1 hr, at room temperature with shaking. After that, the membranes were washed three times with TBS-T, each for 5 min, and at the end the protein antibody complexes were visualized by Versa doc MP chemiluminescence detection system using lumi-light western blotting substrate kit or super signal west femto maximum sensitivity substrate kit.

3.2.7.3. Exchanging antibodies from nitrocellulose membranes

In the first step, the existing antibodies were stripped from the nitrocellulose membranes. To do so, the membranes were incubated with the stripping buffer for exactly 30 min at 50°C with shaking. After that, the membranes were washed 6 times with TBS-T buffer each for 10 min at room temperature. Then, the membranes were incubated with a blocking solution and the proteins were labelled with the primary and secondary as described before.

3.2.8. Molecular biology

3.2.8.1. Determination of relative change in gene expression

3.2.8.1.1. RNA isolation

The experiments were performed using confluent 10 cm dishes of NRCF. Following treatment course, the cells were washed once with PBS, and were incubated afterwards with 0.05 % trypsin-EDTA (2.5 ml/plate) for 3-4 min until most were detached. At this point, 12 ml FGM was added and the cell suspension was collected and centrifuged at 300 g for 5 min at 4°C. The supernatant was removed completely, and the total RNA was extracted from the cell pellet using RNeasy kit according to the manufacturer's instructions. Following RNA extraction, the RNA concentration was determined using Nanodrop 1000 device.

3.2.8.1.2. RNA analysis by formaldehyde (FA) agarose gel-electrophoresis

RNA analysis was performed according to the protocol described in the RNeasy kit manufacturer's instructions. First, 1.2% FA agarose gel was prepared as described in section 2.1.7. After the gel had already condensed, it was incubated for at least 30 min in a horizontal system for submerged gel electrophoresis containing 1x FA gel running buffer, to equilibrate before sample loading. RNA samples were diluted with RNase-free water and were mixed with 5x RNA loading dye. Usually between 0.5 to 2.5 µg RNA was used from each sample. After that, the RNA samples were incubated for 5 min at 65°C for 5 min, then, chilled on ice, centrifuged briefly and loaded onto the equilibrated 1.2% FA agarose gel. The electrophoresis was performed at 7 volts/cm for 25-30 min. Finally, the RNA bands were imaged with the help of Gel doc XR device. The detection of two sharp bands, which reflects the ribosomal RNAs, was considered as an indication of a good RNA integrity.

3.2.8.1.3. RNA reverse transcription into cDNA

Every time, 1000 ng RNA was used from each sample to produce cDNA using Revert Aid First Strand cDNA Synthese Kit according to the manufacturer's instructions.

3.2.8.1.4. Quantitative polymerase chain reaction (qPCR)

The qPCR was performed using 5x HOT FIREPOL EvaGreen qPCR Mix Plus kit, according to the instructions of the manufacturer. The cDNA samples were diluted as 1:20, and the primers for each gene were diluted to 10 μ M. A master mix for each target gene was prepared by scaling up the recipe shown in table 19 according to the number of samples. For each sample four replicates were performed.

| Component | Volume (μ l) |
|---------------------------------------|-------------------|
| Forward primer (10 μ M) | 1 |
| Reverse primer (10 μ M) | 1 |
| 5x HOT FIREPOL EvaGreen qPCR Mix Plus | 4 |
| Water | 13 |

Tables 19: Mix for a single replicate

The experiment was performed in a Micro-Amp optical reaction 384-well plate, where first 1 μ l of the diluted cDNA was added per well, followed by the addition of 19 μ l of the corresponding master mix. After loading the samples on the plate, it was sealed with Micro-Amp optical adhesive film and centrifuged for 5 min at 700 g. Finally the reaction was performed using TaqMan 7900HT Fast Real-Time-PCR System, according to the program shown in table 20.

| Stage | Cycle | Temperature | Time | Repetition | Ramp rate |
|-------|----------------------|-------------------------|--------|------------|-----------|
| I | Initial denaturation | 95°C | 15 min | 1 time | 1.6°C/sec |
| II | Denaturation | 95°C | 15 sec | 40 times | |
| | Annealing | Specified for each gene | 20 sec | | |
| | Elongation | 72°C | 45 sec | | |
| III | Dissociation curve | 95°C | 15 sec | 1 time | |

| | | | | | |
|--|--|------|--------|--|--|
| | | 60°C | 15 sec | | |
| | | 95°C | 15 sec | | |

Table 20: General qPCR program

3.2.8.2. RT-PCR for verification of gene expression

To check whether a certain gene is expressed in NRCF, cDNA was first synthesized from RNA, followed by a PCR step according to the reaction mixture shown in table 21, where the cDNA was used as a template.

| Component | Volume (μ l) |
|-----------------------------|-------------------|
| Forward primer (10 μ M) | 1 |
| Reverse primer (10 μ M) | 1 |
| GoTaq green master mix | 12.5 |
| cDNA | 1 |
| Water | 9.5 |

Table 21: Reaction mixture for the PCR step

The reaction was performed using Mastercycler gradient device according to the program shown in table 22.

| Cycle | Temperature (°C) | Time | Repetition |
|----------------------|-------------------------|--------|------------|
| Initial denaturation | 94 | 2 min | 1 time |
| Denaturation | 94 | 10 sec | 45 times |
| Annealing | Specified for each gene | 5 sec | |
| Elongation | 72 | 85 sec | |
| Final elongation | 72 | 10 min | 1 time |

Table 22: General program for the PCR step

After that, the PCR product was separated by DNA-agarose gel electrophoresis, and the band of the representative DNA fragment was visualized by Gel doc XR device.

3.2.8.3. Construction of an adenovirus for overexpression of tetracycline (TC) tagged CTGF

3.2.8.3.1. Restriction digestion

The conditions and the composition of the reaction mixture for the restriction digestion were according to the manufacturer's instructions, provided with each restriction enzyme.

3.2.8.3.2. DNA agarose gel electrophoresis

DNA samples were pre-mixed with a suitable volume of 6x DNA loading buffer. After that, they were loaded on a DNA agarose gel. The electrophoresis was performed at 7 volts/cm for 15-35 min, depending on the expected size of DNA band. After that, DNA bands were imaged with the help of Gel doc XR device.

3.2.8.3.3. Purification of DNA from agarose gel

After performing DNA agarose gel electrophoresis for PCR products or restriction digests, the regions of the agarose gel containing the DNA bands were excised under UV light using a sharp scalpel. After that, the DNA was extracted using High pure PCR product purification kit according to the manufacturer's instructions.

3.2.8.3.4. Amplification of CTGF gene from cDNA by PCR

As a starting point, cDNA prepared by reverse transcription of total NRCF RNA, was used as a template for CTGF gene amplification, using PrimeSTAR HS DNA polymerase kit. The reaction mixture was prepared according to table 23, and the PCR was performed according to the program shown in table 24.

| Reagent | Volume |
|---------------------------------------------|-----------------------------|
| cDNA | 2 μ l |
| 5x PrimeSTAR buffer (Mg ²⁺ plus) | 10 μ l |
| Forward primer (10 μ M) | 1 μ l |
| Reverse primer (10 μ M) | 1 μ l |
| dNTP mixture (2.5 mM each) | 4 μ l |
| PrimStar HS Polymerase | 0.5 μ l |
| Water | 31.5 μ l |
| Final volume | 50 μl |

Table 23: Reaction mixture for CTGF gene amplification from cDNA

| Cycle | Temperature ($^{\circ}$ C) | Time | Repetition |
|--------------|-----------------------------|--------|------------|
| Denaturation | 95 | 10 sec | 30 times |
| Annealing | 55 | 5 sec | |
| Elongation | 72 | 85 sec | |

Table 24: PCR program for CTGF gene amplification from cDNA

3.2.8.3.5. Addition of *KpnI* and *XhoI* restriction sites to CTGF gene by PCR

After amplification of the CTGF fragment, it was purified as mentioned before, and was further amplified using primers with overhangs, which can add *KpnI* and *XhoI* restriction sites at the 5' and 3' ends of the gene, respectively. The reaction mixture was prepared according to table 25, and by using the program shown in table 26.

| Reagent | Volume |
|--------------------------------------------|-----------------------------|
| CTGF fragment (109 ng/ μ l) | 1 μ l |
| 5x PrimSTAR buffer (Mg ²⁺ plus) | 10 μ l |
| Forward primer (10 μ M) | 1 μ l |
| Reverse primer (10 μ M) | 1 μ l |
| dNTP mixture (2.5 mM each) | 4 μ l |
| PrimStar HS Polymerase | 0.5 μ l |
| Water | 32.5 μ l |
| Final volume | 50 μl |

Table 25: PCR reaction mixture for the addition of restriction sites to the ends of CTGF gene by PCR

| Cycle | Temperature (°C) | Time | Repetition |
|--------------|------------------|--------|------------|
| Denaturation | 95 | 10 sec | 30 times |
| Annealing | 55 | 5 sec | |
| Elongation | 72 | 70 sec | |

Table 26: PCR program for the addition of restriction sites to the ends of CTGF gene

3.2.8.3.6. Hybridization of TC-tag oligonucleotides

The TC-tag was provided as separate sense and antisense DNA oligonucleotides. The lyophilized powder of each oligonucleotide strand was reconstituted in water to achieve a concentration of 1 pmol/ μ l. Equal number of moles from each oligonucleotide was used in the hybridization reaction as shown in table 27. The hybridization mixture was incubated at 95°C for 30 min, and then, it was left to cool down slowly overnight to room temperature.

| Reagent | Volume |
|---------------------------|-----------------------------|
| Sense oligonucleotide | 16.25 μ l (16.25 pmol) |
| Antisense oligonucleotide | 16.25 μ l (16.25 pmol) |
| NEB Buffer 1 | 5 μ l |
| Water | 12.5 μ l |
| Final volume | 50 μl |

Table 27: Hybridization reaction for TC-tag oligonucleotides

3.2.8.3.7. DNA ligation

Quick ligation kit was used to perform different kinds of ligation reactions, according to the manufacturer's instruction. For cohesive end ligation 3:1 molar excess of the insert was used, whereas for linker ligation 20:1 molar excess of the linker was used. As a negative control, equal volume of water was used instead of the insert. The ligation reaction mixture was incubated for 1 hr at room temperature, after that, it was directly used to transform DH10 bacteria by heat shock protocol.

3.2.8.3.8. *Transformation of DH10B bacteria by heat shock protocol*

Initially DH10B bacteria were thawed on ice for 30 min. After that, 25 ng of the transforming DNA was mixed well with 50 µl of the bacteria in pre-cooled tubes, and the tubes were incubated on ice for 30 min. Then, the tubes were incubated in a 42°C water bath for exactly 90 sec, after which they were rapidly transferred into an ice bath, where they were incubated for 2 min. In the next step, 800 µl of SOC medium was added to each tube, warmed to 37°C in a water bath, and then, transferred to a shaking incubator set to 37°C. The Bacteria were incubated for 45 min whilst continuous shaking. After that, under sterile conditions 200 µl of the bacterial culture was transferred to each 10 cm LB agar plate supplied with the appropriate antibiotic. The bacterial suspension was distributed evenly throughout the plate, and was left until the liquid was absorbed. Finally, the plates were transferred in an inverted position to a 37°C incubator. On the next day, the colonies of bacteria that grew on the plates were picked up under sterile conditions and each colony was used to inoculate LB medium containing the proper antibiotic.

3.2.8.3.9. *Transformation of AdEasier cells by Inoue protocol*

A starter culture was made by adding 10 µl AdEasier cell stock to 5 ml of LB medium (containing 50 µg/ml carbenicillin), and was placed in a shaking incubator at 37°C for 8 hr. After that, an overnight culture was prepared by adding the starter culture to 120 ml SOB medium (containing 50 µg/ml carbenicillin). The culture was placed in a shaking incubator at 18-22°C overnight and until the optical density at a wave length of 600 nm (OD₆₀₀) was between 0.45-0.50. At this point, the bacterial suspension was centrifuged for 10 min at 4°C and 2500 g, and the supernatant was poured off completely. Then, the bacterial pellet was resuspended in 8 ml of ice-cold Inoue buffer, and was centrifuged for 10 min at 4°C and 2500 g. Next, the supernatant was poured off completely, the bacterial pellet was resuspended in 2 ml of fresh ice-cold Inoue buffer, and the cells were immediately transformed with the vector of interest by heat shock method as described above.

3.2.8.3.10. *Isopropanol precipitation of DNA*

DNA solution was mixed with 0.1 volume of 3 M sodium acetate solution (pH 5.2) and 0.7 volume of room temperature isopropanol, and incubated overnight at 80°C. The next day, the solution was centrifuged at 15000 g for 30 min at 4°C, and the supernatant was poured off. In the next step, 500 µl of ice-cold 70% ethanol was added, and the solution was centrifuged at 15,000 g for 30 min at 4°C. The supernatant was poured off, the pellet was air dried completely, and finally it was reconstituted with 50 µl sterile distilled water.

3.2.8.3.11. *Transfection of HEK293A cells by recombinant adenovirus plasmid*

One day before transfection, HEK293A cells were seeded in 6 cm dishes with a density allowing to have 70% confluent cells the next day. After that, 4 µg of the linearized plasmid was used to transfect the cells using PolyFect reagent according to the manufacturer's instruction. The transfected cells were maintained in the incubator for 20 days, during which 0.5 ml of HEK293A low serum medium was added every 3rd day.

3.2.8.3.12. *Amplification of recombinant adenovirus by HEK293A cells*

After 20 days of transfection, the HEK293A cells were collected by scraping them off in the presence of the medium, and were thereafter exposed to three cycles of freezing and thawing using liquid nitrogen, followed by vigorous vortexing to disrupt the cells in order to release the virus particles. After that, the resulting suspension was centrifuged at 700 g for 5 min at room temperature to pellet the debris, and the supernatant was mixed with fresh HEK293A low serum medium, which was used to infect 70% confluent HEK293A cells cultured in 10 cm dish. When the cells started to detach (after about three days), they were collected and processed following the same steps mentioned above, and the obtained supernatant was used to infect 2x 15 cm dishes of HEK293A to start a new round of infection. In the next round, the supernatant of virus was used to infect 5x 15 cm dishes of HEK293A cells, and the supernatant obtained from these cells was used in the last round to infect 20x 15 cm dishes of HEK293A cells. At this point, when the cells start to round and slightly detach, they were flushed off the plate by their own medium, collected in 50 ml reaction tubes, centrifuged at 150 g for 10 min at room

temperature. Next, the pellet was resuspended in 50 ml PBS, centrifuged at 150 g for 10 min at room temperature. The supernatant was aspirated and the pellet was resuspended in 10 ml PBS. After that, the cell suspension was exposed to three cycles of freezing and thawing, followed by centrifugation at 700 g for 5 min at room temperature to pellet the cell debris.

3.2.8.3.13. *Purification of recombinant adenovirus*

In a 17 ml ultracentrifugation tube, 5 ml of light CsCl was added followed by the administration of 5 ml of heavy CsCl underneath the light CsCl, and the interphase was marked. After that, 5 ml of virus supernatant was added on top and the tubes were filled completely with PBS. Next, ultracentrifugation was performed using L8-70M device under vacuum, at 22000 g, 8°C for 24 hr. After that, the virus ring was aspirated through the wall of the tube by a syringe. Then, the virus was purified by overnight dialysis: two times against 2000 ml PBS and one time against 2000 ml 1x virus storage buffer (VSB). Finally, the virus was stored in 45% glycerol in 1x VSB at -20°C.

3.2.8.3.14. *Cloning strategy*

Insertion of the TC tag in pcDNA3.1/Zeo(+) 5.0 kb vector

First, the pcDNA3.1/Zeo 5.0 kb expression vector was linearized using KpnI and AflIII restriction enzymes, and the linearized vector was purified as explained before. After that, the TC-tag oligonucleotide, which has AflIII and KpnI overhang, was ligated with the linearized vector, creating a TC-pcDNA3.1/zeo(+) vector. Next, DH10B bacteria were directly transformed with this vector using heat shock method, and minipreps were performed for the resulting bacterial colonies, using Exprep plasmid SV mini kit according to the manufacturer's instructions. The positive colonies were determined by checking the yielded pcDNA with SmaI restriction enzyme, since the corresponding restriction site exists exclusively in the TC-tag. After that, midpreps were performed for

the positive colonies to get enough yield of the vector, using Exprep plasmid SV midi kit according to the manufacturer's instructions.

Insertion of CTGF gene downstream the TC-tag in the expression vector

The CTGF PCR fragment with added restriction sites was processed with KpnI and XhoI restriction enzymes to create sticky ends. In parallel, the TC-pcDNA3.1/zeo(+) vector was linearized by the same restriction enzymes. Both CTGF gene and the linearized vector were isolated and purified as explained before. After that, the CTGF fragment was ligated downstream the TC-tag, creating TC-CTGF-pcDNA3.1/zeo(+) vector, which was used directly to transform DH10B bacteria by the heat shock method. Minipreps were performed for the resulting bacterial colonies, and the positive colonies were determined by checking the yielded pcDNA by KpnI, XhoI and PstI restriction enzymes (PstI can cut within two regions of CTGF gene). The presence of mutation was ruled out by sequencing the pcDNA of positive clones by SeqLab Company. Tsa201 cells were transfected with this construct using PolyFect reagent to validate the expression of TC-CTGF fusion protein.

Insertion of TC-CTGF-pcDNA3.1/zeo(+) vector in pShuttle-CMV vector

TC-CTGF-pcDNA3.1/zeo(+) and pShuttle-CMV vectors were digested by PmeI and EcoRV restriction enzymes, respectively, to create blunt ends. After that, they were purified and ligated together as explained before creating TC-CTGF-pShuttle-CMV vector. Using heat shock method, DH10B bacteria were transformed by the resulting construct, followed by miniprep. Colonies having the correct orientation of ligation were identified by restriction digest using XhoI.

Transformation of AdEasier cells with TC-CTGF-pShuttle-CMV vector to create adenovirus backbone for the expression of TC-CTGF

TC-CTGF-pShuttle-CMV vector was linearized with PmeI restriction enzyme, and after that, it was purified as explained before. Next AdEasier cells were transformed by the linearized vector using Inoue protocol as described before, and miniprep was performed for the obtained colonies. Positive clones, which contain the TC-CTGF-pShuttle-CMV-pAdEasy-1 (TC-CTGF-AdEasy-1) were determined by restriction digestion using PaeI enzyme.

Transfection of HEK293A cells with TC-CTGF-AdEasy-1, and the production of high-titer recombinant adenovirus

First the TC-CTGF-AdEasy-1 vector was linearized using PaeI restriction enzyme. After that, the linearized vector was purified by isopropanol precipitation, and then it was used to transfect HEK293A cells. The cell lysate from these cells was used in repeated infection cycles, as described before, to infect increasing numbers of HEK293A cells. Finally, the recombinant adenovirus was isolated and purified as described before.

3.2.9. Statistical analysis

The data are shown as means \pm standard error means (SEM). To test the differences between groups, one-way analysis of variance (ANOVA) test was performed. To further compare two groups, where the data in the same row are matched, paired student's t-test was used, and otherwise unpaired student's t-test was used. *p*-values less than or equal to 0.05 were considered statistically significant.

4. Results

4.1. Role of Ca²⁺ in the regulation of CTGF

4.1.1. Characterization of Ang II-induced Ca²⁺ transient in CF

4.1.1.1. *Ang II induces Ca²⁺ transient in both NRCF and NHCF-V*

First, the ability of NRCF to induce a Ca²⁺ transient in response to Ang II was investigated. To do so, NRCF were loaded with Fluo-8 Ca²⁺ sensitive fluorescent dye. While recording time lapse as one frame every 5 sec, 100 nM Ang II was applied at the 20th sec, resulting in a sharp increase in the fluorescence intensity that could be detected in the subsequent frame (at 25th sec), which declined gradually until close to baseline level. This transient change in fluorescence intensity reflects a transient increase in the cytoplasmic Ca²⁺ concentration (Fig. 5A). The fluorescence intensity was measured by the arbitrary relative fluorescence unit (RFU) (Fig. 5B). In the next step, a concentration-response curve was performed using 4 different concentrations of Ang II (1, 10, 100 and 1000 nM). For each Ang II concentration, the means \pm SEM of Δ RFU_{Max} (maximal fluorescence – basal fluorescence) was used to calculate a concentration-response curve. The calculated EC₅₀ was 1.7 nM, and it was found that 100 nM Ang II was required to achieve a maximal response (Fig. 5C). In addition, the ability of normal human ventricular CF (NHCF-V) to generate a similar Ca²⁺ transient in response to Ang II was validated (Fig. 5D). In addition, Ang II was able to induce a concentration-dependent change in fluorescence intensities in NHCF-V, preliminary data (Fig. 5E).

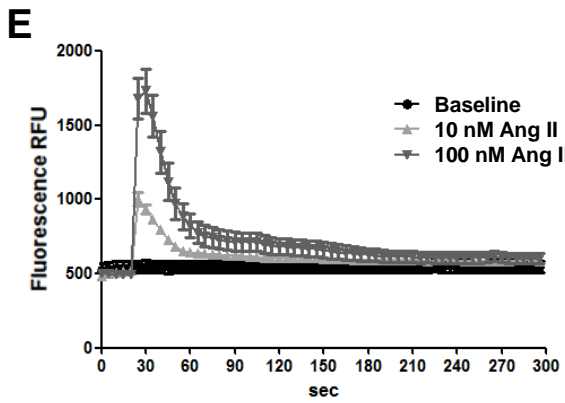
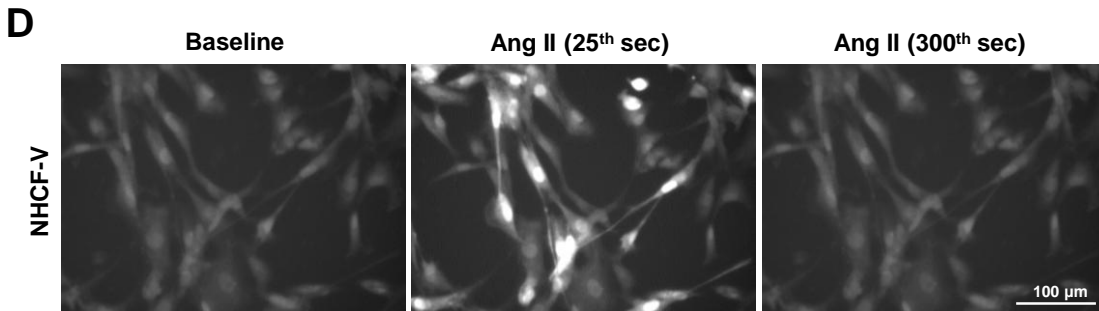
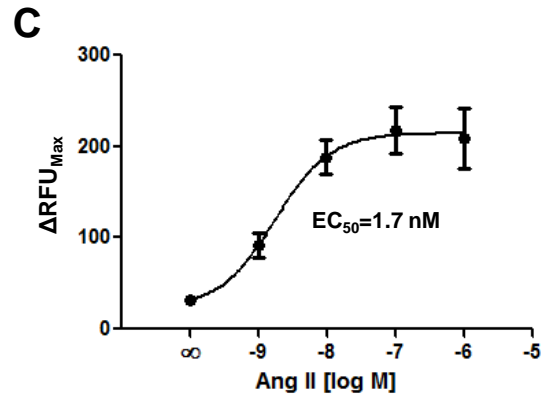
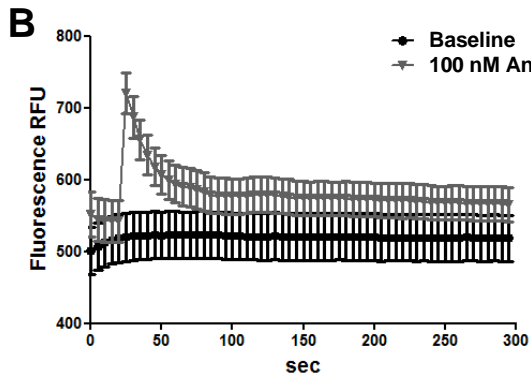
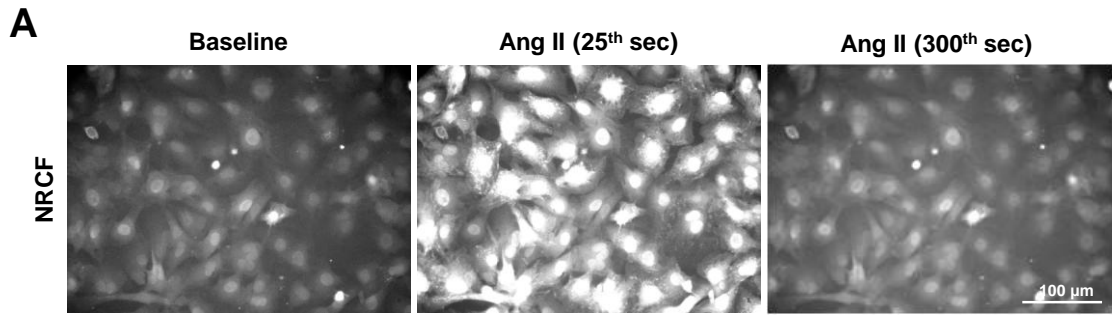


Figure 5: Induction of Ca²⁺ transients in NRCF and NHCF-V by different concentrations of Ang II

NRCF and NHCF-V were loaded with the Ca²⁺ dye, then time lapse was recorded where Ang II was added at the 20th sec. A) Representative images for NRCF taken at 0 sec (baseline), after Ang II (100 nM) application at the 25th sec, and at the end of the time lapse at 300th sec B) The graph shows the analysis of the fluorescence, for control and 100 nM Ang II-treated NRCF, over the time course of the experiment (n=4, for each n at least 3 wells/condition, 40-60 cells/well, means ± SEM). C) Ca²⁺ transients were analyzed in NRCF in the presence of 0, 1, 10, 100 and 1000 nM Ang II. The means ± SEM for ΔRFU_{Max} from each Ang II concentration was used for the concentration-response curve, where the calculated EC₅₀ was 1.7 nM (n=3, for each n at least 3 wells/condition, 40-60 cells/well, means ± SEM). D) Representative images for NHCF-V taken at 0 sec (baseline), after Ang II application at the 25th sec, and at the end of the time lapse at 300th sec E) The graph shows the analysis of the fluorescence for NHCF-V treated with two different concentrations of Ang II, as well as for a baseline (n=1, at least 3 wells for each condition, 30-50 cells/well, means ± SEM, preliminary data).

4.1.1.2. Ca²⁺ handling in NRCF is independent of the differentiation state

To investigate whether the differentiation state of NRCF can influence the handling of Ca²⁺, the Ang II-induced Ca²⁺ transient (Ang II-CaT) was compared between passage 0 (P0) and passage 1 (P1) NRCF. It was found that the basal fluorescence (basal Ca²⁺ level), the maximal fluorescence (peak level of Ca²⁺) and the area under the curve (AUC) (total Ca²⁺ mobilization) were all equal (Fig. 6).

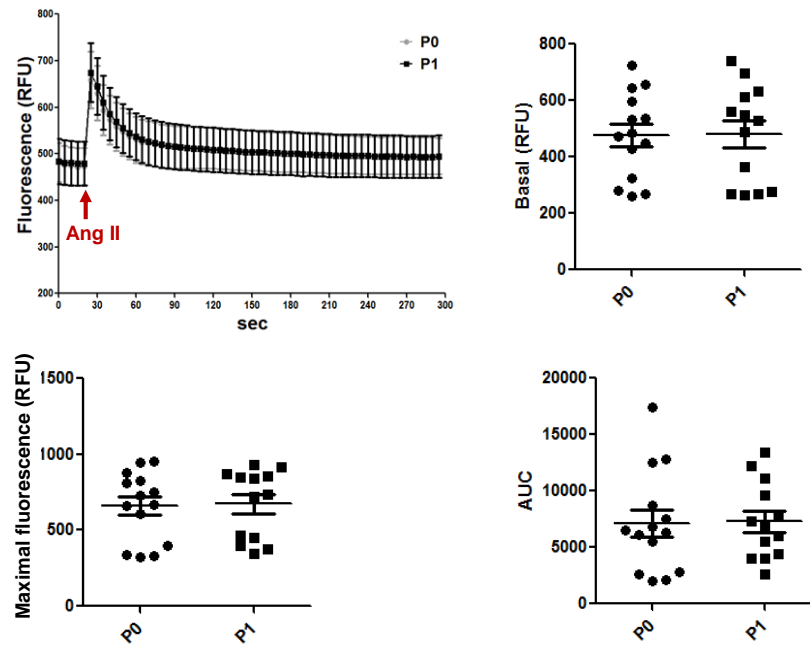


Figure 6: Comparison of the Ang II-CaT in P0 and P1 NRCF

The Ang II-CaT was investigated in P0 and P1 NRCF, in the presence of 100 nM Ang II. The upper left graph demonstrates the trace of the detected fluorescence over 300 sec. The analysis of this graph is shown in the accompanying scatter plots. Upper right scatter plot illustrates the basal fluorescence level in P0 and P1 cells. Lower left scatter plot illustrates the maximal fluorescence intensity. Lower right scatter plot illustrates the area under the curve (AUC) ($n=13$, for each n at least 3 wells/condition, 40-60 cells/well, means \pm SEM).

4.1.1.3. *AT1* receptor -PLC- β signaling cascade mediates the Ang II-CaT

In order to verify that the observed Ca^{2+} transient in response to Ang II is mediated through the AT1 receptor-PLC- β canonical pathway, the Ang II-CaT was studied in NRCF treated with valsartan, which is a clinically used selective AT1 receptor blocker, or with the PLC- β inhibitor U73122 (122). U73343 (343) was used as a negative control for 122. Both treatments significantly reduced the $\Delta\text{RFU}_{\text{Max}}$ (Fig. 7A and B). To further determine whether the components of the signaling cascade are located in the caveolae, NRCF were treated with methyl- β -cyclodextrin (CDX), which disrupts caveolae by

cholesterol depletion, before the Ang II-CaT was measured. This resulted in a significant reduction in the ΔRFU_{Max} (Fig. 7C). The disruption of the caveolae was confirmed by immunofluorescence (IF) analysis of caveolin-1 (Fig. 7D).

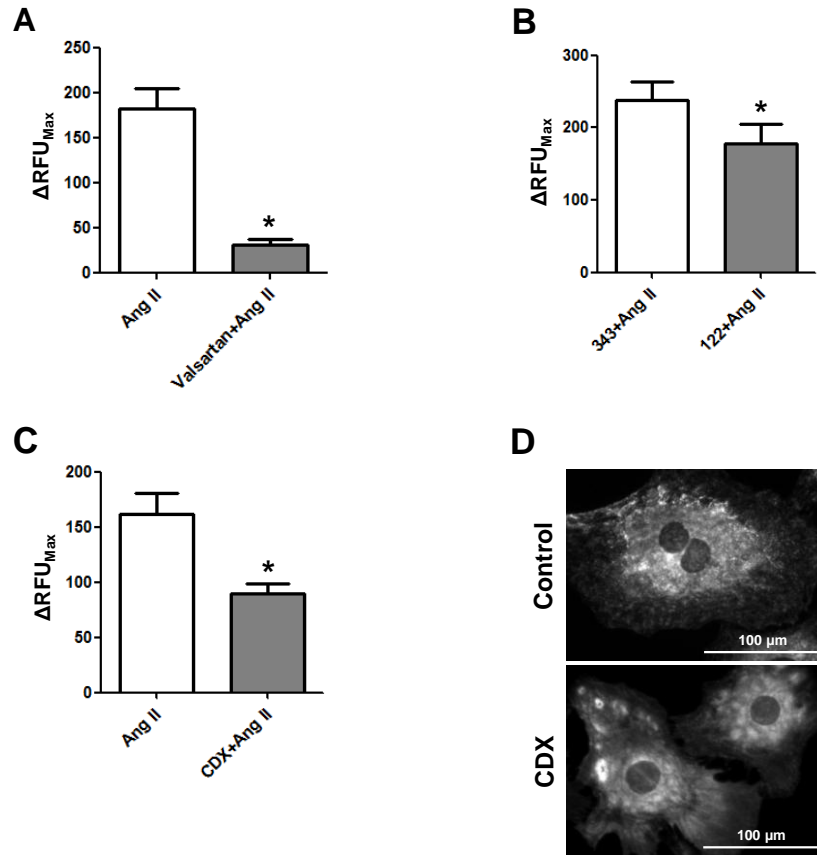


Figure 7: Signaling cascade underlying the Ang II-CaT

NRCF were treated with the inhibitors or the corresponding control conditions for 1 hr, before the Ang II-CaT was investigated. A) Effect of AT1 receptor blockade by 15 nM valsartan on the ΔRFU_{Max} ($n=7$, for each n at least 3 wells/condition, 40-60 cells/well, means \pm SEM, $*p \leq 0.05$) B) Effect of PLC- β inhibition by 1.5 μM 122 on the ΔRFU_{Max} as compared to 1.5 μM of the negative control 343 ($n=5$, for each n at least 3 wells/condition, 40-60 cells/well, means \pm SEM, $*p \leq 0.05$) C) Effect of caveolae disruption by 2.5 mM CDX on the ΔRFU_{Max} ($n=5$, for each n at least 3 wells/condition, 40-60 cells/well, means \pm SEM, $*p \leq 0.05$) D) IF microscopy for caveolin-1 showing the disruption of caveolae by CDX.

4.1.1.4. Intracellular Ca^{2+} stores are the major sources for the Ang II-CaT

In order to investigate the involvement of the intracellular Ca^{2+} stores and the extracellular Ca^{2+} in the Ang II-CaT, the normal cell culture medium was replaced by Ca^{2+} -free Tyrode's solution during the recording of the time lapse, then Ang II was added in the absence of extracellular Ca^{2+} and the impact on the Ca^{2+} transient was studied. Finally, the extracellular Ca^{2+} level was restored. As shown in Fig. 8A, a first increase in cytoplasmic Ca^{2+} level was observed in response to the depletion of the extracellular Ca^{2+} , then a second Ca^{2+} transient was induced in response to Ang II treatment, and finally a third Ca^{2+} transient was induced upon restoring the extracellular Ca^{2+} level. To further validate this finding, an experiment was performed, where first the cell culture medium was exchanged to Ca^{2+} -free Tyrode's solution, followed by restoration of the original extracellular Ca^{2+} level, and finally, the Ang II treatment was applied in the presence of extracellular Ca^{2+} . Comparably, a first Ca^{2+} transient was induced in response to the depletion of the extracellular Ca^{2+} , then a second Ca^{2+} transient occurred upon restoring the original extracellular Ca^{2+} level. Finally, Ang II treatment induced a Ca^{2+} transient. The amplitude of the transient was comparable to that observed in the absence of extracellular Ca^{2+} (Fig. 8B). As this data argued for a more prominent role for the intracellular Ca^{2+} stores in the Ca^{2+} transient, the effect of the intracellular Ca^{2+} store depletion by thapsigargin (TGN) was studied. As shown in Fig. 8C, the $\Delta\text{RFU}_{\text{Max}}$ was significantly reduced in TGN-treated NRCF. This pointed to a role for the inositol-triphosphate receptors (IP3Rs), therefore, the expression of these receptors by NRCF was checked by RT-PCR, which confirmed that all of the three isoforms of the IP3Rs could be detected (Fig. 8D). Next, the effect of IP3Rs blockade by xestospongin C (XeC) was investigated, which showed a significant reduction in the $\Delta\text{RFU}_{\text{Max}}$ (Fig. 8E).

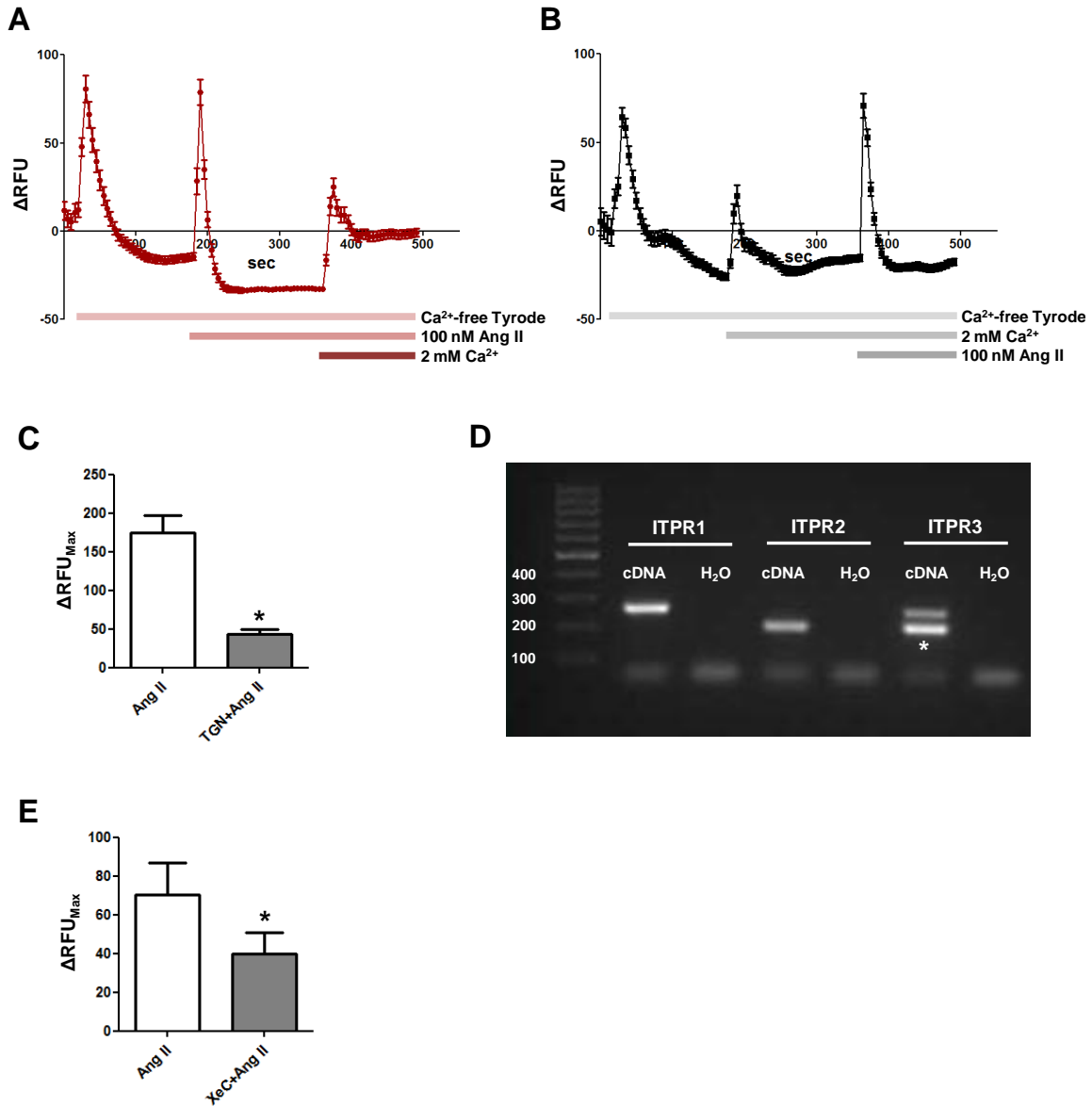


Figure 8: Contribution of the intracellular Ca^{2+} stores to the Ang II-CaT

A) The graphs show the background-subtracted fluorescence intensity (ΔRFU) over time. The cell culture medium was quickly replaced by Ca^{2+} -free Tyrode's solution at the 20th sec. After that, 100 nM Ang II was added at the 180th sec. Finally, Ca^{2+} solution was added at the 360th sec to restore the original extracellular Ca^{2+} level (2 mM) ($n=2$, for each n at least 3 wells/condition, 40-60 cells/well, means \pm SEM). B) The graphs show the ΔRFU over time. The cell culture medium was replaced by Ca^{2+} -free Tyrode's solution at the 20th sec. After that, Ca^{2+} was added at the 180th sec to restore the original extracellular Ca^{2+} level (2 mM). Finally, 100 nM Ang II was added at the 360th sec ($n=2$,

for each n at least 3 wells/condition, 40-60 cells/well, means \pm SEM). C) Effect of pre-depletion of intracellular Ca^{2+} stores by 3 μ M TGN on the ΔRFU_{Max} ($n=4$, for each n at least 3 wells/condition, 40-60 cells/well, means \pm SEM, $*p \leq 0.05$). D) DNA-agarose gel electrophoresis for the products of the RT-PCR showing the expression of IP3R1, IP3R2 and IP3R3. The calculated length of the amplified DNA fragments is 259, 197 and 252 base pairs, respectively. * is an unspecific band. E) Effect of IP3Rs blockade by 100 μ M XeC on the ΔRFU_{Max} ($n=3$, for each n at least 3 wells/condition, 40-60 cells/well, means \pm SEM, $*p \leq 0.05$).

4.1.1.5. Blockade of TRPC3 channels enhances the ΔRFU_{Max} of the Ang II-CaT

To further investigate the impact of different Ca^{2+} sources on the regulation of the Ang II-CaT, the effect of TRPC3 channels blockade by Pyr3 was investigated, which showed that the basal fluorescence intensity was reduced in Pyr3-treated NRCF compared to the control, but the maximal fluorescence was equal in both groups. This led to an increase in the ΔRFU_{Max} (Fig. 9A). The expression of TRPC3 channels by NRCF was confirmed by RT-PCR (Fig. 9B).

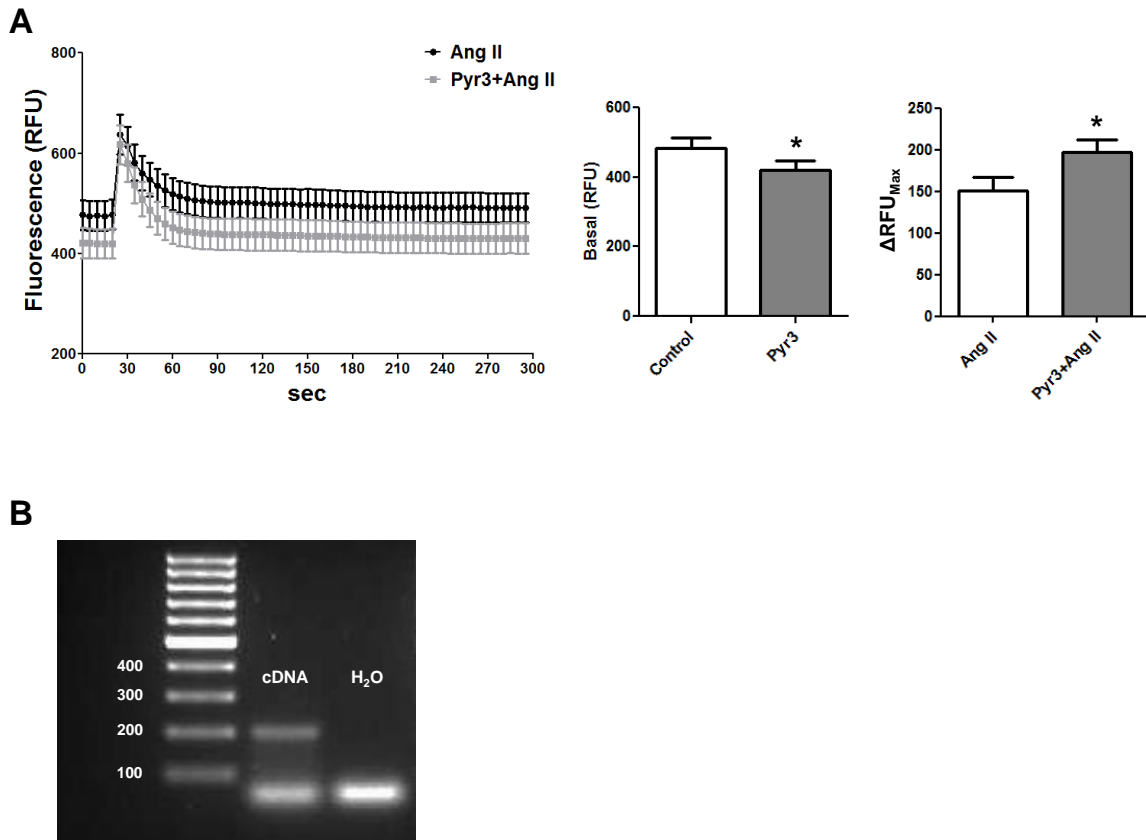


Figure 9: Contribution of TRPC3 channels to the Ang II-CaT in NRCF

A) The cells were treated with 3 μ M Pyr3 for 1 hr before the Ang II-CaT was investigated. The graph shows the traces for the detected absolute fluorescence intensity in response to 100 nM Ang II in the presence and absence of Pyr3. The analysis of this graph is shown in the accompanying column graphs. The middle graph illustrates the basal level of absolute fluorescence intensity. The right graph shows the Δ RFU_{max} ($n=7$, for each n at least 3 wells/condition, 40-60 cells/well, means \pm SEM, * $p \leq 0.05$). B) DNA-agarose gel electrophoresis for the products of the RT-PCR for TRPC3 channel expression. The calculated length of the amplified DNA fragment is 198 base pairs.

4.1.1.6. *TRPC3 channels and the intracellular Ca²⁺ stores play a role in the regulation of the Ang II-induced-Ca²⁺ oscillation*

Besides the induction of a Ca²⁺ transient by Ang II, spontaneous Ca²⁺ oscillation could be detected in NRCF (Fig. 10A). This phenomenon was evaluated by analyzing the percentages of the oscillating to the non-oscillating P0 and P1 cells, in the presence and absence of Ang II, which showed that following Ang II treatment, the proportion of Ca²⁺ oscillating cells was significantly increased, independent of the passage (Fig. 10B). However, this effect could not be prevented by valsartan (Fig. 10C). To study the sensitivity of the NRCF towards Ang II, the effect of 1 nM and 100 nM Ang II was compared. Interestingly, the submaximal concentration of 1 nM Ang II was sufficient to induce a maximal oscillation (Fig. 10D). After that, the contribution of the intracellular Ca²⁺ stores to the Ang II-induced Ca²⁺ oscillation was investigated by using TGN. As a result, the Ca²⁺ oscillation was completely inhibited (Fig. 10E). To investigate whether the TRPC3 channels are also involved in the regulation of Ca²⁺ oscillation, the influence of Pyr3 treatment was analyzed. Similar to TGN, treatment with Pyr3 significantly inhibit the effect of Ang II on Ca²⁺ oscillation (Fig. 10F). Finally, in a first experiment, it could be shown that also the NHCF-V are oscillating Ca²⁺ to a certain extent (Fig. 10G).

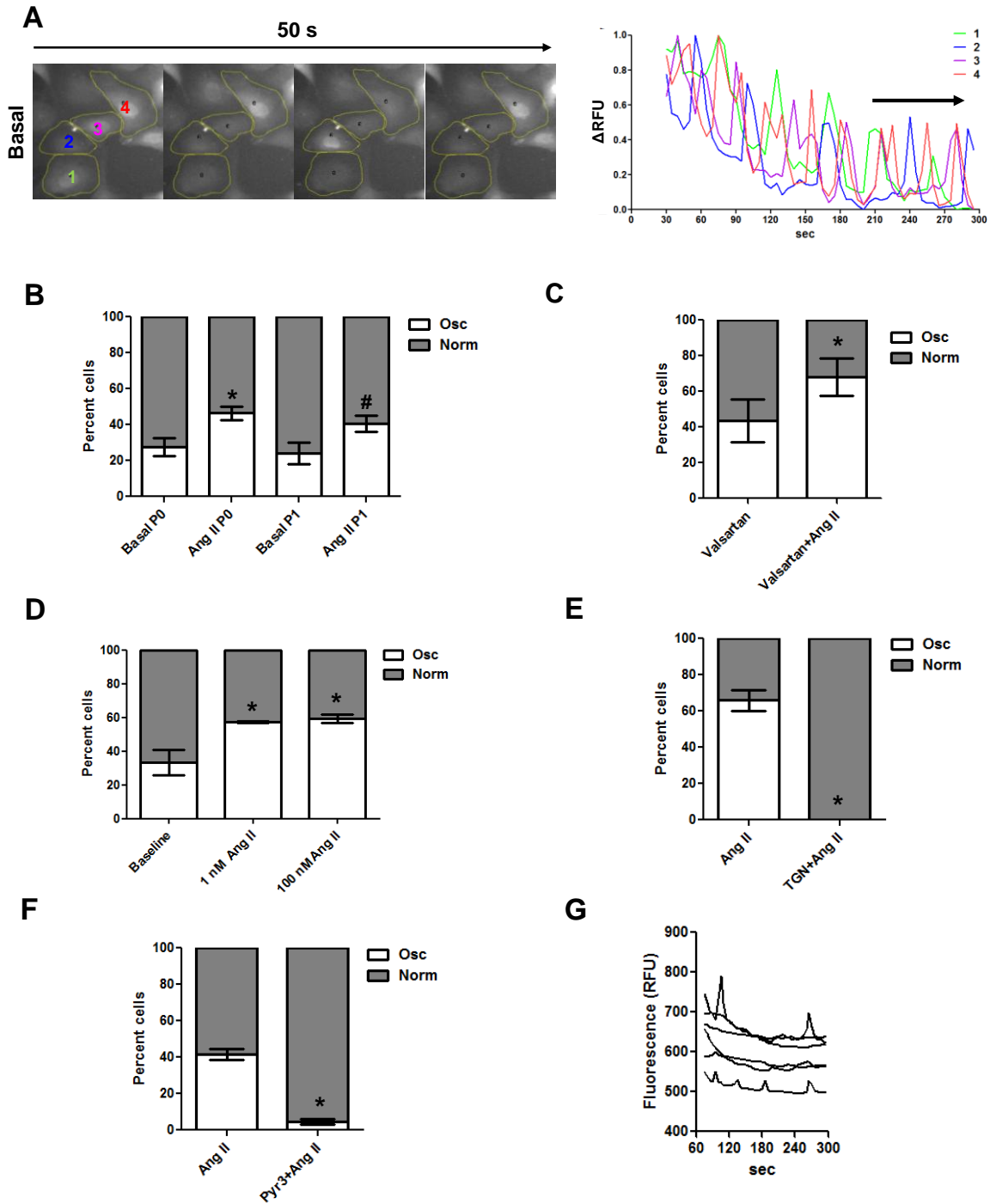


Figure 10: Investigation of Ca^{2+} oscillation in CF

A) Representative series of images of NRCF showing Ca^{2+} oscillation over a time period of 50 sec. The graph shows the ΔRFU for the marked cells. B-F) For each field of the time lapse recording, the percentage of oscillating (Osc) vs. non-oscillating (Norm)

*NRCF was analyzed. B) Percentage of P0 and P1 NRCF that can spontaneously oscillate Ca²⁺ at the basal level and following 100 nM Ang II treatment (n=7, for each n at least 3 wells/condition, 40-60 cells/well, means ± SEM, *p≤0.05 vs. basal P0, #p≤0.05 vs. basal P1). C) Effect of AT1 receptor blockade by 15 nM valsartan on the proportion of Ca²⁺ oscillating NRCF, with and without 100 nM Ang II (n=7, for each n at least 3 wells/condition, 40-60 cells/well, means ± SEM, *p≤0.05). D) Effect of 1 and 100 nM Ang II on the proportion of Ca²⁺ oscillating NRCF (n=3, for each n at least 3 wells/condition, 40-60 cells/well, means ± SEM, *p≤0.05 vs. baseline). E) Effect of pre-depletion of intracellular Ca²⁺ stores by 3 μM TGN on the proportion of Ca²⁺ oscillating NRCF with and without 100 nM Ang II treatment (n=4, for each n at least 3 wells/condition, 40-60 cells/well, means ± SEM, *p≤0.05). F) Effect of TRPC3 channel blockade by 3 μM Pyr3 on the proportion of Ca²⁺ oscillating NRCF with and without 100 nM Ang II treatment (n=7, for each n at least 3 wells/condition, 40-60 cells/well, means ± SEM, *p≤0.05). G) Investigating the occurrence of Ca²⁺ oscillation in NHCF-V. The graph shows the fluorescence traces for 6 individual cells treated with 100 nM Ang II.*

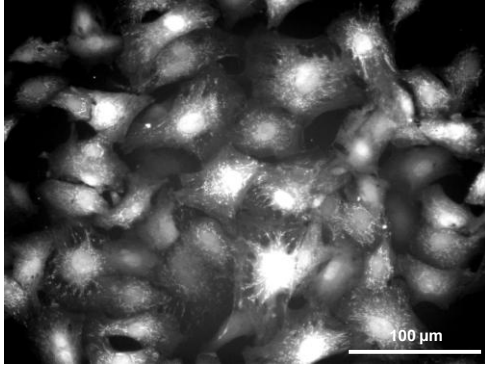
4.1.1.7. The NADPH oxidases (NOXs) and Rac1 GTPases are regulators of the Ang II-CaT in NRCF

Higher magnification imaging revealed that the flux of Ca²⁺ is spatially regulated. In response to Ang II, there was a transient Ca²⁺ loading in the nucleus or the perinuclear space, and a transient Ca²⁺ loading inside the mitochondria in many cells (Fig. 11A). Several processes in the mitochondria are known to involve ROS generation, therefore, the effect of ROS on Ang II-mediated Ca²⁺ handling was investigated by targeting Rac1 activation, which is among others a subunits of NOX1, 2, and 3, and by inhibition of NOX2 subunit gp91 phox activation.

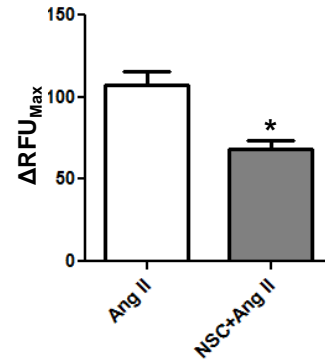
To determine whether the ROS producing NADPH-oxidases are involved in the regulation of Ca²⁺, the Ang II-CaT was investigated in NRCF treated with the Rac1 activation inhibitor NSC23766 (NSC). By analyzing the change in fluorescence in the whole cells, a significant decrease in the $\Delta\text{RFU}_{\text{Max}}$ was detected (Fig. 11B). Moreover, it was found that following Ang II treatment, around 30-40% of the control and NSC-treated cells, showed Ca²⁺ loading in the mitochondria, which resolved over time in the control cells, so that after 170 sec only 10% of the cells showed mitochondrial Ca²⁺

loading, while the mitochondrial Ca^{2+} loading was persistent in the NSC-treated cells. However, the loading of Ca^{2+} in the nuclei or the perinuclear space was not influenced by NSC treatment (Fig. 11C).

A



B



C

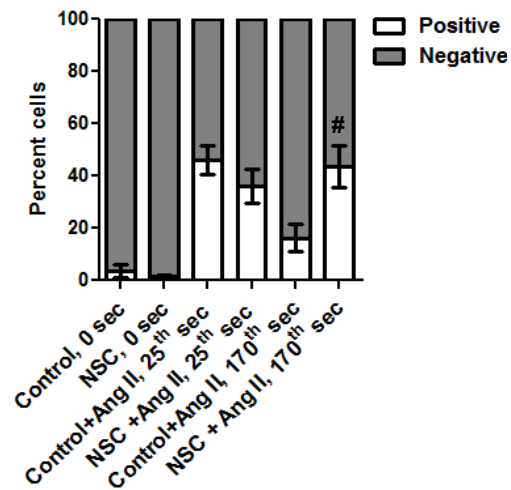
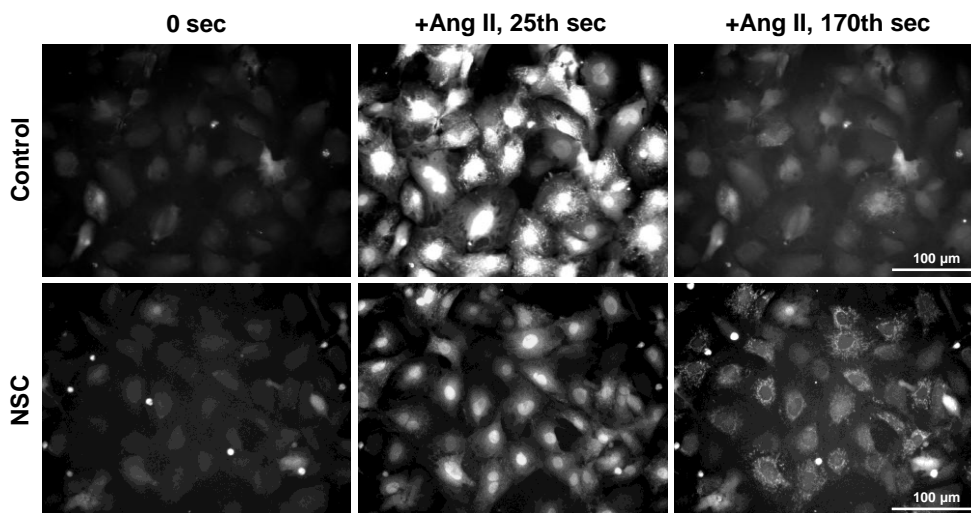


Figure 11: Investigation of the role of Rac1 in Ca²⁺ handling

A) Representative image for the loading of Ca²⁺ in the mitochondria following 100 nM Ang II treatment. B) NRCF were incubated for 1 hr with 50 μM NSC, before the Ang II-CaT was studied, where 100 nM Ang II was added at the 20th sec. The graph shows the effect of NSC treatment on the ΔRFU_{Max} (n=7, for each n at least 3 wells/condition, 40-60 cells/well, means ± SEM, *p≤0.05). C) Upper panel contains representative cell images showing the time-course for Ca²⁺ loading in the mitochondria and nuclei at 0, 25th and 170th sec for control and NSC-treated cells. Lower graph shows the analysis of the proportion of cells with mitochondrial Ca²⁺ loading at the defined time points (n=7, for each n at least 3 wells/condition, 40-60 cells/well, means ± SEM, # vs. control + Ang II at 170th sec, p≤0.05).

To further investigate the role of ROS in the regulation of Ca²⁺ handling in NRCF, a gp91-ds-tat peptide was used to specifically inhibit the association of gp91phox with p47phox, thus preventing the assembly of NOX2 subunits. A scrambled peptide with ds-tat motif (Scr) was used as a negative control. Similar to NSC treatment, the gp91-ds-tat peptide decreased the ΔRFU_{Max} significantly by approximately 40% (Fig. 12A). However, in contrast to the inhibition of the Rac activation, the duration of Ca²⁺ loading in the mitochondria was not prolonged (Fig. 12B).

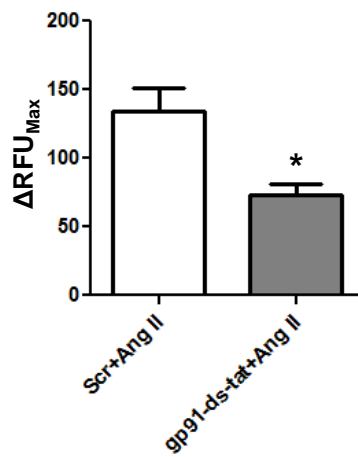
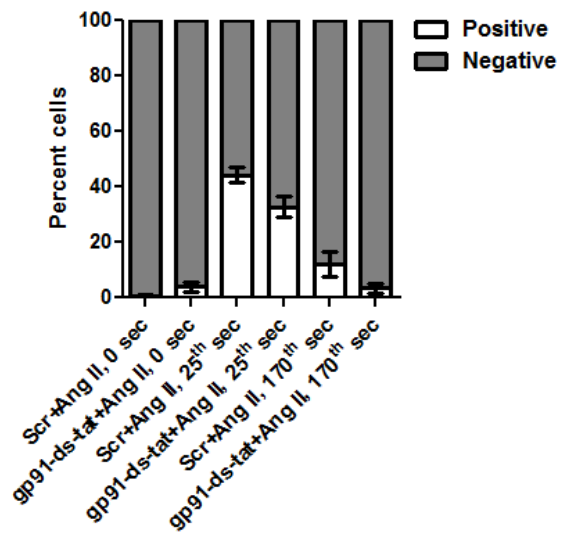
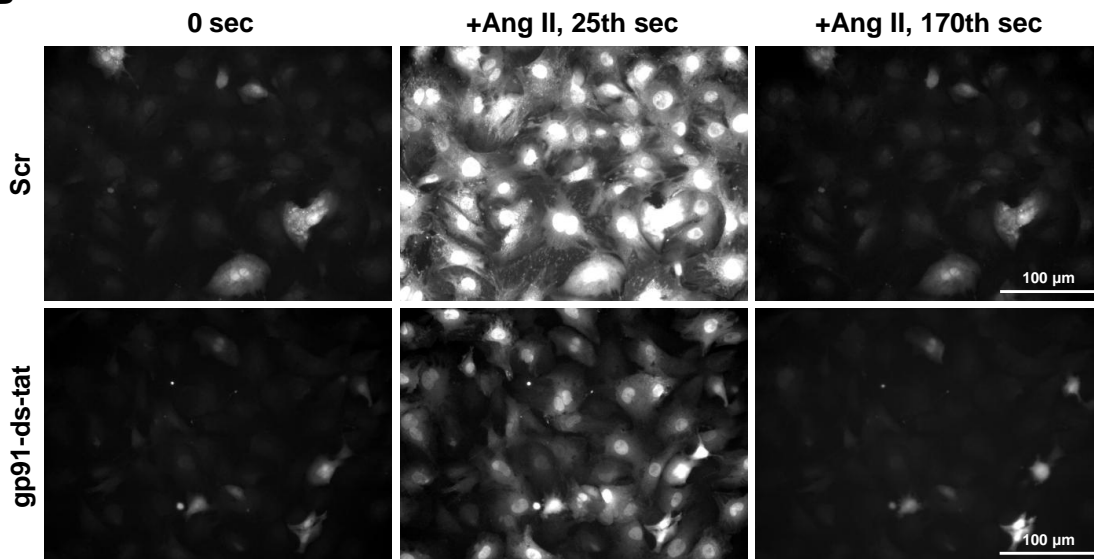
A**B**

Figure 12: Investigation of the role of NOX2 in Ca²⁺ handling

*NRCF were incubated for 1 hr with 5 μM gp91-ds-tat or Scr before the Ang II-CaT was studied. A) Effect of gp91-ds-tat treatment on the ΔRFU_{Max} ($n=3$, for each n at least 3 wells/condition, 40-60 cells/well, means \pm SEM, $*p\leq 0.05$). B) Upper panel contains representative cell images showing the time-course for Ca²⁺ loading in the mitochondria and nuclei at 0, 25th and 170th sec for the Scr and gp91-ds-tat-treated cells. Lower graph shows the analysis of the proportion of the cells with mitochondrial Ca²⁺ loading at the defined time points ($n=3$, for each n at least 3 wells/condition, 40-60 cells/well, means \pm SEM).*

4.1.2. Ca²⁺ controls the expression and secretion of CTGF

4.1.2.1. Chelation of intracellular Ca²⁺ by BAPTA-AM affects the basal and induced levels of CTGF expression and secretion

After the characterization of the Ang II-CaT in NRCF, its impact on CTGF expression and secretion was studied. To do so, first a control experiment was performed in which the NRCF were treated with BAPTA-AM and the effectiveness of Ca²⁺ chelation was studied by Ca²⁺ imaging after Ang II application. Compared to control conditions, BAPTA-AM significantly reduced the ΔRFU_{Max} by 70% reflecting the successful chelation of free Ca²⁺ in these cells (Fig. 13A). In next step, the impact of BAPTA-AM on the transcription of the immediate-early gene CTGF was analyzed under basal conditions and 2 hr after Ang II application, which induced the transcription of CTGF by 3-folds. In the presence of BAPTA-AM, however, this increase was completely suppressed and the basal CTGF gene transcription was also significantly reduced (Fig. 13B). To verify this finding on protein level, the effect of BAPTA-AM was investigated on the regulation of CTGF protein over 24 hr under basal conditions and after Ang II treatment. Ang II treatment alone significantly increased the intracellular CTGF by 0.5-fold and the secreted CTGF by 3.5 fold, however, in the presence of BAPTA-AM, the effect of Ang II was completely suppressed (Fig. 13C).

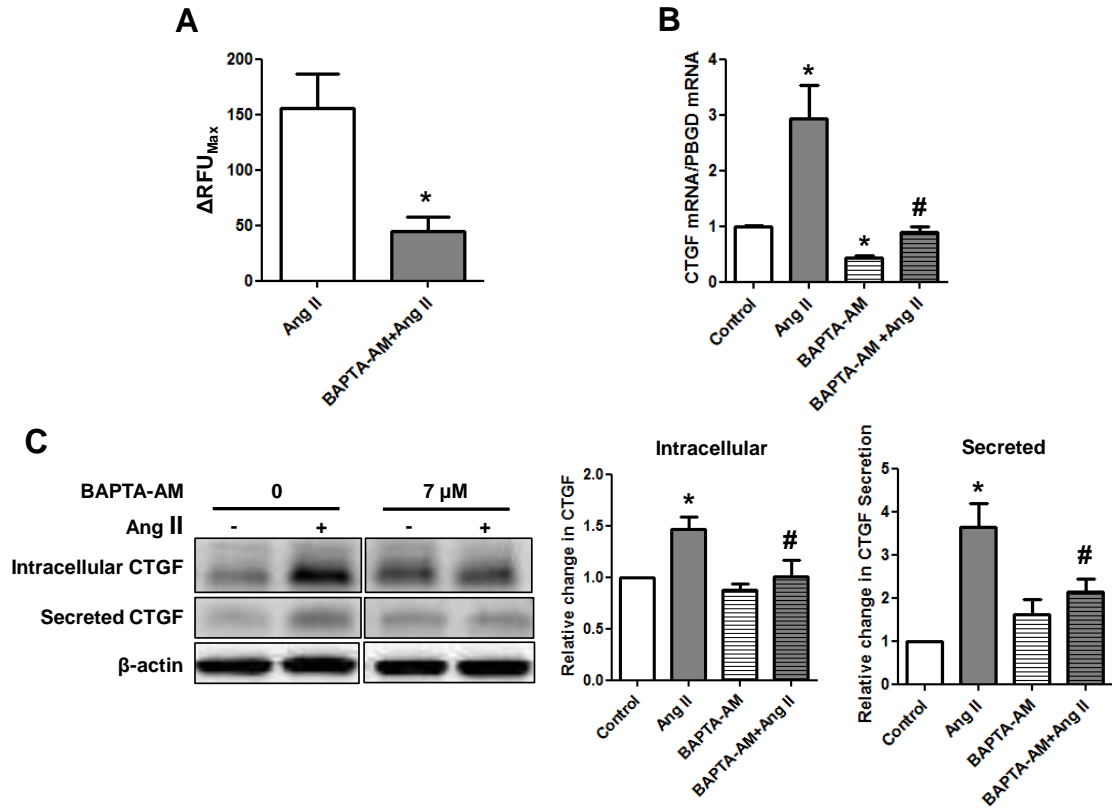


Figure 13: Investigation of the general role of Ca^{2+} in the regulation of CTGF expression and secretion

A) The graph shows ΔRFU_{Max} for the Ang II- CaT , where NRCF were treated for 1 hr with 7 μM BAPTA-AM or the corresponding control condition before 100 nM Ang II was applied ($n=3$, for each n at least 3 wells/condition, 40-60 cells/well, means \pm SEM, $*p \leq 0.05$). For the experiments shown in B and C, NRCF were treated for 1 hr with 7 μM BAPTA-AM or the corresponding control condition before 100 nM Ang II was added. For the qPCR data shown in B, the RNA was isolated 2 hr after Ang II treatment, whereas for the immunoblotting data shown in C the cell lysates and the conditioned media were collected 24 hr after Ang II treatment. B) Effect of BAPTA-AM treatment on CTGF gene transcription. The data were normalized to PBGD, and the change in gene transcription was calculated relative to the control ($n=3$, means \pm SEM, * and # $p \leq 0.05$, * vs. control, # vs. Ang II). C) Effect of BAPTA-AM treatment on the intracellular and secreted CTGF protein levels under basal and Ang II effects. Left are representative immunoblots, right are the relative quantification of the intracellular and secreted CTGF shown. The data

were normalized to β -actin, and the change in CTGF level was calculated relative to the control ($n=5$, means \pm SEM, * and # $p \leq 0.05$, * vs. control, #vs. Ang II).

In addition, fluorescence microscopy was performed for NRCF treated for 24 hr with BAPTA-AM to analyze its effect on CTGF localization and the cytoskeleton's integrity and organization. As shown in Fig. 14, there was no clear effect of the BAPTA-AM treatment on the CTGF localization in the Golgi apparatus, or on the integrity and organization of the actin filaments and microtubules.

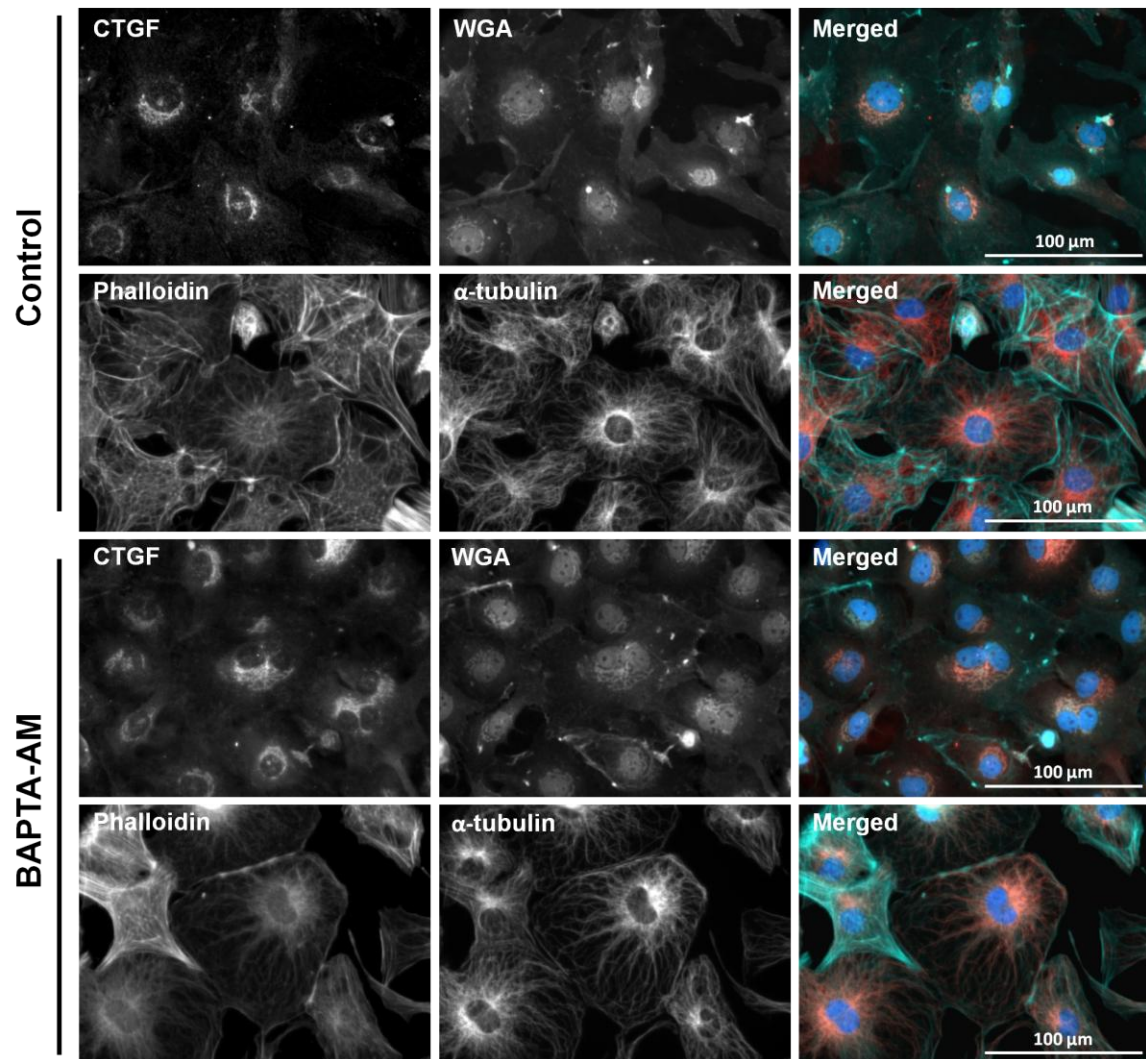


Figure 14: Fluorescence microscopy of NRCF treated for 24 hr with BAPTA-AM

The cells were incubated with 7 μ M BAPTA-AM for 24 hr, after which they were fixed, permeabilized and incubated with a blocking solution. IF staining was performed to detect CTGF (red) and α -tubulin (red). The actin filaments were stained with FITC-phalloidin (green), the membranous structures, including the Golgi apparatus, were stained with Alexa-fluor 488 conjugated-WGA (green), and the nuclei were stained with DAPI (blue).

As shown by the qPCR and immunoblotting data, the effect of BAPTA-AM was more pronounced in the qPCR data, where the cells were treated with BAPTA-AM for only 3 hr. Since BAPTA-AM is known to be unstable for a long time in cell culture, fluorescence microscopy was performed for NRCF treated with BAPTA-AM for 3 hr to explore the impact on the localization of CTGF and on the status of the cytoskeleton. As shown in Fig. 15, BAPTA-AM treatment disrupted of the Golgi apparatus into membranous structures containing CTGF. There was also a disruption of actin filaments and microtubules.

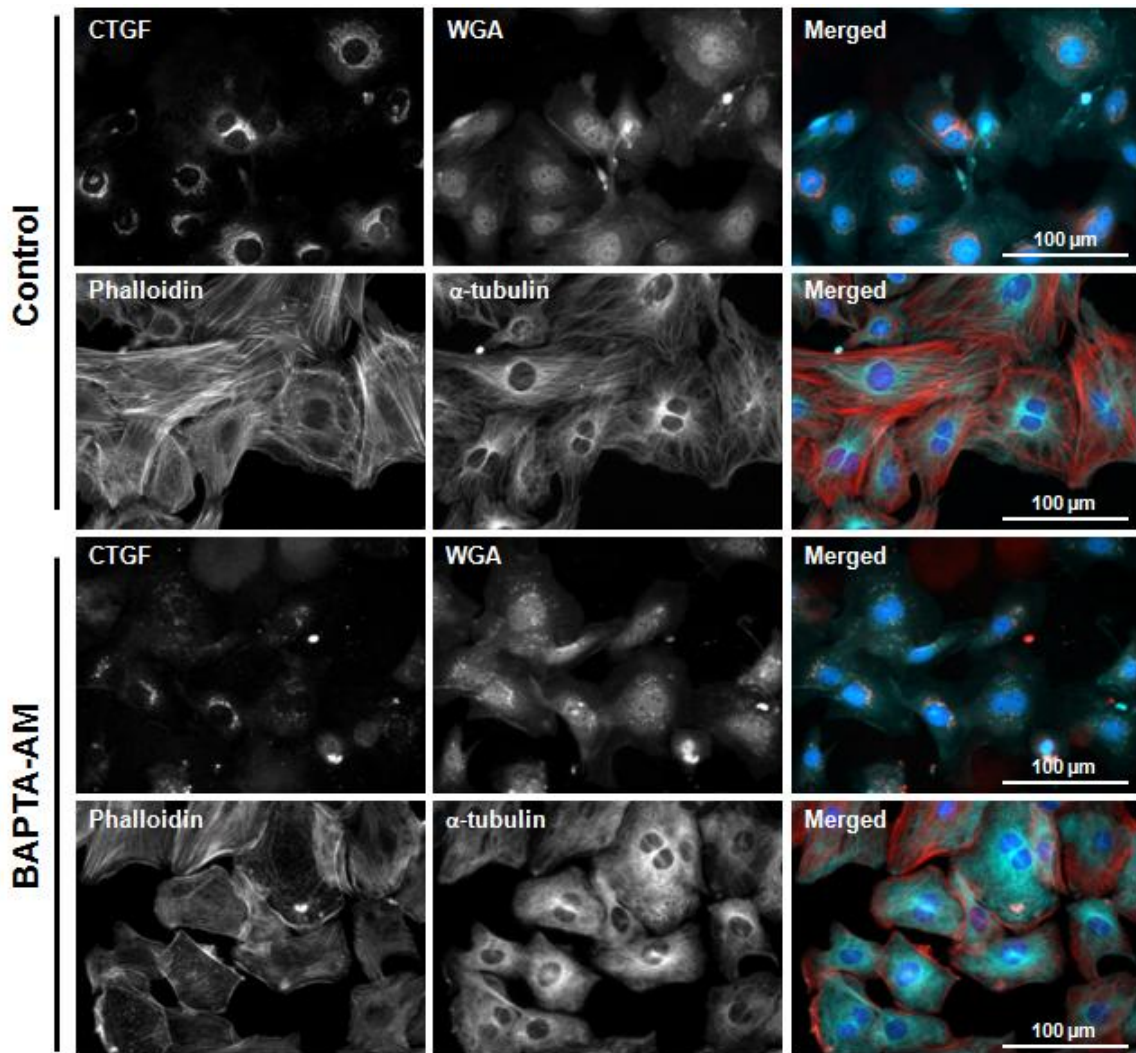


Figure 15: Fluorescence microscopy of NRCF treated for 3 hr with BAPTA-AM

The cells were incubated with 7 μ M BAPTA-AM for 3 hr, after which they were fixed, permeabilized and incubated with a blocking solution. IF staining was performed to detect CTGF (red) and α -tubulin (red). The actin filaments were stained with FITC-phalloidin (green), the membranous structures, including the Golgi apparatus, were stained with Alexa-fluor 488 conjugated-WGA (green), and the nuclei were stained with DAPI (blue).

4.1.2.2. Depletion of intracellular Ca^{2+} by TGN affects mainly CTGF secretion

After the effect of Ca^{2+} chelation was investigated, further experiments were performed to determine the effect of the intracellular Ca^{2+} depletion by TGN on the regulation of CTGF by Ang II, which showed that in the presence of TGN the stimulatory effect of Ang II on CTGF secretion was completely suppressed, but there was no effect on the basal level of secretion. Also, there was no significant effect for TGN on the intracellular CTGF (Fig. 16).

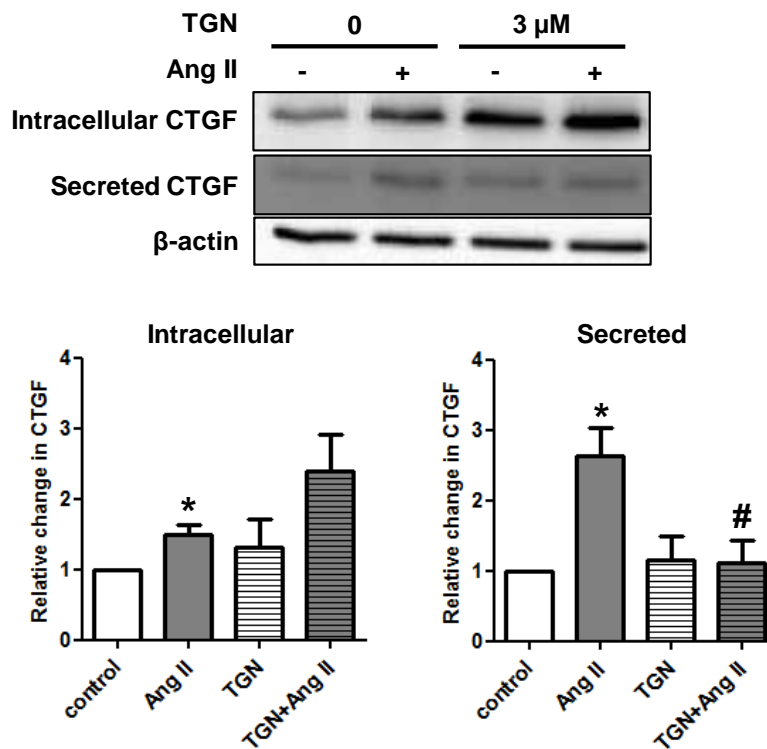


Figure 16: Investigating the effect of intracellular Ca^{2+} depletion by TGN on CTGF regulation

NRCF were treated for 1 hr with 3 μM TGN or the corresponding control condition, before they were treated with 100 nM Ang II. After 24 hr, the cell lysates and the conditioned media were collected. Upper panel showing representative immunoblots. The graphs below show the relative quantification of the intracellular and secreted CTGF. The data were normalized to β -actin, and the change in CTGF level was

calculated relative to the control ($n=4$, means \pm SEM, * and # $p \leq 0.05$, * vs. control, # vs. Ang II).

Moreover, fluorescence microscopy was performed for NRCF treated with TGN to analyze its effect on CTGF localization and the cytoskeleton's integrity and organization, which revealed that TGN treatment disrupted the morphology of Golgi apparatus, while CTGF protein was dispersed throughout the cytosol. Moreover, TGN treatment affected the integrity of the actin filaments, but not of the microtubules (Fig. 17).

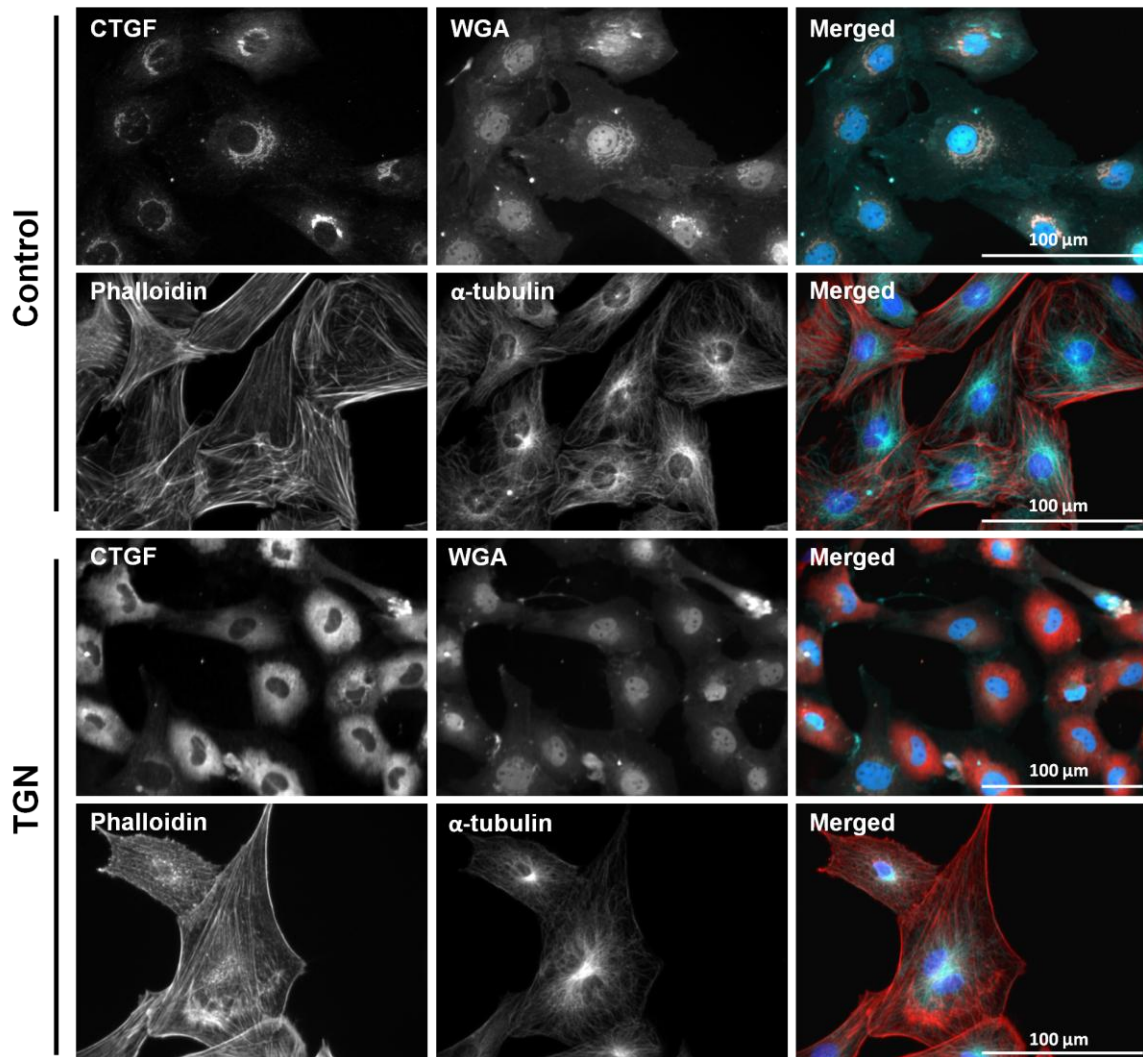


Figure 17: Fluorescence microscopy of TGN-treated NRCF

The cells were incubated for 24 hr with 3 μM TGN, after which they were fixed, permeabilized and incubated with a blocking solution. IF staining was performed to detect CTGF (red) and α -tubulin (green). The actin filaments were stained with TRITC-phalloidin (red), the membranous structures, including the Golgi apparatus, were stained with Alexa-fluor 488 conjugated-WGA (green), and the nuclei were stained with DAPI (blue).

4.1.2.3. Blockade of IP3Rs by XeC inhibits CTGF secretion

After it was found that the depletion of intracellular Ca^{2+} stores suppresses the secretion of CTGF, the effect of IP3Rs blockade by XeC was evaluated on the regulation of CTGF protein in the presence and absence of Ang II. Immunoblotting data analysis revealed that XeC significantly reduced the basal and induced levels of CTGF secretion, without showing a clear reduction in the intracellular level of CTGF (Fig. 18).

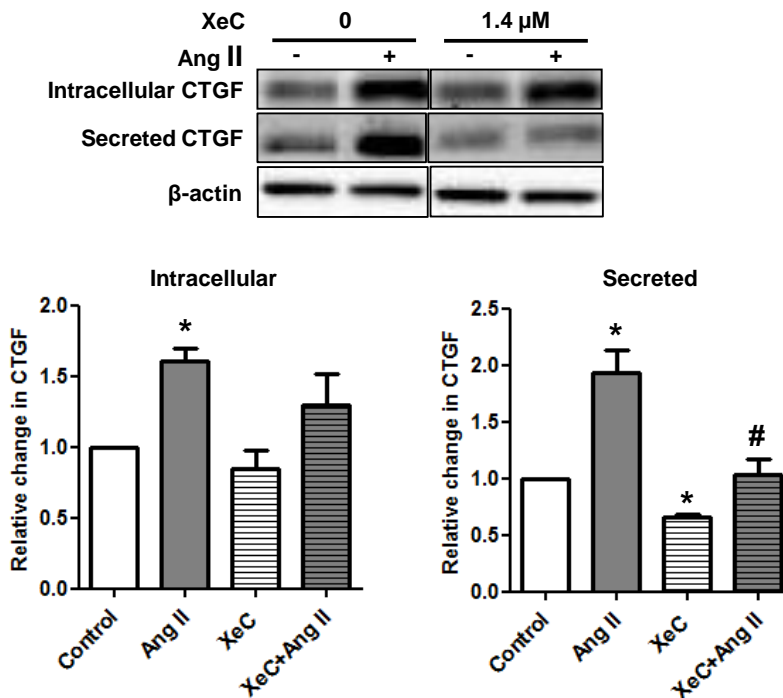


Figure 18: Evaluating the effect of IP3R blockade by XeC on CTGF regulation

*NRCF were treated for 1 hr with 1.4 μ M TGN or the corresponding control condition, before they were treated with 100 nM Ang II. After 24 hr, the cell lysates and the conditioned media were collected. Upper panel showing representative immunoblots. The graphs below show the relative quantification of the intracellular and secreted CTGF. The data were normalized to β -actin, and the change in CTGF level was calculated relative to the control (n=5, means \pm SEM, * and # $p \leq 0.05$, * vs. control, # vs. Ang II).*

IF microscopy was also performed to determine the effect of XeC treatment on the localization of CTGF as well as on the integrity and organization of actin filaments and microtubules. As shown in Fig. 19, XeC partially disrupted the morphology of Golgi apparatus, and the cytoplasm of XeC-treated cells seemed to contain more CTGF vesicles. In the same time, no effect could be detected on the status of actin filaments and microtubules.

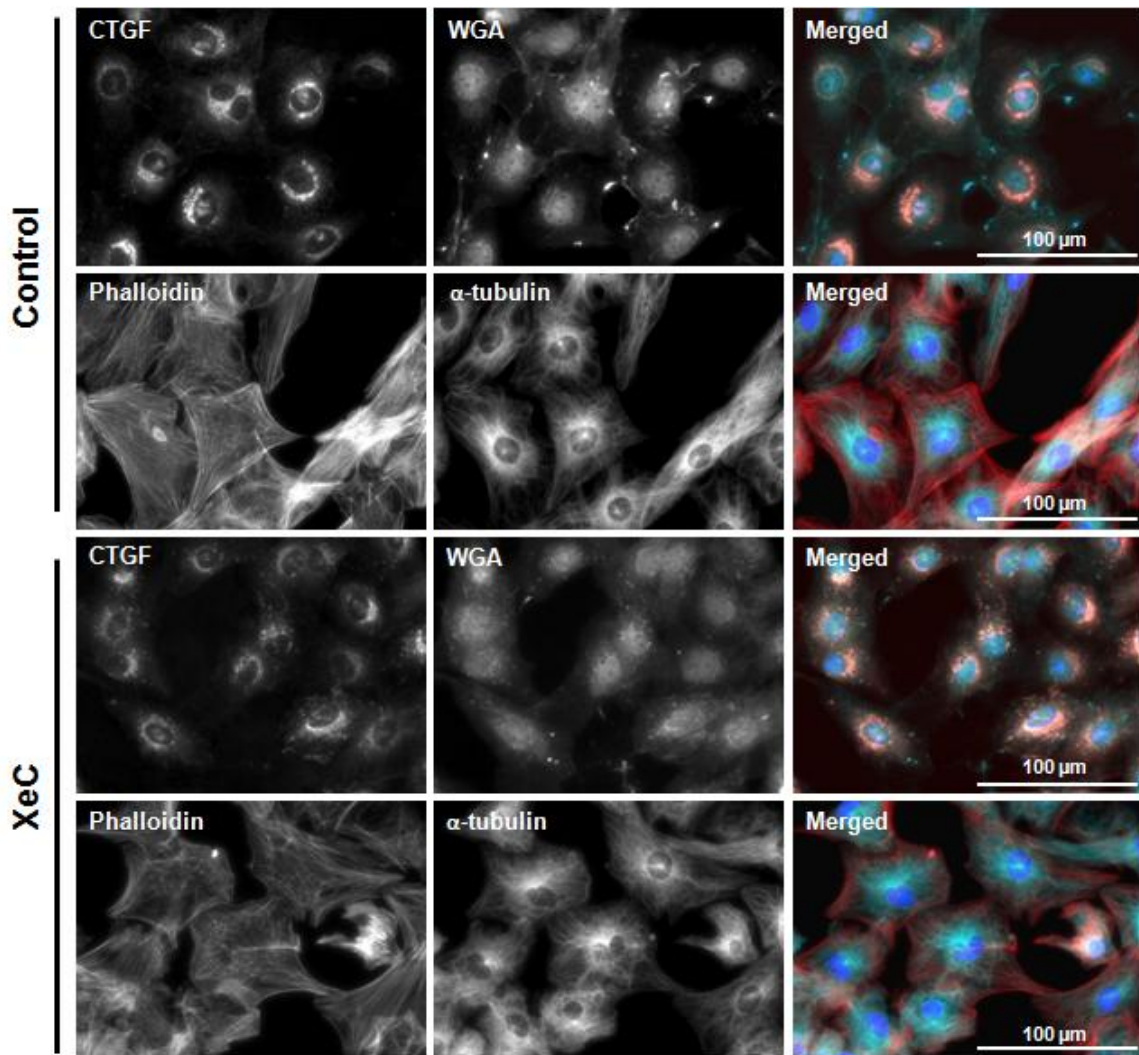


Figure 19: Fluorescence microscopy of XeC-treated NRCF

The cells were incubated for 24 hr with 1.4 μM TGN, after which they were fixed, permeabilized and incubated with a blocking solution. IF staining was performed to detect CTGF (red) and α-tubulin (green). The actin filaments were stained with TRITC-phalloidin (red), the membranous structures, including the Golgi apparatus, were stained with Alexa-fluor 488 conjugated-WGA (green), and the nuclei were stained with DAPI (blue).

4.1.2.4. Blockade of TRPC3 channels induces CTGF secretion, without influencing the expression

As shown in Fig. 9A and Fig. 10F, TRPC3 channels were found to play a role in the regulation of the Ang II-CaT and the Ang II-induced Ca^{2+} oscillation. The next step was to determine whether TRPC3 channels can therefore play a role in the regulation of CTGF expression by Ang II. To do so, the effect of Pyr3 on the transcription of the immediate-early gene CTGF was analyzed under basal conditions and 2 hr following Ang II application, which revealed that treatment with Pyr3 had no effect on the basal or induced levels of CTGF gene transcription (Fig. 20A). In addition, immunoblotting analysis was performed to evaluate the effect of Pyr3 on the intracellular and secreted CTGF protein under basal and Ang II treatment, which showed that treatment with Pyr3 had no effect on the basal levels of intracellular and secreted CTGF, but upon Ang II treatment, the intracellular level of CTGF was significantly reduced while the secreted CTGF was significantly increased (Fig. 20B).

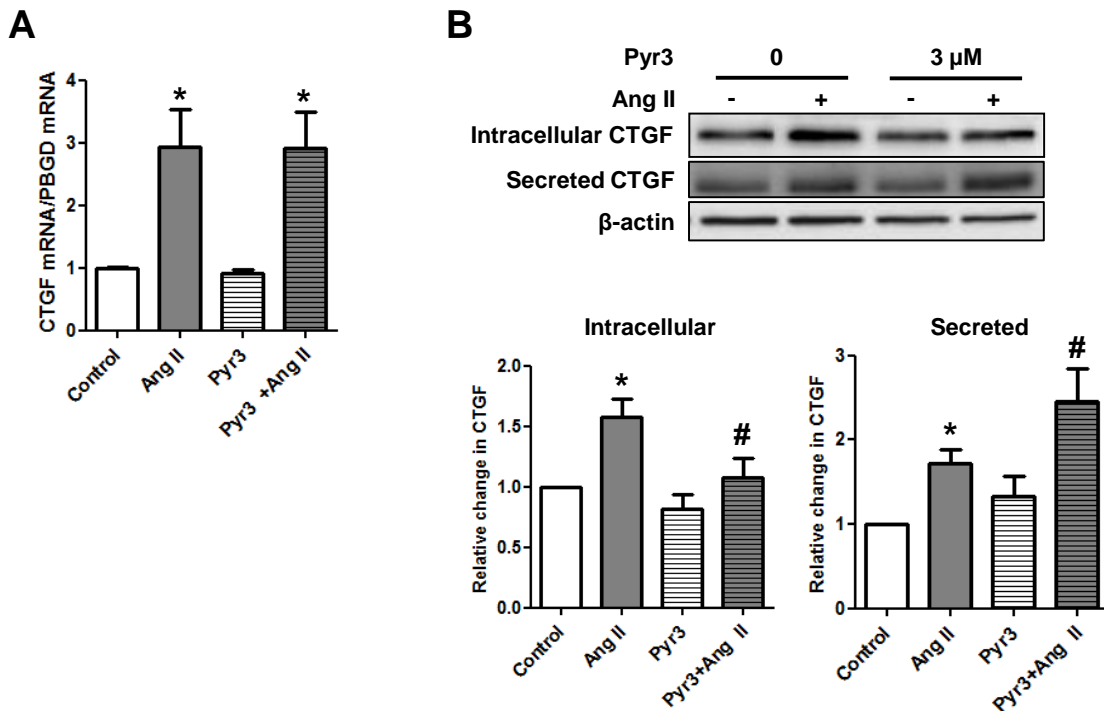


Figure 20: Investigating the effect of TRPC3 blockade on CTGF regulation

*NRCF were treated for 1 hr with 3 μ M Pyr3 or the corresponding control condition, before 100 nM Ang II was added. For the qPCR data shown in A, the RNA was isolated 2 hr following Ang II treatment, whereas for the immunoblotting data shown in B, the cell lysates and the conditioned media were collected 24 hr after Ang II treatment. A) Effect of Pyr3 treatment on CTGF gene transcription under basal and Ang II effects. The data were normalized to PBGD, and the change in gene transcription was calculated relative to the control (n=3, means \pm SEM, * and #p \leq 0.05, * vs. control, # vs. Ang II). B) Effect of Pyr3 treatment on the intracellular and secreted CTGF levels, under basal and Ang II effects. Upper panel shows representative immunoblots, the graphs below show the relative quantification for the intracellular and secreted CTGF. The data were normalized to β -actin, and the change in CTGF level was calculated relative to the control (n=8, means \pm SEM, * and #p \leq 0.05, * vs. control, # vs. Ang II).*

Besides, NRCF treated with Pyr3 were examined by fluorescence microscopy to determine the effect of Pyr3 on CTGF localization and the cytoskeleton's integrity and organization. As shown in Fig. 21, there was no clear effect for Pyr3 treatment on CTGF localization in Golgi apparatus, or on the integrity and organization of the actin filaments and microtubules.

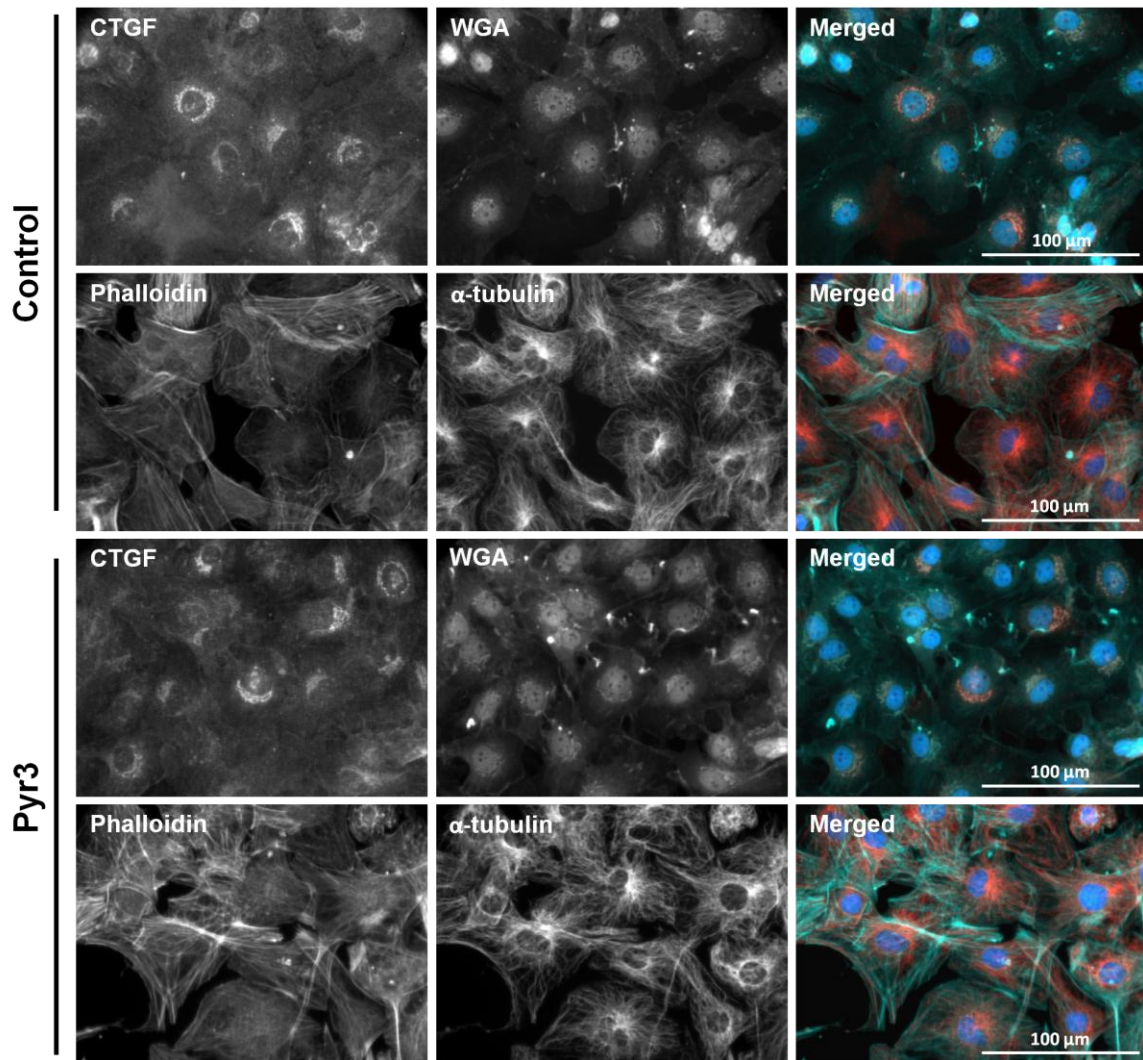


Figure 21: Fluorescence microscopy for NRCF treated with Pyr3

The cells were incubated for 24 hr with 3 μ M Pyr3. After that, they were fixed, permeabilized and incubated with a blocking solution. IF staining was performed to detect CTGF (red) and α -tubulin (red). The actin filaments were stained with FITC-phalloidin (green), the membranous structures, including Golgi apparatus, were stained with Alexa-fluor 488 conjugated-WGA (green), and the nuclei were stained with DAPI (blue).

4.1.2.5. Inhibition of NOX2 subunits assembly has no impact on the regulation of CTGF

After it has been shown that the inhibition of NOX2 subunits assembly by gp91-ds-tat interfered with the regulation of Ca²⁺ handling in NRCF, the effect of gp91-ds-tat treatment on the regulation of CTGF was investigated by immunoblotting, which showed no impact for gp91-ds-tat treatment on the basal or induced levels of the intracellular or secreted CTGF (Fig. 22).

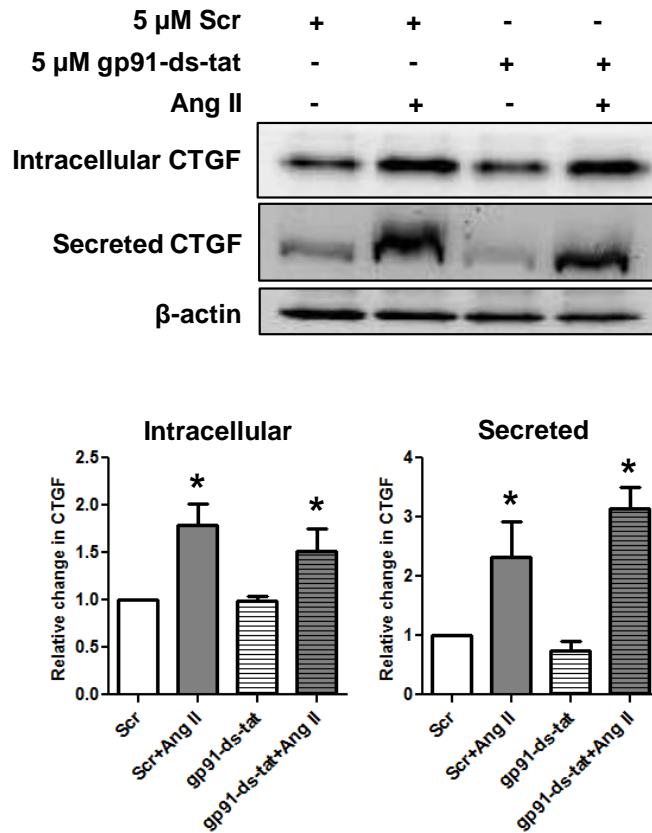


Figure 22: Evaluation of the effect of NOX2 inhibition by gp91-ds-tat on CTGF regulation

NRCF were incubated for 1 hr with 5 μ M Scr (negative control) or 5 μ M gp91-ds.tat, before 100 nM Ang II was applied. After 24 hr, the cell lysates and the conditioned media

were collected. Upper panel are representative immunoblots. Lower graphs show the relative quantification for the intracellular and secreted CTGF. The data were normalized to β -actin, and the change in CTGF level was calculated relative to the Scr ($n=3$, means \pm SEM, $*p\leq 0.05$, * vs. Scr).

4.1.3. Determination of downstream targets for Ca^{2+} that mediate CTGF regulation

4.1.3.1. Calcineurin and PKC oppositely regulate CTGF expression

After it had been established that Ca^{2+} plays a role in the regulation of CTGF, the next step was to determine downstream targets through which Ca^{2+} can influence CTGF expression and secretion. Therefore, PKC (Ca^{2+} -dependent kinases) and calcineurin (Ca^{2+} -dependent phosphatase) were investigated.

In order to confirm that both PKC and calcineurin are located downstream Ca^{2+} and have no impact on the handling of Ca^{2+} itself, Ang II-CaT was investigated in the presence of the PKC inhibitor Go 6983 and the calcineurin inhibitor CsA. As shown in Fig. 23A and B, there was no effect for either of these two inhibitors on the $\Delta\text{RFU}_{\text{Max}}$. In addition, the impact of Go 6983, CsA and a combination of both on the transcription of the immediate-early gene CTGF was analyzed under basal conditions and 2 hr after Ang II application, which showed that Go 6983 significantly reduced the basal and induced levels of CTGF gene transcription. In contrast, CsA significantly increased the basal and induced levels of CTGF gene transcription. However, when a combination of both treatments was applied, CsA was no longer able to enhance CTGF gene transcription (Fig. 23C). Moreover, the effect of Go 6983 was investigated on the regulation of CTGF at the protein level by immunoblotting, which demonstrated that treatment with Go 6983 significantly reduced the basal and induced levels of intracellular and secreted CTGF (Fig. 23D). In parallel, the effect of CsA on the regulation of CTGF at the protein level was also evaluated by immunoblotting analysis, which revealed that treatment with CsA significantly reduced the basal and induced levels of the intracellular CTGF, without showing a significant effect on the basal and induced levels of CTGF secretion (Fig. 23E).

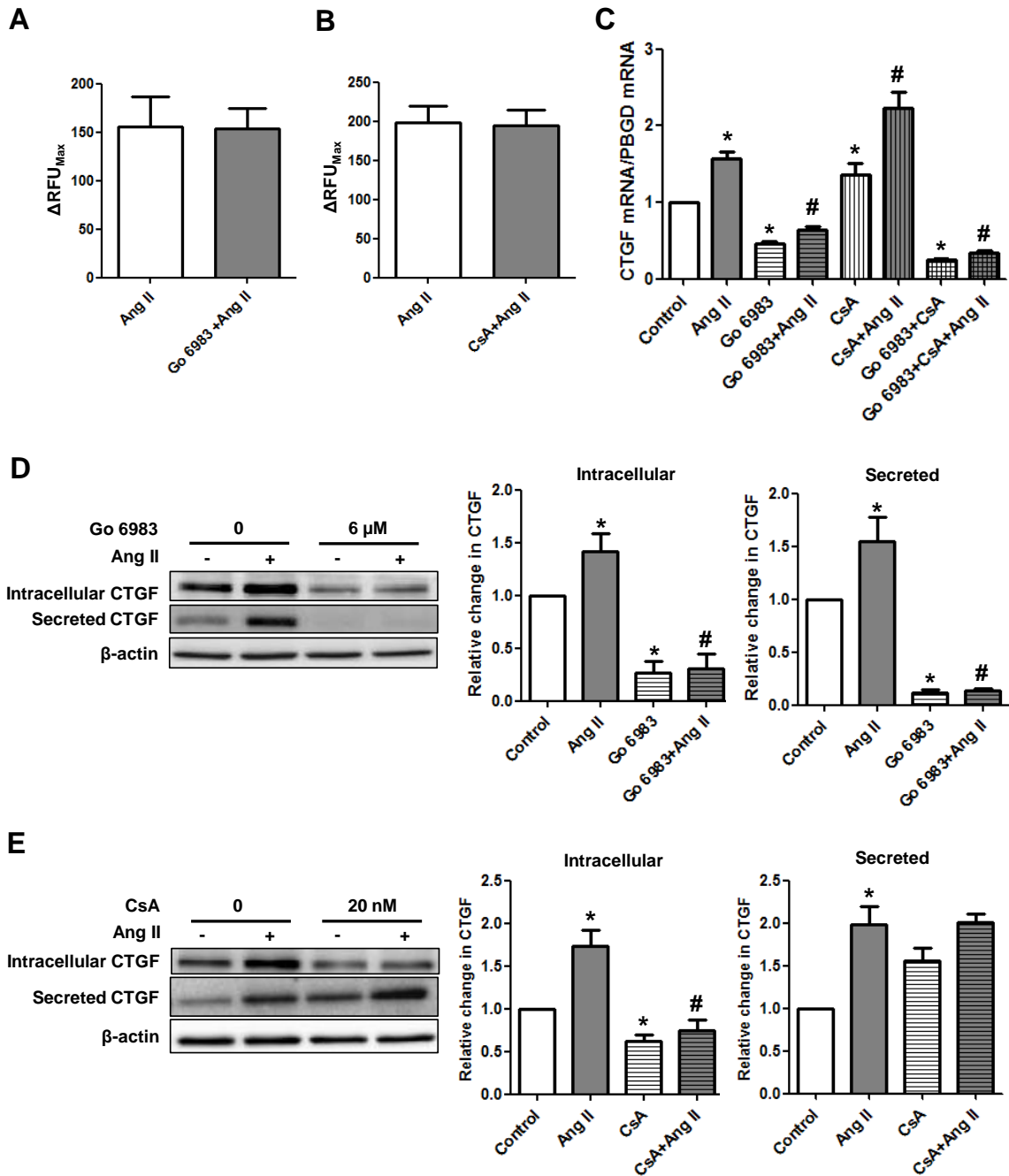


Figure 23: Investigating the role of PKC and calcineurin in CTGF regulation

A) NRCF were incubated with 6 μ M Go 6983 before the Ang II-CaT was investigated. The graph shows the effect of Go 6983 on the ΔRFU_{Max} ($n=3$, for each n at least 3 wells/condition, 40-60 cells/well, means \pm SEM * $p \leq 0.05$). B) NRCF were incubated with

20 nM CsA before the Ang II-CaT was investigated. The graph shows the effect of CsA on the ΔRFU_{Max} ($n=3$, for each n at least 3 wells/condition, 40-60 cells/well, means \pm SEM, $*p \leq 0.05$). C) NRCF were incubated with 6 μ M Go 6983, 20 nM CsA or a combination of both for 1 hr, before 100 nM Ang II was added. The RNA was isolated 2 hr following Ang II treatment and was used to analyze the change in CTGF gene transcription by qPCR. The data were normalized to PBGD, and the change in gene transcription was calculated relative to the control ($n=3$, means \pm SEM, $*p \leq 0.05$ vs. control, $^{\#}p \leq 0.05$ vs. Ang II). D) NRCF were treated for 1 hr with 6 μ M Go 6983 or the corresponding control condition, after that 100 nM Ang II was added. The cell lysates and the conditioned media were collected 24 hr later. Left are representative immunoblots shown. The graphs on the right show the relative quantification for the intracellular and secreted CTGF. The data were normalized to β -actin, and the change in CTGF level was calculated relative to the control ($n=4$, means \pm SEM, $*p \leq 0.05$ vs. control, $^{\#}p \leq 0.05$ vs. Ang II). E) NRCF were treated for 1 hr with 20 nM CsA or the corresponding control conditions, after that 100 nM Ang II was added. The cell lysates and the conditioned media were collected 24 hr later. Left are representative immunoblots shown. The graphs on the right show the relative quantification for the intracellular and secreted CTGF. The data were normalized to β -actin, and the change in CTGF level was calculated relative to the control ($n=4$, means \pm SEM, $*p \leq 0.05$ vs. control, $^{\#}p \leq 0.05$ vs. Ang II).

The effect of 24 hr-treatment with Go 6983 on CTGF localization and the cytoskeleton's integrity and organization was determined by fluorescence microscopy, which revealed that Go 6983 treatment resulted in the collapse and condensation of the Golgi apparatus and the disruption of the actin filaments. CTGF remained localized in the Golgi apparatus, and the microtubules appeared normal (Fig. 24).

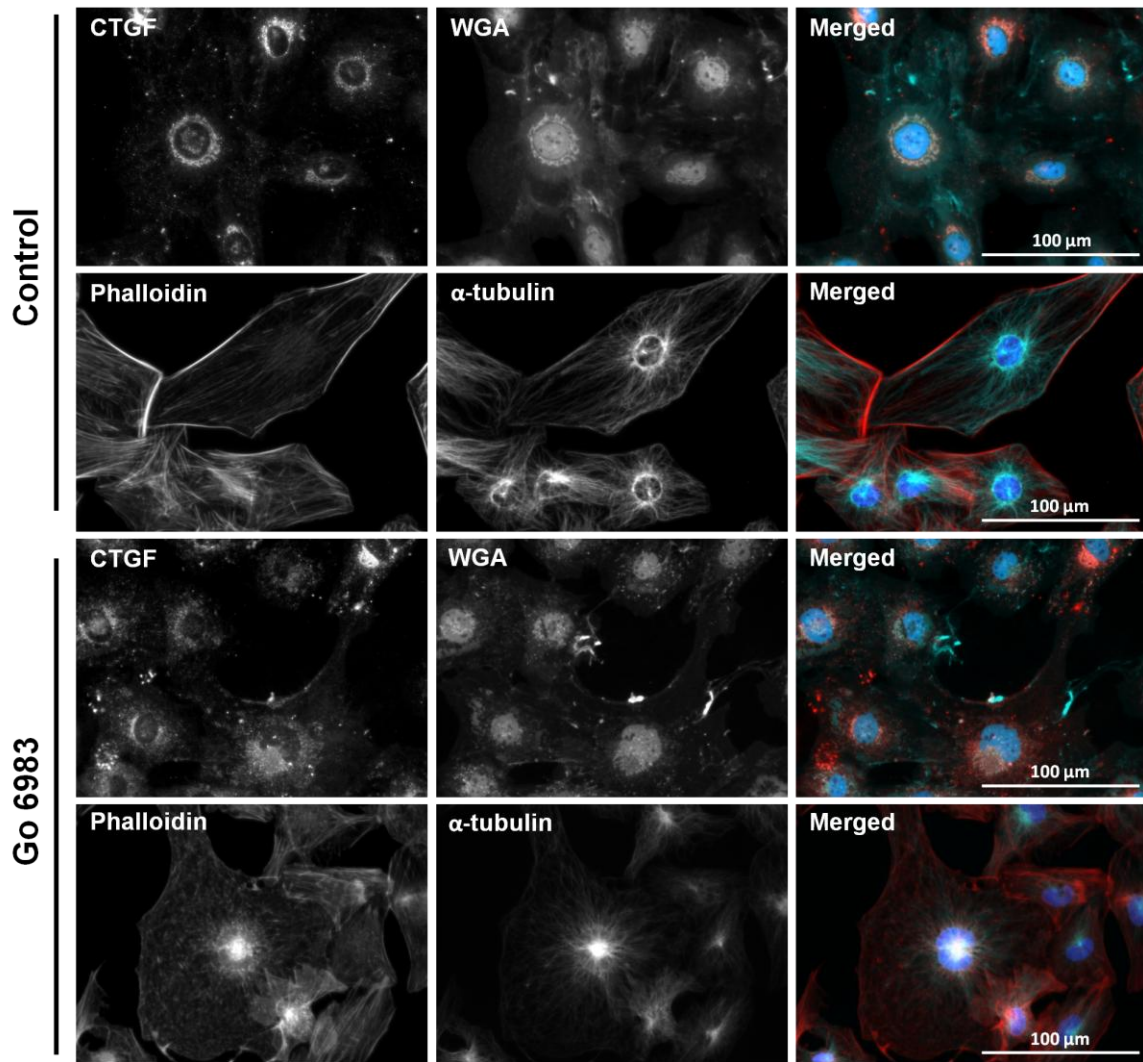


Figure 24: Fluorescence microscopy for NRCF treated for 24 hr with Go 6983

The cells were incubated for 24 hr with 6 μM Go 6983. After that, they were fixed, permeabilized and incubated with a blocking solution. IF staining was performed to detect CTGF (red) and α-tubulin (green). The actin filaments were stained with TRITC-phalloidin (red), the membranous structures, including the Golgi apparatus, were stained with Alexa-fluor 488 conjugated-WGA (green), and the nuclei were stained with DAPI (blue).

In order to determine, whether 3 hr-treatment with Go 6983 can also cause structural changes in NRCF, fluorescence microscopy was performed for this purpose, which

revealed that the disruption of the Golgi apparatus can already be observed within this short time interval . However, the impact on the integrity of actin filaments was not clear (Fig. 25).

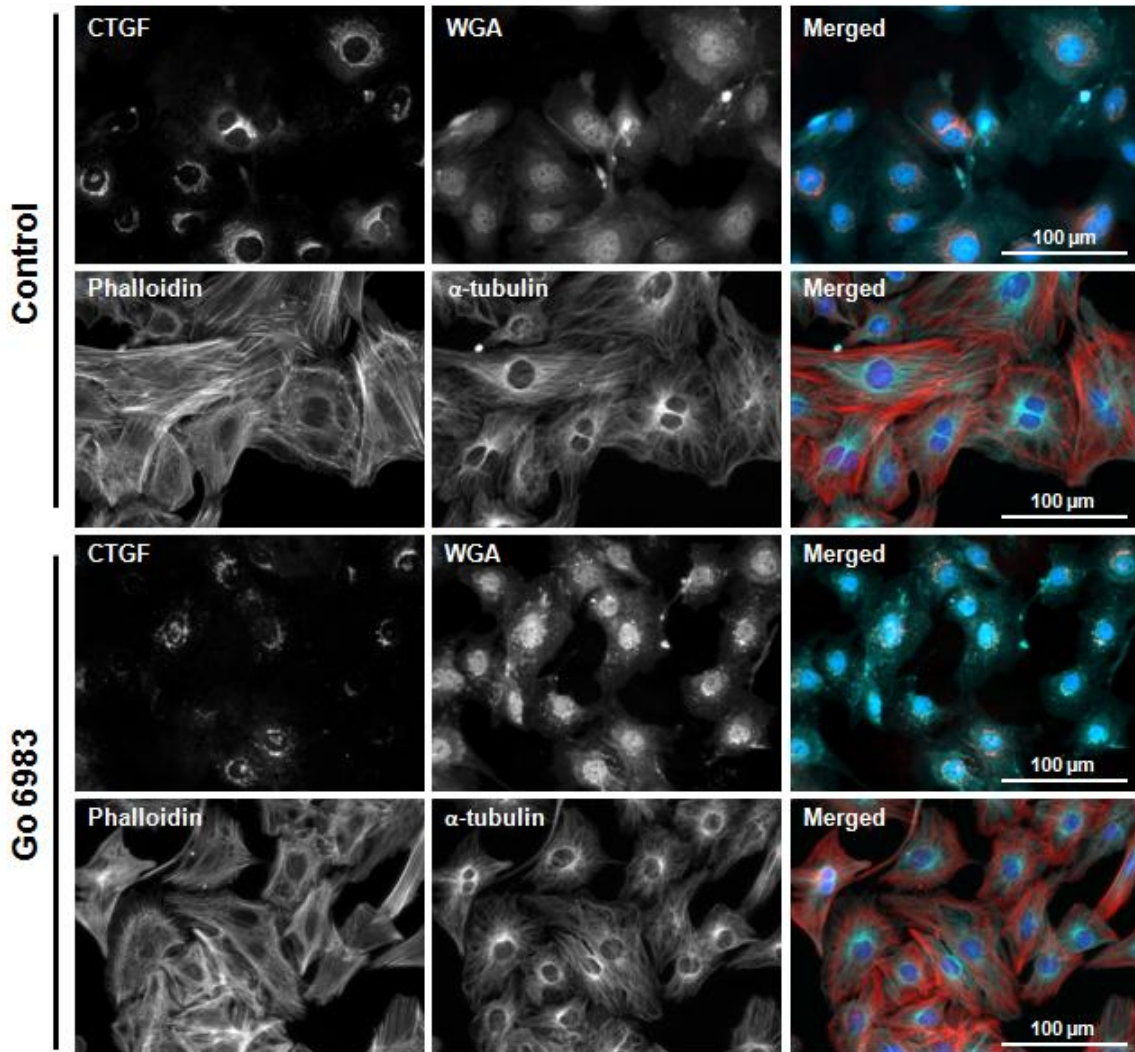


Figure 25: Fluorescence microscopy for NRCF treated for 3 hr with Go 6983

The cells were incubated for 3 hr with 6 μM Go 6983. After that, they were fixed, permeabilized and incubated with a blocking solution. IF staining was performed to detect CTGF (red) and α-tubulin (green). The actin filaments were stained with TRITC-phalloidin (red), the membranous structures, including the Golgi apparatus, were stained

with Alexa-fluor 488 conjugated-WGA (green), and the nuclei were stained with DAPI (blue).

The effect of CsA treatment on CTGF localization and the cytoskeleton's status was also investigated by fluorescence microscopy. As shown in Fig. 26, the complexities of the cell membrane in the CsA-treated cells were lost, and the morphology of the Golgi apparatus became unclear, but it was not disrupted. However, there was no clear effect on the actin filaments or microtubules.

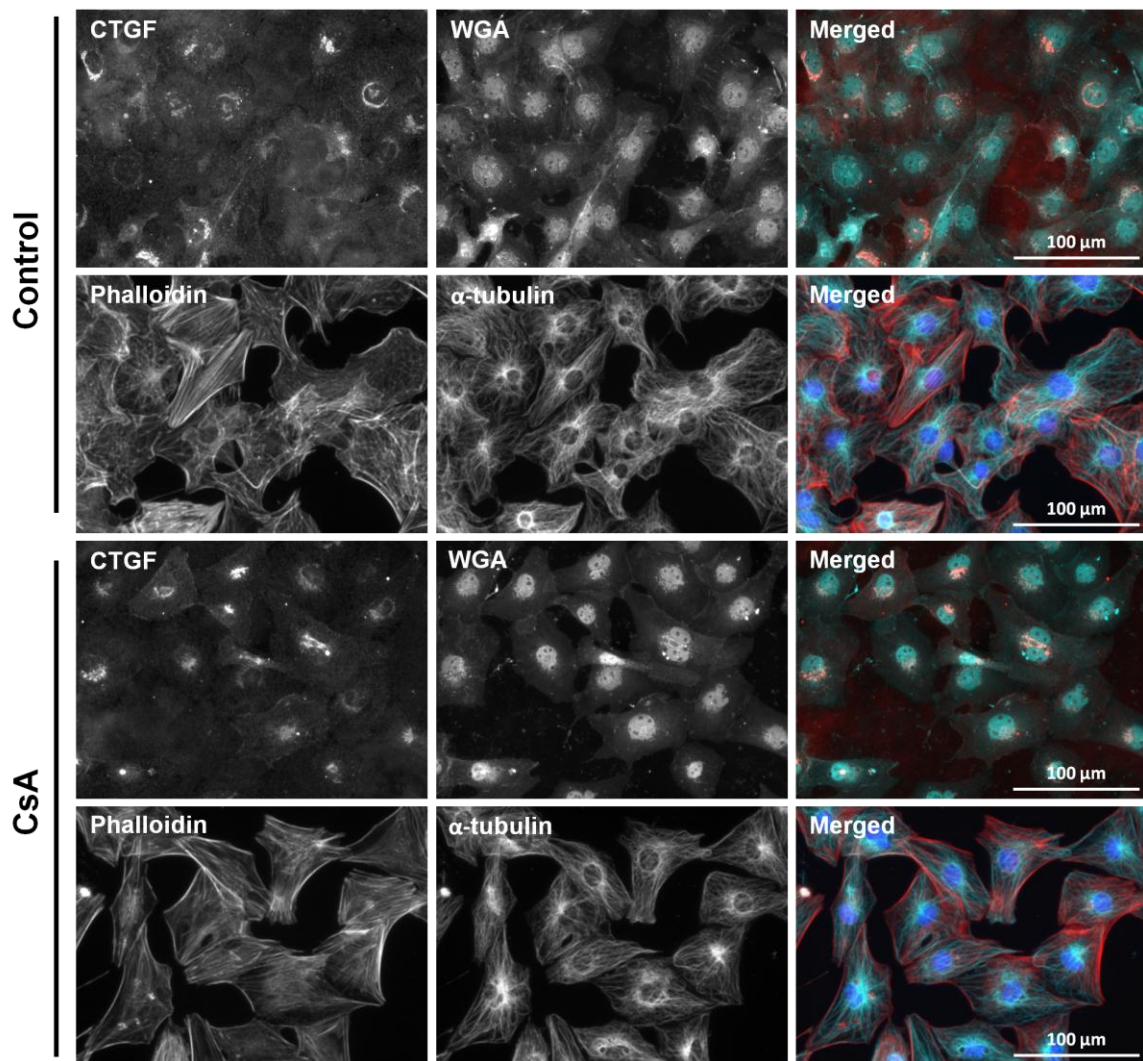


Figure 26: Fluorescence microscopy for CsA-treated NRCF

The cells were incubated for 24 hr with 20 nM CsA. After that, they were fixed, permeabilized and incubated with a blocking solution. IF staining was performed to detect CTGF (red) and α -tubulin (green). The actin filaments were stained with TRITC-phalloidin (red), the membranous structures, including the Golgi apparatus, were stained with Alexa-fluor 488 conjugated-WGA (green), and the nuclei were stained with DAPI (blue).

4.1.3.2. Ca^{2+} regulates CTGF independently of ERK1/2 or Ca^{2+} /calmodulin-dependent protein kinase II δ (CaMKII δ) signaling

Other downstream targets of Ca^{2+} , which could be involved in the regulation of CTGF, were also investigated including ERK1/2 and CaMKII δ . To do so, the phosphorylation of ERK1/2 by Ang II was investigated in NRCF in the presence and absence of BAPTA-AM, which demonstrated that Ang II-induced ERK1/2 phosphorylation was not influenced by intracellular Ca^{2+} chelation (Fig. 27A). In addition, the effect of Ang II on CaMKII phosphorylation was investigated in the presence of the CaMKII phosphorylation inhibitor Kn-93 and its negative control Kn-92. As shown in Fig. 27B, Ang II did not induce CaMKII phosphorylation (preliminary data). Moreover, CaMKII inhibition did not affect the Ang II-CaT (preliminary data) (Fig. 27C). Thus, a role of CaMKII could be excluded.

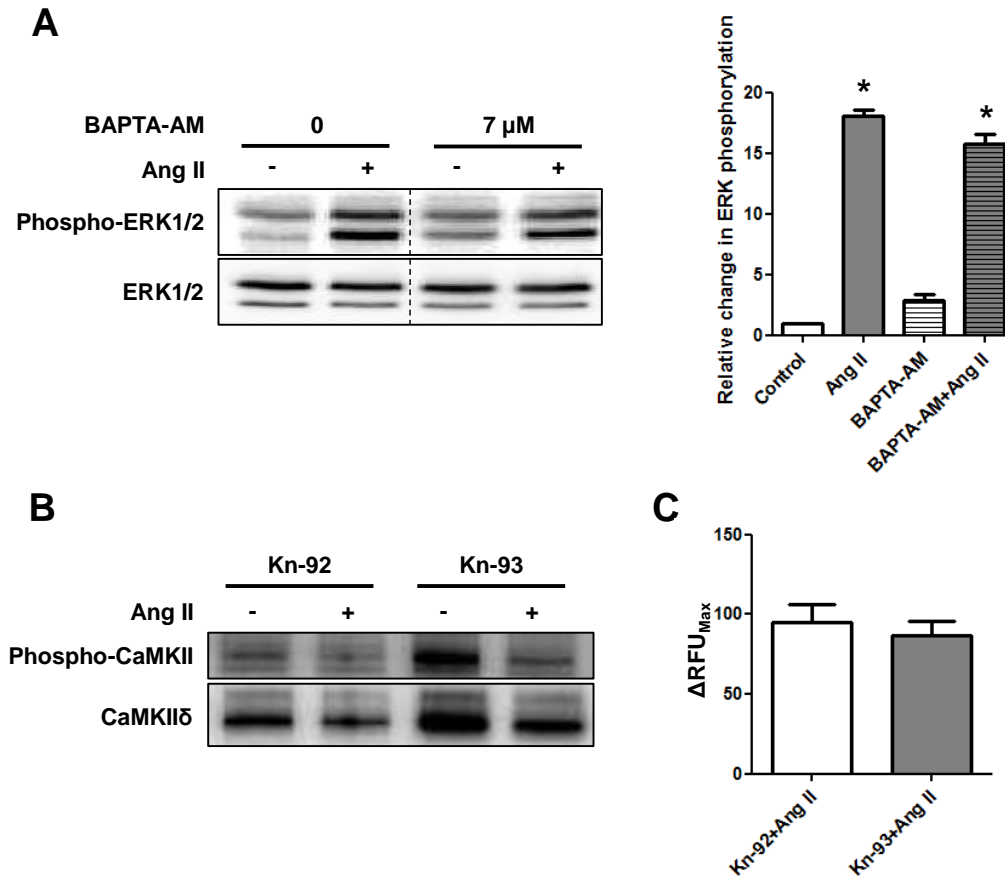


Figure 27: Verification of the role of ERK1/2 and CaMKII in the Ca²⁺-dependent Ang II signaling

A) NRCF were incubated for 1 hr with 7 μ M BAPTA-AM or the corresponding control conditions before treatment with 100 nM Ang II. The cell lysates were collected 5 min thereafter. Left are representative immunoblots of phospho and total ERK1/2 proteins. Right graph shows the analysis of the change in ERK1/2 phosphorylation. The data were normalized to total ERK1/2, and the change in phosphorylation was calculated relative to the control ($n=4$, means \pm SEM, * $p<0.05$ vs. control). B) NRCF were incubated for 1 hr with 2 μ M Kn-92 or Kn-93, before treatment with 100 nM Ang II. The cell lysates were collected 5 min thereafter. Representative immunoblots for phospho-and total CaMKII are shown (preliminary data). C) NRCF were incubated with 2 μ M Kn-93 or 2 μ M of the negative control Kn-92 before the Ang II-CaT was investigated. The graph shows the effect of CaMKII phosphorylation inhibition on the Δ RFU_{Max} ($n=1$, 3 wells/condition, 40-60 cells/well, means (of replicates) \pm SEM, preliminary data).

4.1.3.3. Ca^{2+} , PKC and Rac1 are involved in CTGF regulation in NHCF-V

To validate the role of Ca^{2+} , PKC and Rac1 in the regulation of CTGF in human cardiac fibroblasts, NHCF-V were incubated with BAPTA-AM, Go 6983 and NSC before they were treated with Ang II. As shown in the immunoblot in Fig. 28, BAPTA-AM was at least able to inhibit the secretion of CTGF, Go 6983 reduced both the intracellular and secreted CTGF, and NSC reduced mainly the intracellular CTGF. This experiment was performed only once.

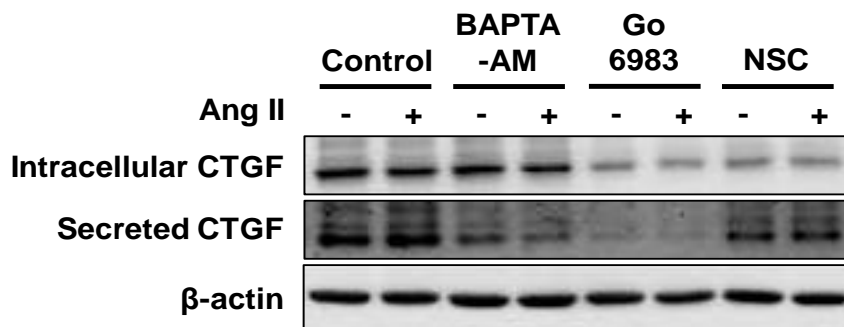


Figure 28: Validating the role of Ca^{2+} , PKC and Rac1 in the regulation of CTGF in NHCF-V

NHCF-V were incubated for 1 hr with 7 μ M BAPTA-AM, 6 μ M Go 6983, 50 μ M NSC or the corresponding control condition before they were treated with 100 nM Ang II. The cell lysates and the conditioned media were collected 24 hr following Ang II treatment. Shown are immunoblots of the intracellular and secreted CTGF. β -actin is shown as a loading control (preliminary data).

4.2. Role of the cytoskeleton in CTGF regulation

4.2.1. Role of the actin filaments in CTGF regulation

The role of the actin filaments in the regulation of CTGF in NRCF was investigated using latrunculin-A (LAT-A), which is a natural compound known to disrupt actin filaments. First of all, fluorescence microscopy was performed to confirm the effect of LAT-A on the actin filaments, and to study the consequences of the disruption of the actin filaments on CTGF localization. Cell imaging by fluorescence microscopy clearly showed that the actin filaments were disrupted by LAT-A treatment, and that the Golgi apparatus became condensed, but not disrupted. CTGF remained localized to the Golgi apparatus (Fig. 29).

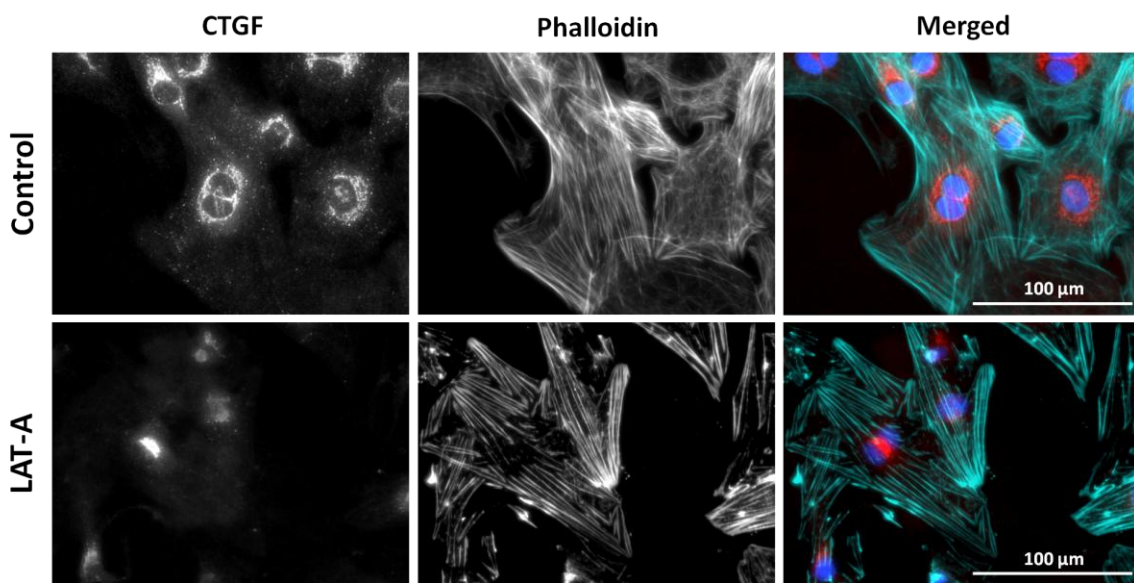


Figure 29: Fluorescence microscopy of NRCF treated with LAT-A

NRCF were incubated for 24 hr with 8.5 ng/ml LAT-A. After that, they were fixed, permeabilized and incubated with a blocking solution. CTGF was detected by IF staining (red), the actin filaments were stained with FITC-phalloidin (green), and the nuclei were stained with DAPI (blue).

To rule out the possibility that LAT-A might influence the microtubules, co-fluorescence staining for actin filaments and microtubules was performed in LAT-A-treated cells, which showed no clear effect for LAT-A on the integrity or organization of microtubules (Fig. 30).

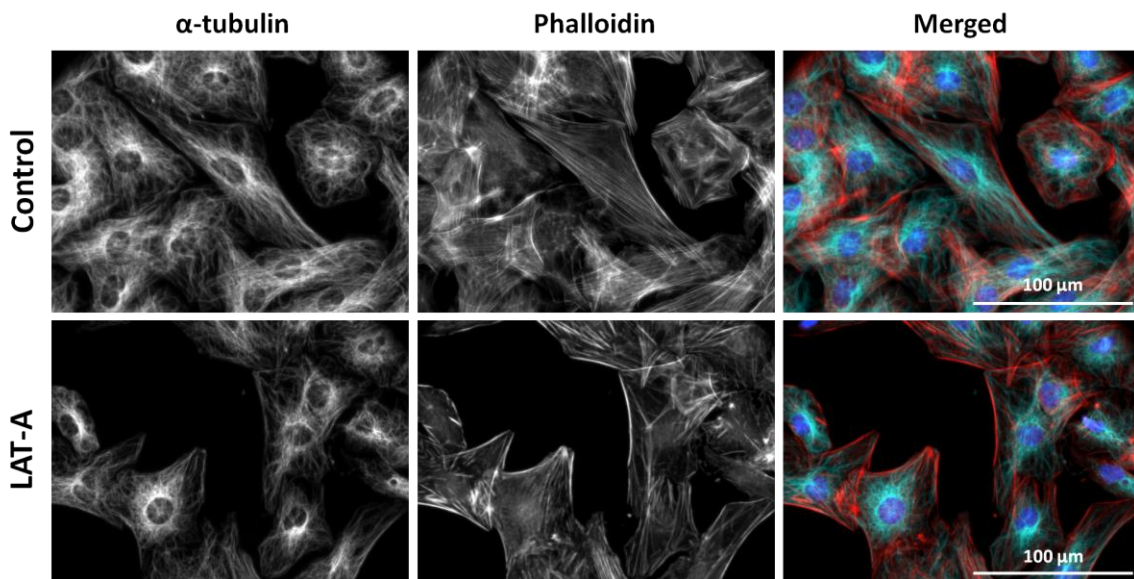


Figure 30: Fluorescence microscopy of the effect of LAT-A on microtubules

NRCF were incubated for 24 hr with 8.5 ng/ml LAT-A. After that, they were fixed, permeabilized and incubated with a blocking solution. The actin filaments were stained with TRITC-phalloidin (red), α -tubulin was detected by IF staining (green) and the nuclei were stained with DAPI (blue).

In the next step, the consequences of the actin filaments disruption by LAT-A on the regulation of CTGF by Ang II was investigated at the level of gene expression. The analysis of the qPCR data showed that treatment with LAT-A significantly inhibited the basal and Ang II-induced levels of CTGF gene transcription (Fig. 31A). In the same time, immunoblotting analysis was performed to evaluate CTGF regulation at the protein level, which showed that upon disruption of the actin filaments, Ang II was no longer able to increase the intracellular or the secreted CTGF. Also, the basal level of intracellular

CTGF was significantly reduced, while the basal level of secretion was not affected (Fig. 31B).

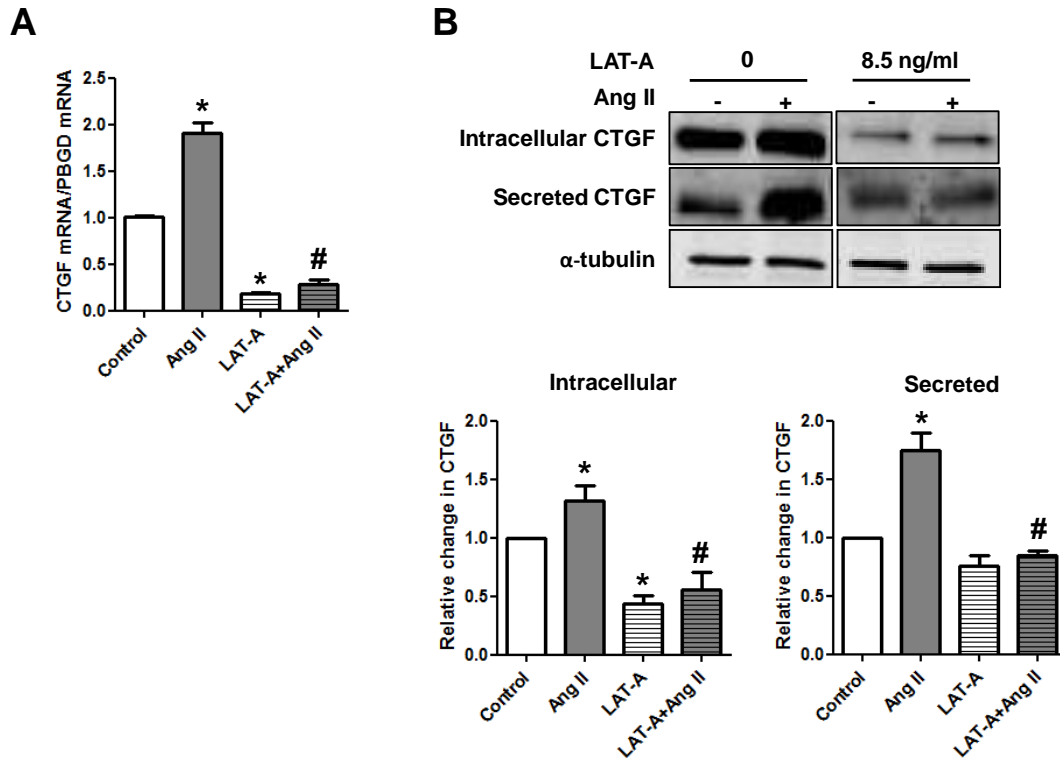


Figure 31: Investigating the effects of the actin filaments disruption on CTGF regulation

NRCF were incubated for 1 hr with 8.5 ng/ml, before they were treated with 100 nM Ang II. For the qPCR data shown in A, the RNA was isolated 2 hr following Ang II treatment, whereas for the immunoblotting data shown in B, the cell lysates and the conditioned media were collected 24 hr following Ang II treatment. A) Effect of LAT-A treatment on CTGF gene transcription under basal and Ang II effect. The data were normalized to PBGD, and the change in gene transcription was calculated relative to the control ($n=3$, means \pm SEM, * and # $p \leq 0.05$, * vs. control, # vs. Ang II). B) Effect of LAT-A treatment on the intracellular and secreted CTGF levels, under basal and Ang II effects. Upper panel demonstrates representative immunoblots. The graphs below show the relative quantification of the intracellular and secreted CTGF. The data were normalized to α -tubulin, and the change in CTGF level was calculated relative to the control ($n=5$, means \pm SEM, * and # $p \leq 0.05$, * vs. control, # vs. Ang II).

4.2.2. Role of the microtubules in the regulation of CTGF

The role of microtubules in the regulation of CTGF was verified in NRCF using colchicine, which is a clinically used drug that disrupts microtubules. In the first step, fluorescence microscopy was performed to confirm the effect of colchicine on the microtubules, and to study the consequences on the localization of CTGF. As shown in Fig. 32, the microtubules were depolymerised and randomly dispersed throughout the cytosol in the form of tubulin aggregates. In addition, the Golgi apparatus, where CTGF is normally stored, was fragmented and dispersed randomly throughout the cytosol.

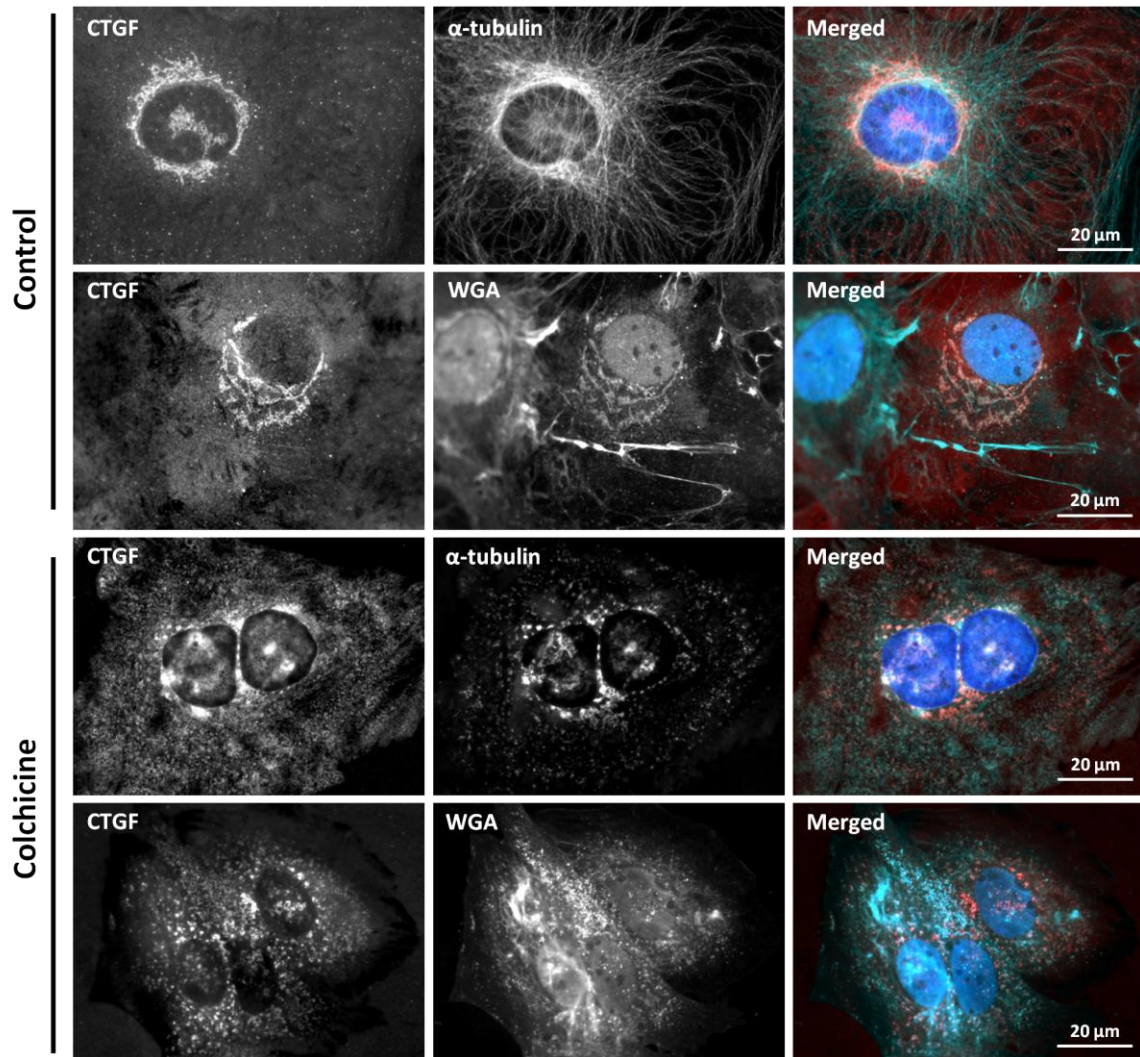


Figure 32: Fluorescence microscopy for NRCF treated with colchicine

The cells were incubated for 24 hr with 5 µg/ml colchicine. After that, they were fixed, permeabilized and incubated with a blocking solution. IF staining was performed to detect CTGF (red) and α-tubulin (green). The membranous structures, including the Golgi apparatus, were stained with Alexa-fluor 488 conjugated-WGA (green), and the nuclei were stained with DAPI (blue).

In the next step, the consequence of the microtubules disruption was investigated on the regulation of CTGF gene transcription at the basal level and 2 hr following Ang II treatment. The analysis of the qPCR data showed that treatment with colchicine significantly enhanced the level of CTGF gene transcription, which could not be increased further by Ang II (Fig. 33A). The successful disruption of microtubules within 2 hr was confirmed by immunofluorescence microscopy of α-tubulin (Fig. 33B). Further biochemical analysis, by immunoblotting of protein samples from cells treated over 24 hr with colchicine in the presence and absence of Ang II, showed that upon disruption of the microtubules, the intracellular and secreted levels of CTGF were significantly increased, and that Ang II was no longer able to enhance it further. In addition, the level of α-tubulin was significantly reduced (Fig. 33C). In addition, by using sirius red-based colorimetric microassay it was found that colchicine treatment had no effect on the amount of collagen deposition over 24 hr (preliminary data) (Fig. 33D).

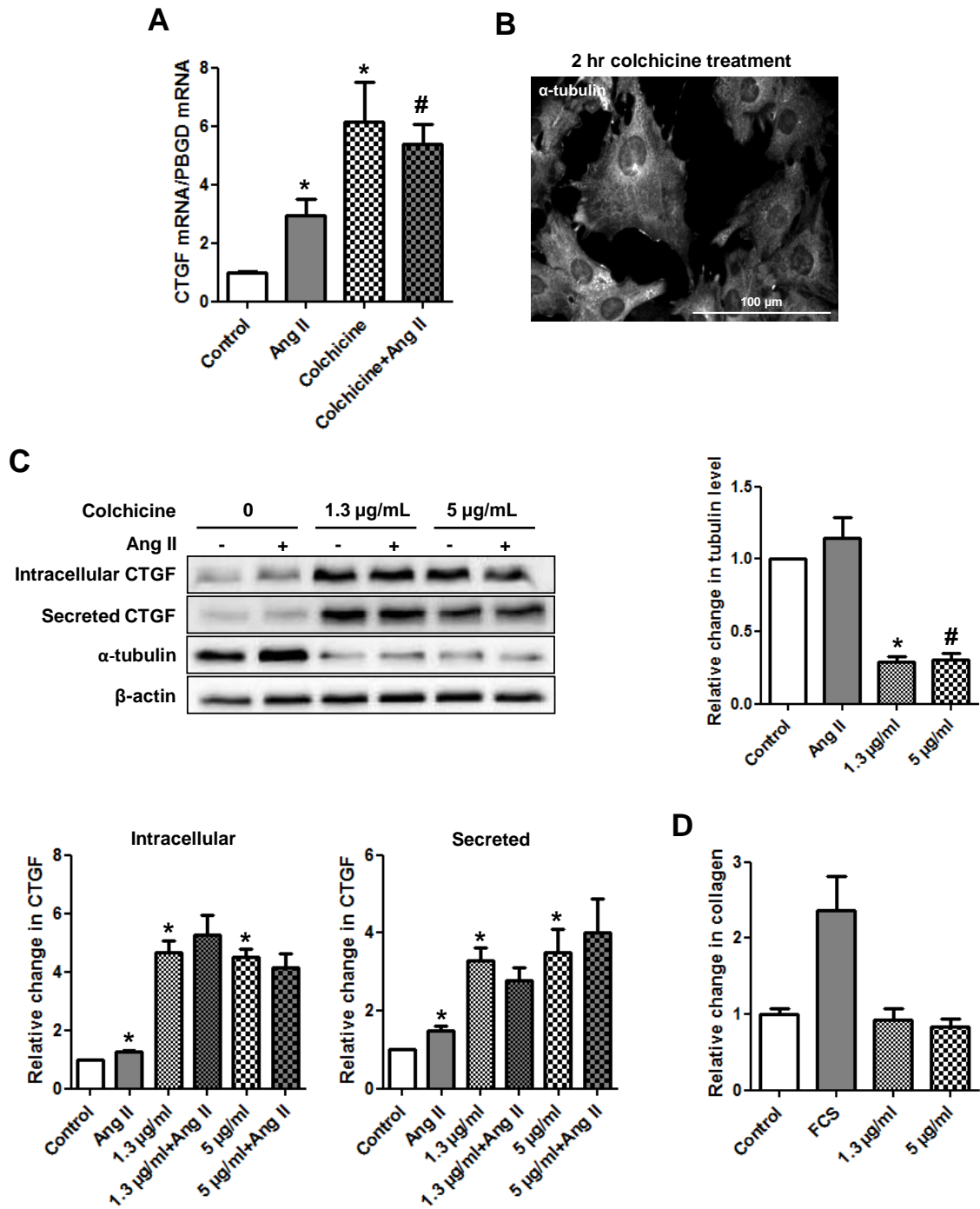


Figure 33: Disruption of microtubules by colchicine significantly induces CTGF expression and secretion

A) NRCF were treated for 1 hr with 5 µg/ml colchicine or the corresponding control conditions, before they were treated with 100 nM Ang II. After 2 hr, the RNA was isolated

for the analysis of CTGF gene transcription by qPCR. The data were normalized to PBGD, and the change in gene transcription was calculated relative to the control ($n=3$, means \pm SEM, * and # $p\leq 0.05$, * vs. control, # vs. Ang II). B) IF staining for the detection of α -tubulin in NRCF treated with 5 $\mu\text{g/ml}$ colchicine over 2 hr. C) NRCF were treated for 1 hr with two different concentrations of colchicine (1.3, 5 $\mu\text{g/ml}$) or the corresponding control conditions, before they were treated with 100 nM Ang II. The cell lysates and the conditioned media were collected 24 hr following Ang II treatment. Representative immunoblots are presented along with graphs showing the relative quantification for α -tubulin and the intracellular and secreted CTGF. The data were normalized to β -actin, and the change in CTGF and α -tubulin levels were calculated relative to the control ($n=6$, means \pm SEM, * and # $p\leq 0.05$, * vs. control, # vs. Ang II). D) NRCF were treated overnight with two different concentrations of colchicine (1.3, 5 $\mu\text{g/ml}$), 10% FCS (positive control) or the corresponding negative control condition. After that sirius red-based colorimetric microassay was performed. The graph shows the relative quantification for the deposited collagen (preliminary data, $n=2$, 6 replicates, means \pm SEM).

4.3. Prospects for studying CTGF by live cell imaging using Ad.TC-CTGF

After construction of the adenovirus encoding the TC-CTGF fusion protein (Ad.TC-CTGF), the functionality of the virus was evaluated in NRCF. First, IF microscopy was performed for NRCF infected with Ad.TC-CTGF or the control virus Ad.EGFP, which showed that in case of Ad.TC-CTGF infection EGFP-positive cells displayed a strong expression of CTGF (Fig. 34A). The next step was to confirm that the over-expressed CTGF was tagged by TC, and that it can be secreted. To do so, NRCF were infected with Ad.EGFP, Ad.TC-CTGF and an adenovirus over-expressing hemagglutinin (HA) tagged-CTGF (Ad.HA-CTGF), which was considered as a positive control. As shown in the immunoblot in Fig. 34B, single bands of CTGF were observed in the lysate and conditioned medium of the Ad.EGFP-infected cells, whereas, double bands were observed in the cell lysate and conditioned medium of the Ad.HA-CTGF-infected cells, but for the Ad.TC-CTGF-infected NRCF, double bands of CTGF were observed in the cell lysate only, while there was only a single band of CTGF in the medium.

From this immunoblot, it was concluded that the TC-CTGF could be over-expressed in NRCF, but during certain stages of processing the TC- tag was cleaved, and only the

untagged CTGF could be secreted, which explains why greater amounts of the endogenous CTGF could be detected in the cell lysate and conditioned medium.

Regarding the positive control virus Ad.HA-CTGF, the HA-tag was similarly cloned in front of the CTGF cDNA as in the Ad.TC-CTGF, however, cleavage was not as effective. The most probable reason for this finding is the difference in the tag length. The HA-tag seems to be cloned as a multicopy construct and thus cleavage by the signal peptide peptidase was not effective. In principle, the tagging of CTGF by TC is still an interesting strategy for real time tracking of CTGF in living cells, with assumedly minimal interference with the behavior of CTGF, due to the relatively small molecular weight of the tag, but the cloning strategy should be modified to overcome the problem of tag cleavage. Although the cloning of multiple TC tags at the N-terminus of CTGF gene sounds a good idea, the risk that this could influence the behavior of the CTGF protein becomes higher. In addition, the fact that the cleavage process of the tag is still occurring makes it impossible to distinguish between the endogenous and the cleaved TC-CTGF, which restricts the readout of certain experiments. Therefore, it is worthy to try to clone the TC tag within the first 130 amino acids, but verification steps would be required to rule out problems in protein folding and behavior.

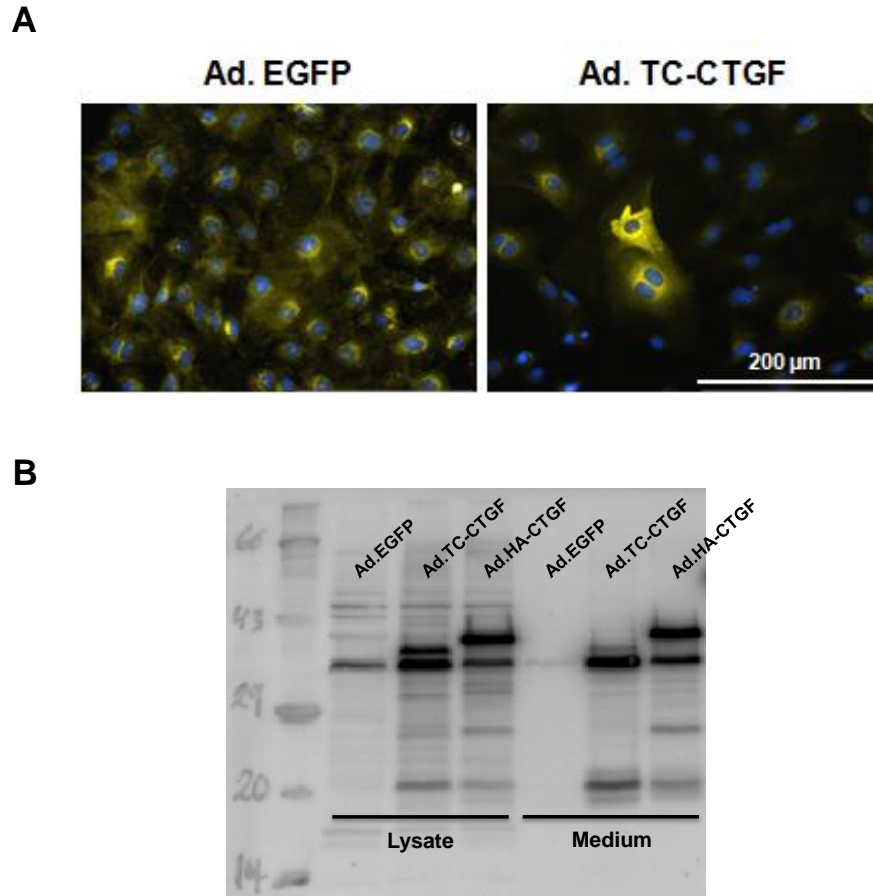


Figure 34: Evaluation of the Ad.TC-CTGF in NRCF

A) NRCF were incubated for 48 hr with Ad.EGFP (negative control adenovirus) or Ad.TC-CTGF, 10 μ l of each virus stock was used per 1 ml medium. After that, the cells were fixed, permeabilized and incubated with a blocking solution. CTGF detected by IF staining (yellow) and the nuclei were stained with DAPI (blue). B) NRCF were incubated for 48 hr with Ad.EGFP, Ad.TC-CTGF or Ad.HA-CTGF (positive control). 10 μ l of each virus stock was used per 1 ml medium. After that, the cells lysates and conditioned media were collected and analyzed by immunoblotting.

5. Discussion

A hallmark for heart failure is remodeling of the cardiac tissue, which is characterized by myocardial hypertrophy and fibrosis. Fibrosis occurs due to dysregulation of the extracellular matrix homeostasis. In the last few years, there was increasing interest in the contribution of the numerically predominant CF in this process, because these cells are largely responsible for the deposition and organization of the extracellular matrix components. In addition, these cells secrete a variety of growth factors and cytokines, which contribute to the progression of heart disease via autocrine and paracrine mechanisms. CTGF is one of the interesting proteins that are secreted by fibroblasts. The expression and secretion of this factor are upregulated not only in cardiac diseases, but also in almost all other fibrotic diseases occurring in various tissues. Moreover, several recent publications have reported increasing evidences for its direct role in the process of fibrosis. However, the mechanisms controlling the expression and secretion of CTGF in CF are still unclear. This work provides novel findings on the regulation of CTGF in CF by cytoskeleton-dependent and Ca^{2+} -dependent signaling pathways. It provides thorough investigations on the Ca^{2+} handling in these cells, and discusses the role of actin filaments and microtubules on the status of the Golgi apparatus and the regulation of CTGF. It also pinpoints Ca^{2+} as a major regulator of the expression of CTGF with potential role for the actin and microtubules cytoskeleton in the underlying mechanism. Mechanistically, this work highlights PKC and calcineurin as major downstream targets for Ca^{2+} and shows potential crosstalk between their signaling pathways. At the same time, the Golgi apparatus and actin filaments were identified as targets for Ca^{2+} , PKC and calcineurin, which creates a link between Ca^{2+} -dependent and cytoskeleton-dependent signaling pathways.

5.1. Regulation of the Ca^{2+} transient in CF

Within this work, it could be shown that the Ang II-CaT involves the activation of the AT1R, Gq/11 proteins, PLC- β and IP3 receptors. This canonical Ca^{2+} release pathway has been already demonstrated to play a substantial role in the regulation of Ca^{2+} in diverse other cells like smooth muscle cells [81, 82]. However, in contrast to rat aortic smooth muscle cells [63] it was found by cholesterol depletion with CDX that this signaling cascade seems to reside at least partly in caveolae. Moreover, by inhibiting the

ER Ca^{2+} ATPase with TGN, and by analysing the effect of extracellular Ca^{2+} on the Ca^{2+} transient, it was found that the ER is probably the most important source of this ion. This is in line with a report by Brilla and coworkers, who demonstrated in adult rat CF that the Ang II-CaTs in the absence and presence of extracellular Ca^{2+} were comparable, therefore, they also suggested the intracellular Ca^{2+} stores to be the major source for the acute increase in the cytoplasmic Ca^{2+} levels in response to Ang II [173]. However, there is increasing evidence that the influx of Ca^{2+} from the extracellular space via diverse channels also plays a role in the Ca^{2+} homeostasis in CF. This includes a study from Chen and coworkers who demonstrated that at least on the mRNA level the expression of diverse channels including Ca(V)1.2, NCX3, PMCA1,3,4, TRPC1,3,4,6, STIM1, and Orai1-3 in human CF [174]. Ikeda and coworkers then confirmed the expression of the unselective $\text{Ca}^{2+}/\text{Na}^{+}$ TRPC1,3,4,6 channels in these cells. Furthermore, they showed that these channels and the reverse-mode of the $\text{Na}^{+}/\text{Ca}^{2+}$ exchanger influences the proliferative behavior of these cells [175]. This is in line with data presented by Harada and coworkers, who also showed that the specific TRPC3 inhibitor Pyr3 inhibited the proliferation of CF. As a mechanism, the authors analyzed the impact of Pyr3 on the regulation of Ca^{2+} . They showed that the relatively slow, Ang II-induced Ca^{2+} influx in adult CF could be blocked by Pyr3 [176]. This type of Ang II-dependent, slow and persistent Ca^{2+} influx could not be detected within this work in a similar time frame. However, the incubation of neonatal CF with Pyr3 led to significant reduction of the basal cytoplasmic Ca^{2+} concentration. This discrepancy between data obtained in adult and neonatal CF might be explained by several reasons. First, it has been shown that the TRPC3 possesses a substantial constitutive activity, which could be of different height. Second, Schleifer and coworkers demonstrated recently that Pyr3 additionally inhibits the store-operated Ca^{2+} influx, which could be also differently involved [177]. Third, the already in smooth muscle cell described coupling between the TRPC3 and the IP3R [125-127] might play a so far unevaluated role in CF. Further studies are needed to address this issue.

In addition to the decrease in the basal cytosolic Ca^{2+} concentration, Pyr3 substantially inhibited the oscillation of Ca^{2+} in CF in this work. Ca^{2+} oscillation is a repetitive cyclical change in the cytoplasmic Ca^{2+} concentration, which has been observed in different non-excitable cell types under not only basal conditions, but also in response to different physiological stimuli.

5.2. Regulation of the Ca²⁺ oscillation in CF

In summary, in this thesis it could be shown that the Ca²⁺ oscillation occurred in around one third of the cells independent of the passage number and could be increased by submaximal Ang II concentrations and inhibited by TGN and Pyr3, arguing for a role of intracellular Ca²⁺ stores but also for an influx of Ca²⁺ from the extracellular space. Although, so far only few data is available for CF on the oscillation of Ca²⁺, this finding is in line with data presented by Chen and coworkers, who reported that spontaneous Ca²⁺ oscillation occurred in 29% of primary human CF. With respect to the mechanism the authors discussed a role of the PLC-β/IP3R system and of L-type Ca²⁺ channels [174]. For other cell types, it has already been described that the TRPC3 channels can mediate agonist-activated Ca²⁺ oscillation via non-capacitative Ca²⁺ entry [117]. But also other mechanisms have been attributed to this process which has not been evaluated within this work, such as extracellular and intracellular mechanical stress [128].

Independent of the mechanism how Ca²⁺ oscillations are generated, the outcome of these cyclic changes is not clear. There is evidence that the amplitude, frequency and duration of these signals actually play a major role in the regulation of different cellular processes such as, proliferation, contraction and secretion [117, 118], and it was shown by several publications that it is involved in the efficiency and specificity of gene expression [178], but it was not possible to find a link between this process and the regulation of CTGF expression in NRCF. However, the inhibition of TRPC3 channels augmented the CTGF secretion in CF. Future experiments have to be performed to unravel the role of this long known phenomenon in CF.

5.3. Influence of ROS-regulating mediators on the Ca²⁺ handling in CF

Within this thesis, the role of the reactive oxygen species (ROS) producing NADPH oxidase in the regulation of the Ca²⁺ handling in CF was analyzed. By using the specific peptide gp91-ds-tat, which can penetrate the plasma membrane and inhibit the association of the essential p47phox with the transmembrane subunits of the NADPH oxidase NOX2, it could be demonstrated that the amplitude of the Ang II-CaT was

significantly reduced. Similar results were obtained by inhibiting the activation of the accessory activator Rac1 with NSC, which argues for a role of ROS in the regulation of Ca^{2+} in CF. With this respect, it has already been demonstrated by Colston and coworkers that a short exposure of CF to exogenously added H_2O_2 can induce a Ca^{2+} transient without any other stimulus [179]. So far, however, it is not clear which mechanism is responsible for this regulation. On one hand, Colston and coworkers could partly block this transient by IP3R inhibition with XeC and TGN, but also by the depletion of extracellular Ca^{2+} . These findings suggested that the ROS-induced increase in Ca^{2+} is not only dependent on intracellular Ca^{2+} stores, but also on the influx of Ca^{2+} from the extracellular space. On the other hand, Takahashi and coworkers postulated the involvement of the TRPM2 channel in the ROS-induced Ca^{2+} influx in CF. The TRPM2 is a non-selective Ca^{2+} -permeable channel, which is upregulated in hypoxia and stimulated by ROS [180]. Finally, data presented by Fujii supported the idea of the Ca^{2+} influx as the main ROS target, because they showed that in CF in the absence of extracellular Ca^{2+} the Ang II-CaT could not be decreased by the expression of dominant negative variants of Rac1 and p47phox [67]. To finally understand the role of ROS in the handling of Ca^{2+} in CF further studies have to be performed.

Besides the inhibitory effect of the gp91-ds-tat peptide and of the inhibitor of Rac1 activation on the amplitude of the Ang II-CaT, distinct effects of both molecules on the Ca^{2+} loading in the mitochondria was observed. The uptake of Ca^{2+} in the mitochondria is a well-documented process, which occurs in most cells when the Ca^{2+} concentration rises above 1 μM [88, 181]. Depending on the increase of Ca^{2+} in the mitochondria the outcome is either an increase in ATP synthesis or in case of a Ca^{2+} overload the enhanced generation of ROS, triggering of the permeability transition pore, and cytochrome c release, leading to cell apoptosis. Recently, a new junction has been identified which allows the direct, spatially highly controlled flux of Ca^{2+} from the ER into the mitochondria. This region has been called mitochondria-associated ER membranes (MAM) or the ER-mitochondria-juxtaposition. It has been shown that within this junction several Ca^{2+} channels are clustered, including the IP3R in the ER membrane, the voltage-dependent anion channel in the outer mitochondrial membrane and the mitochondrial Ca^{2+} uniporter in the inner mitochondrial membrane. With respect to the Ca^{2+} efflux from the mitochondria, the Na^+ - Ca^{2+} -exchanger 3 (NCX3) in the outer mitochondrial membrane was identified as a possible candidate [182]. Although, it is not

clear in this thesis how the observed decrease and increase in the duration of the rise in mitochondrial Ca^{2+} by gp91-ds-tat and NSC, respectively, takes place, there is increasing evidence data that most of the proteins involved in the mitochondrial Ca^{2+} flux are redox-sensitive [183]. In addition, it was shown that in endothelial cells glucose induces total and mitochondrial ROS, mitochondrial DNA damage and cell apoptosis, which could be blocked by NSC [184]. Moreover, Rac1 has been found at the membrane of mitochondria where it interacts with Bcl-2 and its functional inhibition or silencing decrease mitochondrial O_2^- levels and enhances apoptosis sensitivity [185]. However, these studies provided no links to a potential role of the mitochondrial Ca^{2+} regulation.

In summary, the obtained data in this thesis and the recent literature suggest that ROS production is important for the cytosolic Ca^{2+} transient and for the regulation of the Ca^{2+} flux in mitochondria, however, the underlying mechanisms are still obscure. It has to be also taken into account that Rac1 is not only a functional part of some isoforms of the NADPH oxidases but also possess other downstream target like the p21-activated kinases.

5.4. Mechanism of CTGF regulation by cytoskeleton-dependent and Ca^{2+} -dependent signaling pathways

The mechanical properties of cells are strongly dependent on the organization and degree of actin filaments polymerization. LAT-A can inhibit the polymerization of these filaments mainly by binding to G-actin monomers in the cytosol [186]. Interestingly, the chelation or depletion of the intracellular Ca^{2+} by BAPTA-AM or TGN, respectively, disrupted actin filaments, which is in line with a recent publication by Kuwahara, who reported that the elevation of the intracellular Ca^{2+} concentration in mesothelial cells was associated with increased actin filaments polymerization and organization [187]. Moreover, it was shown by this thesis that the inhibition of PKC, the downstream target of Ca^{2+} , was also associated with the disruption of actin filaments. Several working groups reported that PKC mediates the activation of RhoA-ROCK in different cell types including smooth muscle cells and endothelial cells [188, 189]. A mechanistic study by Dovas and coworkers in fibroblasts provided evidence that PKC α mediates the activation of RhoA by syndican 4, a transmembrane heparin sulphate proteoglycan that works with integrin in the formation of the focal adhesions. In addition, the study provided evidence

that syndican 4–PKC α –RhoA signaling pathway was necessary for the formation and maintenance of the actin stress fibers [190]. RhoA maintains the stability of actin filaments via ROCK-mediated LIM-kinase phosphorylation, which in turn phosphorylates and inhibits cofilin, the actin filaments depolymerizing protein [136]. RhoA in addition, activates diaphanous-related formins (mDia1 and mDia2), which nucleate the formation of actin filaments and prevent the binding of plus-end capping proteins, thus keeping the progress of actin filaments polymerization [191-194]. Within this thesis, the disruption of actin filaments was most of the times associated with the inhibition of CTGF expression and secretion. With this respect, it has already been demonstrated by Muehlich and coworkers that the level of CTGF expression in endothelial cells was proportionally related to the degree of actin filaments polymerization, which was dependent on RhoA activation, and mediated via SRF transcription factor [168]. The activation of SRF was shown to be inhibited consequently to actin filaments depolymerization and the elevation of G-actin monomers concentration that sequester MRTF, thus preventing it from complexing with SRF in the nucleus, as reviewed in section 2.7.4.

In this project, the depolymerization of actin filaments, whether directly by LAT-A or indirectly via interference with Ca²⁺ signaling, was associated with the disruption of the Golgi apparatus and the inhibition of CTGF secretion. Consistent with these findings, Lazaro-Diequez and coworkers reported that the disruption of actin filament changes the morphology and integrity of the Golgi apparatus [195], which was found by another group to inhibit protein transportation through the cisternae of the Golgi apparatus, resulting in the inhibition of the cellular secretion [196]. In addition, Chen and coworkers demonstrated that the localization of CTGF to the Golgi apparatus was essential for successful CTGF secretion [197]. In the same time as reviewed in section 2.6.1, Ca²⁺ has already been demonstrated to be involved in the trafficking of the secretory vesicles and in the fusion of the these vesicles with the target cell membrane during exocytosis. Moreover, several reports highlighted the role of Ca²⁺-dependent actin coating of secretory vesicles as an important factor for the efficient release of the content of secretory vesicles during exocytosis [198, 199]. Therefore, it can be postulated that the regulation of CTGF secretion involves actin-dependent and Ca²⁺-dependent mechanisms, with potential crosstalk between these two mechanisms, and involves functional Golgi apparatus. However, the inhibition of CTGF expression per se is also expected to contribute to the inhibition of secretion.

In the same context, the role of calcineurin in the regulation of CTGF was also investigated within this thesis. It was found that the inhibition of calcineurin by CsA significantly enhanced CTGF expression. This was associated with the loss of the cell membrane complexities and changes in the morphology of the Golgi apparatus, but without clear effects on the actin filaments and microtubules. Several reports have already highlighted a role for calcineurin in the dynamic regulation of the actin cytoskeleton. Zhang and coworkers demonstrated that calcineurin mediated the activation of cofilin [200]. A mechanistic study by Wang and coworkers using cell-free assays demonstrated that calcineurin dephosphorylated slingshot 1L protein phosphatase, which in turn dephosphorylated and activated cofilin [201]. Moreover, Li and coworkers recently reported that CsA could inhibit the dephosphorylation of cofilin, resulting in the stabilization of actin filaments [202]. This effect is speculated to enhance CTGF gene expression, as it would negatively influence the level of the monomeric-G actin and enhance SRF-induced gene expression as reviewed in section 2.7.4. On the other hand, Akool and coworkers demonstrated in mesangial cells that the inhibition of calcineurin by CsA was associated with rapid activation of TGF- β /Smad signaling and increased DNA binding of Smad-2, -3 and -4 to the Smad-binding promoter element, resulting in the induction of expression of several genes including CTGF. Mechanistically, they suggested that CsA could induce ROS generation that activated latent TGF- β , which in turn induced gene expression via activation of Smad and p38 MAPK signaling pathways [203]. In another approach, a proteomics study by Van Summeren and coworkers demonstrated that CsA induced endoplasmic reticulum (ER) stress in a cell culture of hepatocytes. The authors showed that CsA treatment was associated with the differential expression of several chaperone proteins, which are normally associated with the induction of ER stress and the disruption of the ER-Golgi transport [204]. Consistent with these findings, Cheng and coworkers showed that treatment of rat kidney epithelial cells with CsA was associated with the induction of ER stress response related proteins including ATF6 [205], which was shown by another group to be involved in the activation of SRF [206]. Therefore, it can be hypothesized that the induction of CTGF expression by CsA results, at least in part, from the ATF6-induced ER-stress. Further experiments are required to test this hypothesis.

The role of microtubules in the regulation of CTGF was also investigated within this thesis by using colchicine, which is a clinically used drug known to depolymerize

microtubules. The disruption of the microtubules by colchicine resulted in the fragmentation of the Golgi apparatus into CTGF-containing membranous structures, which were dispersed randomly throughout the cytosol. At the same time, CTGF expression and secretion were strongly induced and were uncoupled from the AT1R signaling cascade. The disruption of the Golgi apparatus subsequently to microtubule disruption is in line with previous findings by Miller and coworkers, who reported that the spatial organization of the Golgi apparatus is regulated by two subsets of microtubules: the radial centrosomal microtubule array that positions the Golgi apparatus in the center of the cell, and the Golgi-derived microtubules that draw the Golgi ministacks together to maintain the continuity and proper morphology of the Golgi apparatus complex [207]. The augmenting effect of colchicine on CTGF expression was reported previously in immortalized human renal fibroblasts by Ott and coworkers, who demonstrated that the induction of CTGF by colchicine was associated with the activation of RhoA, and that the pharmacological inhibition of RhoA-ROCK was associated with a reduction in colchicine-induced CTGF expression [208]. In addition, Graness and coworkers demonstrated in the same cell type that the colchicine-induced CTGF expression was associated with the recruitment of patchy actin filaments to the cell cortex. This was associated with the reorganization of the focal contact into strong clusters, and with the activation of RhoA-ROCK, focal adhesion kinase and Src-family kinases [170]. Consistent with these findings, several other reports provided evidences that colchicine treatment could alter the G-actin/filamentous actin ratio by inducing actin filaments polymerization and stress fiber formation, thus increasing the cellular rigidity [209-211].

In summary, the obtained data in this thesis and the discussed literature suggest that both the cytoskeleton-dependent signaling pathway and the Ca^{2+} -dependent signaling pathway influence the integrity and morphology of the Golgi apparatus, and play a critical role in the regulation of CTGF, with potential crosstalk between these two signaling pathways.

5.4.1. Role of ROS in the regulation of CTGF

The role of ROS in the regulation of CTGF was evaluated within this thesis by specifically targeting NOX2 isozyme by the inhibitory peptide gp91-ds-tat. Although treatment with gp91-ds-tat inhibited the $\Delta\text{RFU}_{\text{Max}}$ of the Ang II-CaT, it did not influence the expression or secretion of CTGF. On the other hand, the inhibition of Rac1 activation by NSC significantly inhibited $\Delta\text{RFU}_{\text{Max}}$ of the Ang II-CaT, and was shown to reduce the level of intracellular CTGF (personal communication). Rupérez and coworkers reported that H_2O_2 increased CTGF mRNA and protein expression independently of TGF- β [59]. Park and coworkers demonstrated that this effect could be mediated by Janus kinase (JAK)-2 and -3 signaling pathway [212]. In addition, Adam and coworkers showed that the inhibition of Rac1 activation by NSC significantly inhibited the induction effect of Ang II on the expression of CTGF in both NRCF and neonatal rat cardiomyocytes. The authors suggested that the underlying mechanism could involve the generation of ROS [213]. However, Rac1 is a cofactor not only of NOX2 complex but also of NOX1 and NOX3 complexes [214], suggesting that the potential regulation of CTGF by ROS could involve NOX1 and NOX3 isozymes. Therefore, targeted studies on NOX1 and NOX3 are required to unravel the potential role of ROS in the regulation of CTGF.

5.4.2. Ca^{2+} is involved in the regulation of CTGF in human cardiac fibroblasts

Preliminary data obtained from experiments in normal human ventricular cardiac fibroblasts (NHCF-V) showed that Ca^{2+} and PKC were involved in the regulation of CTGF, which is in line with the findings in NRCF. In addition, these preliminary data showed that Rac1 is also involved in CTGF regulation, which is consistent with previous findings in NRCF (personal communication) and in other cell types like chondrocytes [215].

6. Bibliography

1. Nag, A.C., *Study of non-muscle cells of the adult mammalian heart: a fine structural analysis and distribution*. Cytobios, 1980. **28**(109): p. 41-61.
2. Rook, M.B., et al., *Differences in gap junction channels between cardiac myocytes, fibroblasts, and heterologous pairs*. Am J Physiol, 1992. **263**(5 Pt 1): p. C959-77.
3. Lee, A.A., et al., *Angiotensin II stimulates the autocrine production of transforming growth factor-beta 1 in adult rat cardiac fibroblasts*. J Mol Cell Cardiol, 1995. **27**(10): p. 2347-57.
4. Souders, C.A., S.L. Bowers, and T.A. Baudino, *Cardiac fibroblast: the renaissance cell*. Circ Res, 2009. **105**(12): p. 1164-76.
5. Bui, A.L., T.B. Horwich, and G.C. Fonarow, *Epidemiology and risk profile of heart failure*. Nat Rev Cardiol, 2011. **8**(1): p. 30-41.
6. DiPiro, J.T., ed. *Pharmacotherapy: A Pathophysiologic Approach*. 6th ed., ed. A.H. Michael Brown, Karen G. Edmonson, and Peter J. Boyle. 2005, McGraw-Hill Companies, Inc: United States of America. 2856.
7. Mancini, D. and D. Burkhoff, *Mechanical device-based methods of managing and treating heart failure*. Circulation, 2005. **112**(3): p. 438-48.
8. Maack, C., T. Elter, and M. Bohm, *Beta-blocker treatment of chronic heart failure: comparison of carvedilol and metoprolol*. Congest Heart Fail, 2003. **9**(5): p. 263-70.
9. Muhl, C., W.R. Dassen, and H. Kuipers, *Cardiac remodelling: concentric versus eccentric hypertrophy in strength and endurance athletes*. Neth Heart J, 2008. **16**(4): p. 129-33.
10. Creemers, E.E. and Y.M. Pinto, *Molecular mechanisms that control interstitial fibrosis in the pressure-overloaded heart*. Cardiovasc Res, 2011. **89**(2): p. 265-72.
11. Banerjee, I., et al., *Determination of cell types and numbers during cardiac development in the neonatal and adult rat and mouse*. Am J Physiol Heart Circ Physiol, 2007. **293**(3): p. H1883-91.
12. Kapur, N.K., *Transforming growth factor-beta: governing the transition from inflammation to fibrosis in heart failure with preserved left ventricular function*. Circ Heart Fail, 2011. **4**(1): p. 5-7.
13. Gaudesius, G., et al., *Coupling of cardiac electrical activity over extended distances by fibroblasts of cardiac origin*. Circ Res, 2003. **93**(5): p. 421-8.
14. Snider, P., et al., *Origin of cardiac fibroblasts and the role of periostin*. Circ Res, 2009. **105**(10): p. 934-47.
15. Porter, K.E. and N.A. Turner, *Cardiac fibroblasts: at the heart of myocardial remodeling*. Pharmacol Ther, 2009. **123**(2): p. 255-78.
16. Santiago, J.J., et al., *Cardiac fibroblast to myofibroblast differentiation in vivo and in vitro: expression of focal adhesion components in neonatal and adult rat ventricular myofibroblasts*. Dev Dyn, 2010. **239**(6): p. 1573-84.
17. Gabbiani, G., G.B. Ryan, and G. Majne, *Presence of modified fibroblasts in granulation tissue and their possible role in wound contraction*. Experientia, 1971. **27**(5): p. 549-50.
18. Baum, J. and H.S. Duffy, *Fibroblasts and myofibroblasts: what are we talking about?* J Cardiovasc Pharmacol, 2011. **57**(4): p. 376-9.
19. Gurtner, G.C., et al., *Wound repair and regeneration*. Nature, 2008. **453**(7193): p. 314-21.

20. Willems, I.E., et al., *The alpha-smooth muscle actin-positive cells in healing human myocardial scars*. Am J Pathol, 1994. **145**(4): p. 868-75.
21. Sun, Y. and K.T. Weber, *Infarct scar: a dynamic tissue*. Cardiovasc Res, 2000. **46**(2): p. 250-6.
22. Wang, J., et al., *Mechanical force regulation of myofibroblast differentiation in cardiac fibroblasts*. Am J Physiol Heart Circ Physiol, 2003. **285**(5): p. H1871-81.
23. Blaauboer, M.E., et al., *Cyclic mechanical stretch reduces myofibroblast differentiation of primary lung fibroblasts*. Biochem Biophys Res Commun, 2011. **404**(1): p. 23-7.
24. Fowlkes, V., et al., *Type II diabetes promotes a myofibroblast phenotype in cardiac fibroblasts*. Life Sci, 2013. **92**(11): p. 669-76.
25. Petrov, V.V., R.H. Fagard, and P.J. Lijnen, *Stimulation of collagen production by transforming growth factor-beta1 during differentiation of cardiac fibroblasts to myofibroblasts*. Hypertension, 2002. **39**(2): p. 258-63.
26. Hinz, B., et al., *Alpha-smooth muscle actin is crucial for focal adhesion maturation in myofibroblasts*. Mol Biol Cell, 2003. **14**(6): p. 2508-19.
27. Serner, G.G., et al., *Cardiac angiotensin II formation in the clinical course of heart failure and its relationship with left ventricular function*. Circ Res, 2001. **88**(9): p. 961-8.
28. Wang, Y., S.W. Seto, and J. Golledge, *Angiotensin II, sympathetic nerve activity and chronic heart failure*. Heart Fail Rev, 2014. **19**(2): p. 187-98.
29. Lu, Y. and S. Yang, *Angiotensin II induces cardiomyocyte hypertrophy probably through histone deacetylases*. Tohoku J Exp Med, 2009. **219**(1): p. 17-23.
30. Olson, E.R., et al., *Inhibition of cardiac fibroblast proliferation and myofibroblast differentiation by resveratrol*. Am J Physiol Heart Circ Physiol, 2005. **288**(3): p. H1131-8.
31. Lijnen, P.J., V.V. Petrov, and R.H. Fagard, *Angiotensin II-induced stimulation of collagen secretion and production in cardiac fibroblasts is mediated via angiotensin II subtype 1 receptors*. J Renin Angiotensin Aldosterone Syst, 2001. **2**(2): p. 117-22.
32. Lijnen, P.J., V.V. Petrov, and R.H. Fagard, *Induction of cardiac fibrosis by transforming growth factor-beta(1)*. Mol Genet Metab, 2000. **71**(1-2): p. 418-35.
33. Che, Z.Q., et al., *Angiotensin II-stimulated collagen synthesis in aortic adventitial fibroblasts is mediated by connective tissue growth factor*. Hypertens Res, 2008. **31**(6): p. 1233-40.
34. Matsubara, H., et al., *Differential gene expression and regulation of angiotensin II receptor subtypes in rat cardiac fibroblasts and cardiomyocytes in culture*. J Clin Invest, 1994. **93**(4): p. 1592-601.
35. Crabos, M., et al., *Characterization of angiotensin II receptors in cultured adult rat cardiac fibroblasts. Coupling to signaling systems and gene expression*. J Clin Invest, 1994. **93**(6): p. 2372-8.
36. Busche, S., et al., *Expression of angiotensin AT(1) and AT(2) receptors in adult rat cardiomyocytes after myocardial infarction. A single-cell reverse transcriptase-polymerase chain reaction study*. Am J Pathol, 2000. **157**(2): p. 605-11.
37. Freeman, E.J. and E.A. Tallant, *Vascular smooth-muscle cells contain AT1 angiotensin receptors coupled to phospholipase D activation*. Biochem J, 1994. **304 (Pt 2)**: p. 543-8.
38. Roberts, J. and Z. Camacho, *Oxidation of NADPH by polymorphonuclear leucocytes during phagocytosis*. Nature, 1967. **216**(5115): p. 606-7.

39. Hohn, D.C. and R.I. Lehrer, *NADPH oxidase deficiency in X-linked chronic granulomatous disease*. J Clin Invest, 1975. **55**(4): p. 707-13.
40. Scheuer, J. and F. Lai, *Early changes in myocardial hypoxia: relations among mechanical function, pH, and intracellular redox states*. Recent Adv Stud Cardiac Struct Metab, 1975. **7**: p. 237-41.
41. Baud, L. and R. Ardaillou, *Reactive oxygen species: production and role in the kidney*. Am J Physiol, 1986. **251**(5 Pt 2): p. F765-76.
42. Droge, W., *Free radicals in the physiological control of cell function*. Physiol Rev, 2002. **82**(1): p. 47-95.
43. Brown, D.I. and K.K. Griendling, *Nox proteins in signal transduction*. Free Radic Biol Med, 2009. **47**(9): p. 1239-53.
44. Ushio-Fukai, M., *Compartmentalization of redox signaling through NADPH oxidase-derived ROS*. Antioxid Redox Signal, 2009. **11**(6): p. 1289-99.
45. Griendling, K.K., D. Sorescu, and M. Ushio-Fukai, *NAD(P)H oxidase: role in cardiovascular biology and disease*. Circ Res, 2000. **86**(5): p. 494-501.
46. Lyle, A.N., et al., *Poldip2, a novel regulator of Nox4 and cytoskeletal integrity in vascular smooth muscle cells*. Circ Res, 2009. **105**(3): p. 249-59.
47. Gorin, Y., et al., *Nox4 mediates angiotensin II-induced activation of Akt/protein kinase B in mesangial cells*. Am J Physiol Renal Physiol, 2003. **285**(2): p. F219-29.
48. Hafstad, A.D., A.A. Nabeebaccus, and A.M. Shah, *Novel aspects of ROS signalling in heart failure*. Basic Res Cardiol, 2013. **108**(4): p. 359.
49. Rocic, P. and P.A. Lucchesi, *NAD(P)H oxidases and TGF-beta-induced cardiac fibroblast differentiation: Nox-4 gets Smad*. Circ Res, 2005. **97**(9): p. 850-2.
50. Geiszt, M., et al., *Identification of renox, an NAD(P)H oxidase in kidney*. Proc Natl Acad Sci U S A, 2000. **97**(14): p. 8010-4.
51. Cave, A., et al., *NADPH oxidase-derived reactive oxygen species in cardiac pathophysiology*. Philos Trans R Soc Lond B Biol Sci, 2005. **360**(1464): p. 2327-34.
52. Toledo-Pereyra, L.H., F. Lopez-Neblina, and A.H. Toledo, *Reactive oxygen species and molecular biology of ischemia/reperfusion*. Ann Transplant, 2004. **9**(1): p. 81-3.
53. Grieve, D.J. and A.M. Shah, *Oxidative stress in heart failure. More than just damage*. Eur Heart J, 2003. **24**(24): p. 2161-3.
54. Biernacka, A. and N.G. Frangogiannis, *Aging and Cardiac Fibrosis*. Aging Dis, 2011. **2**(2): p. 158-173.
55. Chang, J., et al., *NADPH oxidase-dependent formation of reactive oxygen species contributes to angiotensin II-induced epithelial-mesenchymal transition in rat peritoneal mesothelial cells*. Int J Mol Med, 2011. **28**(3): p. 405-12.
56. Cheng, T.H., et al., *Involvement of reactive oxygen species in angiotensin II-induced endothelin-1 gene expression in rat cardiac fibroblasts*. J Am Coll Cardiol, 2003. **42**(10): p. 1845-54.
57. Liu, R.M. and K.A. Gaston Pravia, *Oxidative stress and glutathione in TGF-beta-mediated fibrogenesis*. Free Radic Biol Med, 2010. **48**(1): p. 1-15.
58. Li, P.F., R. Dietz, and R. von Harsdorf, *Superoxide induces apoptosis in cardiomyocytes, but proliferation and expression of transforming growth factor-beta1 in cardiac fibroblasts*. FEBS Lett, 1999. **448**(2-3): p. 206-10.
59. Ruperez, M., et al., *Connective tissue growth factor is a mediator of angiotensin II-induced fibrosis*. Circulation, 2003. **108**(12): p. 1499-505.

60. Choi, H., et al., *Mechanism of angiotensin II-induced superoxide production in cells reconstituted with angiotensin type 1 receptor and the components of NADPH oxidase*. J Biol Chem, 2008. **283**(1): p. 255-67.
61. Mehta, P.K. and K.K. Griendling, *Angiotensin II cell signaling: physiological and pathological effects in the cardiovascular system*. Am J Physiol Cell Physiol, 2007. **292**(1): p. C82-97.
62. Yang, B. and V. Rizzo, *TNF-alpha potentiates protein-tyrosine nitration through activation of NADPH oxidase and eNOS localized in membrane rafts and caveolae of bovine aortic endothelial cells*. Am J Physiol Heart Circ Physiol, 2007. **292**(2): p. H954-62.
63. Wuertz, C.M., et al., *p63RhoGEF--a key mediator of angiotensin II-dependent signaling and processes in vascular smooth muscle cells*. FASEB J, 2010. **24**(12): p. 4865-76.
64. Ushio-Fukai, M. and R.W. Alexander, *Caveolin-dependent angiotensin II type 1 receptor signaling in vascular smooth muscle*. Hypertension, 2006. **48**(5): p. 797-803.
65. Pagano, P.J., et al., *Angiotensin II induces p67phox mRNA expression and NADPH oxidase superoxide generation in rabbit aortic adventitial fibroblasts*. Hypertension, 1998. **32**(2): p. 331-7.
66. Guo, R., et al., *[Angiotensin II increases ROS production in cardiac fibroblasts by inducing p22phox over-expression]*. Nan Fang Yi Ke Da Xue Xue Bao, 2009. **29**(2): p. 202-4.
67. Fujii, T., et al., *Galpha12/13-mediated production of reactive oxygen species is critical for angiotensin receptor-induced NFAT activation in cardiac fibroblasts*. J Biol Chem, 2005. **280**(24): p. 23041-7.
68. Nian, M., et al., *Inflammatory cytokines and postmyocardial infarction remodeling*. Circ Res, 2004. **94**(12): p. 1543-53.
69. Hein, S., et al., *Progression from compensated hypertrophy to failure in the pressure-overloaded human heart: structural deterioration and compensatory mechanisms*. Circulation, 2003. **107**(7): p. 984-91.
70. Desmouliere, A., et al., *Transforming growth factor-beta 1 induces alpha-smooth muscle actin expression in granulation tissue myofibroblasts and in quiescent and growing cultured fibroblasts*. J Cell Biol, 1993. **122**(1): p. 103-11.
71. Cucoranu, I., et al., *NAD(P)H oxidase 4 mediates transforming growth factor-beta1-induced differentiation of cardiac fibroblasts into myofibroblasts*. Circ Res, 2005. **97**(9): p. 900-7.
72. Chen, M.M., et al., *CTGF expression is induced by TGF-beta in cardiac fibroblasts and cardiac myocytes: a potential role in heart fibrosis*. J Mol Cell Cardiol, 2000. **32**(10): p. 1805-19.
73. Wenzel, S., et al., *Redox-sensitive intermediates mediate angiotensin II-induced p38 MAP kinase activation, AP-1 binding activity, and TGF-beta expression in adult ventricular cardiomyocytes*. FASEB J, 2001. **15**(12): p. 2291-3.
74. Weigert, C., et al., *Angiotensin II induces human TGF-beta 1 promoter activation: similarity to hyperglycaemia*. Diabetologia, 2002. **45**(6): p. 890-8.
75. Lijnen, P. and V. Petrov, *Antagonism of the renin-angiotensin system, hypertrophy and gene expression in cardiac myocytes*. Methods Find Exp Clin Pharmacol, 1999. **21**(5): p. 363-74.
76. Liu, C., E. Adamson, and D. Mercola, *Transcription factor EGR-1 suppresses the growth and transformation of human HT-1080 fibrosarcoma cells by induction of transforming growth factor beta 1*. Proc Natl Acad Sci U S A, 1996. **93**(21): p. 11831-6.

77. Liu, G., et al., *c-Fos is required for TGFbeta1 production and the associated paracrine migratory effects of human colon carcinoma cells*. *Mol Carcinog*, 2006. **45**(8): p. 582-93.
78. Baker, K.M. and H.A. Singer, *Identification and characterization of guinea pig angiotensin II ventricular and atrial receptors: coupling to inositol phosphate production*. *Circ Res*, 1988. **62**(5): p. 896-904.
79. Nishizuka, Y., *Intracellular signaling by hydrolysis of phospholipids and activation of protein kinase C*. *Science*, 1992. **258**(5082): p. 607-14.
80. Mikoshiba, K., *IP3 receptor/Ca2+ channel: from discovery to new signaling concepts*. *J Neurochem*, 2007. **102**(5): p. 1426-46.
81. Schelling, J.R., et al., *Angiotensin II activates the beta 1 isoform of phospholipase C in vascular smooth muscle cells*. *Am J Physiol*, 1997. **272**(5 Pt 1): p. C1558-66.
82. Ohtsu, H., et al., *Central role of Gq in the hypertrophic signal transduction of angiotensin II in vascular smooth muscle cells*. *Endocrinology*, 2008. **149**(7): p. 3569-75.
83. Farrar, W.L., T.P. Thomas, and W.B. Anderson, *Altered cytosol/membrane enzyme redistribution on interleukin-3 activation of protein kinase C*. *Nature*, 1985. **315**(6016): p. 235-7.
84. Garg, R., M.C. Caino, and M.G. Kazanietz, *Regulation of Transcriptional Networks by PKC Isozymes: Identification of c-Rel as a Key Transcription Factor for PKC-Regulated Genes*. *PLoS One*, 2013. **8**(6): p. e67319.
85. Caino, M.C., et al., *Differential regulation of gene expression by protein kinase C isozymes as determined by genome-wide expression analysis*. *J Biol Chem*, 2011. **286**(13): p. 11254-64.
86. Trebak, M., et al., *The TRPC3/6/7 subfamily of cation channels*. *Cell Calcium*, 2003. **33**(5-6): p. 451-61.
87. Hofmann, T., et al., *Direct activation of human TRPC6 and TRPC3 channels by diacylglycerol*. *Nature*, 1999. **397**(6716): p. 259-63.
88. Rizzuto, R., et al., *Mitochondria as sensors and regulators of calcium signalling*. *Nat Rev Mol Cell Biol*, 2012. **13**(9): p. 566-78.
89. Mellor, H. and P.J. Parker, *The extended protein kinase C superfamily*. *Biochem J*, 1998. **332** (Pt 2): p. 281-92.
90. Newton, A.C., *Regulation of the ABC kinases by phosphorylation: protein kinase C as a paradigm*. *Biochem J*, 2003. **370**(Pt 2): p. 361-71.
91. Dempsey, E.C., et al., *Protein kinase C isozymes and the regulation of diverse cell responses*. *Am J Physiol Lung Cell Mol Physiol*, 2000. **279**(3): p. L429-38.
92. Rybin, V.O., et al., *Cross-regulation of novel protein kinase C (PKC) isoform function in cardiomyocytes. Role of PKC epsilon in activation loop phosphorylations and PKC delta in hydrophobic motif phosphorylations*. *J Biol Chem*, 2003. **278**(16): p. 14555-64.
93. Stawowy, P., et al., *Protein kinase C epsilon mediates angiotensin II-induced activation of beta1-integrins in cardiac fibroblasts*. *Cardiovasc Res*, 2005. **67**(1): p. 50-9.
94. Boyle, A.J., et al., *Inhibition of protein kinase C reduces left ventricular fibrosis and dysfunction following myocardial infarction*. *J Mol Cell Cardiol*, 2005. **39**(2): p. 213-21.
95. Wakasaki, H., et al., *Targeted overexpression of protein kinase C beta2 isoform in myocardium causes cardiomyopathy*. *Proc Natl Acad Sci U S A*, 1997. **94**(17): p. 9320-5.

96. Klein, G., et al., *Increased collagen deposition and diastolic dysfunction but preserved myocardial hypertrophy after pressure overload in mice lacking PKCepsilon*. *Circ Res*, 2005. **96**(7): p. 748-55.
97. Braun, M.U. and D. Mochly-Rosen, *Opposing effects of delta- and zeta-protein kinase C isozymes on cardiac fibroblast proliferation: use of isozyme-selective inhibitors*. *J Mol Cell Cardiol*, 2003. **35**(8): p. 895-903.
98. He, Z., et al., *Differential regulation of angiotensin II-induced expression of connective tissue growth factor by protein kinase C isoforms in the myocardium*. *J Biol Chem*, 2005. **280**(16): p. 15719-26.
99. Merat, D.L. and W.Y. Cheung, *Calmodulin-dependent protein phosphatase: isolation of subunits and reconstitution to holoenzyme*. *Methods Enzymol*, 1987. **139**: p. 79-87.
100. Stemmer, P.M. and C.B. Klee, *Dual calcium ion regulation of calcineurin by calmodulin and calcineurin B*. *Biochemistry*, 1994. **33**(22): p. 6859-66.
101. Cope, A.P., *Studies of T-cell activation in chronic inflammation*. *Arthritis Res*, 2002. **4 Suppl 3**: p. S197-211.
102. Schulz, R.A. and K.E. Yutzey, *Calcineurin signaling and NFAT activation in cardiovascular and skeletal muscle development*. *Dev Biol*, 2004. **266**(1): p. 1-16.
103. Molkentin, J.D., et al., *A calcineurin-dependent transcriptional pathway for cardiac hypertrophy*. *Cell*, 1998. **93**(2): p. 215-28.
104. Fu, M., et al., *Involvement of calcineurin in angiotensin II-induced cardiomyocyte hypertrophy and cardiac fibroblast hyperplasia of rats*. *Heart Vessels*, 1999. **14**(6): p. 283-8.
105. Fernandez, R.A., et al., *Pathogenic role of store-operated and receptor-operated ca(2+) channels in pulmonary arterial hypertension*. *J Signal Transduct*, 2012. **2012**: p. 951497.
106. Pedersen, S.F., G. Owsianik, and B. Nilius, *TRP channels: an overview*. *Cell Calcium*, 2005. **38**(3-4): p. 233-52.
107. Eder, P. and J.D. Molkentin, *TRPC channels as effectors of cardiac hypertrophy*. *Circ Res*, 2011. **108**(2): p. 265-72.
108. Freichel, M., et al., *Lack of an endothelial store-operated Ca²⁺ current impairs agonist-dependent vasorelaxation in TRP4^{-/-} mice*. *Nat Cell Biol*, 2001. **3**(2): p. 121-7.
109. Millay, D.P., et al., *Calcium influx is sufficient to induce muscular dystrophy through a TRPC-dependent mechanism*. *Proc Natl Acad Sci U S A*, 2009. **106**(45): p. 19023-8.
110. Maroto, R., et al., *TRPC1 forms the stretch-activated cation channel in vertebrate cells*. *Nat Cell Biol*, 2005. **7**(2): p. 179-85.
111. Spassova, M.A., et al., *A common mechanism underlies stretch activation and receptor activation of TRPC6 channels*. *Proc Natl Acad Sci U S A*, 2006. **103**(44): p. 16586-91.
112. Bush, E.W., et al., *Canonical transient receptor potential channels promote cardiomyocyte hypertrophy through activation of calcineurin signaling*. *J Biol Chem*, 2006. **281**(44): p. 33487-96.
113. Kuwahara, K., et al., *TRPC6 fulfills a calcineurin signaling circuit during pathologic cardiac remodeling*. *J Clin Invest*, 2006. **116**(12): p. 3114-26.
114. Ohba, T., et al., *Upregulation of TRPC1 in the development of cardiac hypertrophy*. *J Mol Cell Cardiol*, 2007. **42**(3): p. 498-507.
115. Brenner, J.S. and R.E. Dolmetsch, *TrpC3 regulates hypertrophy-associated gene expression without affecting myocyte beating or cell size*. *PLoS One*, 2007. **2**(8): p. e802.

116. Nakayama, H., et al., *Calcineurin-dependent cardiomyopathy is activated by TRPC in the adult mouse heart*. FASEB J, 2006. **20**(10): p. 1660-70.
117. Bird, G.S. and J.W. Putney, Jr., *Capacitative calcium entry supports calcium oscillations in human embryonic kidney cells*. J Physiol, 2005. **562**(Pt 3): p. 697-706.
118. Berridge, M.J., P. Lipp, and M.D. Bootman, *The versatility and universality of calcium signalling*. Nat Rev Mol Cell Biol, 2000. **1**(1): p. 11-21.
119. Wollman, R. and T. Meyer, *Coordinated oscillations in cortical actin and Ca²⁺ correlate with cycles of vesicle secretion*. Nat Cell Biol, 2012. **14**(12): p. 1261-9.
120. Nash, M.S., et al., *Intracellular signalling. Receptor-specific messenger oscillations*. Nature, 2001. **413**(6854): p. 381-2.
121. Harootunian, A.T., et al., *Generation of calcium oscillations in fibroblasts by positive feedback between calcium and IP₃*. Science, 1991. **251**(4989): p. 75-8.
122. Woll, E., et al., *Mechanism of intracellular calcium oscillations in fibroblasts expressing the ras oncogene*. Pflugers Arch, 1992. **420**(2): p. 208-12.
123. Brandman, O., et al., *STIM2 is a feedback regulator that stabilizes basal cytosolic and endoplasmic reticulum Ca²⁺ levels*. Cell, 2007. **131**(7): p. 1327-39.
124. Peltonen, H.M., et al., *Involvement of TRPC3 channels in calcium oscillations mediated by OX(1) orexin receptors*. Biochem Biophys Res Commun, 2009. **385**(3): p. 408-12.
125. Treves, S., et al., *Junctate is a key element in calcium entry induced by activation of InsP₃ receptors and/or calcium store depletion*. J Cell Biol, 2004. **166**(4): p. 537-48.
126. Kiselyov, K., et al., *Functional interaction between InsP₃ receptors and store-operated Htrp3 channels*. Nature, 1998. **396**(6710): p. 478-82.
127. Kiselyov, K., et al., *The N-terminal domain of the IP₃ receptor gates store-operated hTrp3 channels*. Mol Cell, 1999. **4**(3): p. 423-9.
128. Godbout, C., et al., *The mechanical environment modulates intracellular calcium oscillation activities of myofibroblasts*. PLoS One, 2013. **8**(5): p. e64560.
129. Follonier, L., et al., *Myofibroblast communication is controlled by intercellular mechanical coupling*. J Cell Sci, 2008. **121**(Pt 20): p. 3305-16.
130. Manneville, J.B., et al., *Interaction of the actin cytoskeleton with microtubules regulates secretory organelle movement near the plasma membrane in human endothelial cells*. J Cell Sci, 2003. **116**(Pt 19): p. 3927-38.
131. Schnee, M.E., et al., *Calcium-dependent synaptic vesicle trafficking underlies indefatigable release at the hair cell afferent fiber synapse*. Neuron, 2011. **70**(2): p. 326-38.
132. Fon, E.A. and R.H. Edwards, *Molecular mechanisms of neurotransmitter release*. Muscle Nerve, 2001. **24**(5): p. 581-601.
133. Lin, R.C. and R.H. Scheller, *Mechanisms of synaptic vesicle exocytosis*. Annu Rev Cell Dev Biol, 2000. **16**: p. 19-49.
134. dos Remedios, C.G., et al., *Actin binding proteins: regulation of cytoskeletal microfilaments*. Physiol Rev, 2003. **83**(2): p. 433-73.
135. Kishino, A. and T. Yanagida, *Force measurements by micromanipulation of a single actin filament by glass needles*. Nature, 1988. **334**(6177): p. 74-6.
136. Maekawa, M., et al., *Signaling from Rho to the actin cytoskeleton through protein kinases ROCK and LIM-kinase*. Science, 1999. **285**(5429): p. 895-8.
137. Schonichen, A. and M. Geyer, *Fifteen formins for an actin filament: a molecular view on the regulation of human formins*. Biochim Biophys Acta, 2010. **1803**(2): p. 152-63.

138. Olson, E.N. and A. Nordheim, *Linking actin dynamics and gene transcription to drive cellular motile functions*. Nat Rev Mol Cell Biol, 2010. **11**(5): p. 353-65.
139. Desai, A. and T.J. Mitchison, *Microtubule polymerization dynamics*. Annu Rev Cell Dev Biol, 1997. **13**: p. 83-117.
140. Sept, D., *Microtubule polymerization: one step at a time*. Curr Biol, 2007. **17**(17): p. R764-6.
141. Cho, S.G., et al., *Analysis of gene expression induced by microtubule-disrupting agents in HeLa cells using microarray*. Cancer Lett, 2006. **241**(1): p. 110-7.
142. Dong, C., et al., *Microtubule binding to Smads may regulate TGF beta activity*. Mol Cell, 2000. **5**(1): p. 27-34.
143. Ziegelbauer, J., et al., *Transcription factor MIZ-1 is regulated via microtubule association*. Mol Cell, 2001. **8**(2): p. 339-49.
144. Shin, H., et al., *The transcription factor Egr3 is a putative component of the microtubule organizing center in mouse oocytes*. PLoS One, 2014. **9**(4): p. e94708.
145. Gressner, O.A. and A.M. Gressner, *Connective tissue growth factor: a fibrogenic master switch in fibrotic liver diseases*. Liver Int, 2008. **28**(8): p. 1065-79.
146. Igarashi, A., et al., *Regulation of connective tissue growth factor gene expression in human skin fibroblasts and during wound repair*. Mol Biol Cell, 1993. **4**(6): p. 637-45.
147. Bradham, D., et al., *Connective Tissue Growth Factor: a Cysteine-rich Mitogen Secreted by Human Vascular Endothelial Cells Is Related to the SRC-induced Immediate Early Gene Product CEF10* The Journal of Cell Biology, 1991. **114**(6): p. 1285-94.
148. de Winter, P., P. Leoni, and D. Abraham, *Connective tissue growth factor: structure-function relationships of a mosaic, multifunctional protein*. Growth Factors, 2008. **26**(2): p. 80-91.
149. Brigstock, D.R., et al., *Purification and characterization of novel heparin-binding growth factors in uterine secretory fluids. Identification as heparin-regulated Mr 10,000 forms of connective tissue growth factor*. J Biol Chem, 1997. **272**(32): p. 20275-82.
150. Heng, E.C., et al., *CCN2, connective tissue growth factor, stimulates collagen deposition by gingival fibroblasts via module 3 and alpha6- and beta1 integrins*. J Cell Biochem, 2006. **98**(2): p. 409-20.
151. Tong, Z.Y. and D.R. Brigstock, *Intrinsic biological activity of the thrombospondin structural homology repeat in connective tissue growth factor*. J Endocrinol, 2006. **188**(3): p. R1-8.
152. Leask, A., *TGFbeta, cardiac fibroblasts, and the fibrotic response*. Cardiovasc Res, 2007. **74**(2): p. 207-12.
153. Ivkovic, S., et al., *Connective tissue growth factor coordinates chondrogenesis and angiogenesis during skeletal development*. Development, 2003. **130**(12): p. 2779-91.
154. Kennedy, L., et al., *CCN2 is necessary for the function of mouse embryonic fibroblasts*. Exp Cell Res, 2007. **313**(5): p. 952-64.
155. Gao, R. and D.R. Brigstock, *A novel integrin alpha5beta1 binding domain in module 4 of connective tissue growth factor (CCN2/CTGF) promotes adhesion and migration of activated pancreatic stellate cells*. Gut, 2006. **55**(6): p. 856-62.
156. Gao, R., et al., *Connective tissue growth factor induces c-fos gene activation and cell proliferation through p44/42 MAP kinase in primary rat hepatic stellate cells*. J Hepatol, 2004. **40**(3): p. 431-8.

157. Song, J.J., et al., *Connective tissue growth factor (CTGF) acts as a downstream mediator of TGF-beta1 to induce mesenchymal cell condensation*. J Cell Physiol, 2007. **210**(2): p. 398-410.
158. Weston, B.S., N.A. Wahab, and R.M. Mason, *CTGF mediates TGF-beta-induced fibronectin matrix deposition by upregulating active alpha5beta1 integrin in human mesangial cells*. J Am Soc Nephrol, 2003. **14**(3): p. 601-10.
159. Grotendorst, G.R. and M.R. Duncan, *Individual domains of connective tissue growth factor regulate fibroblast proliferation and myofibroblast differentiation*. FASEB J, 2005. **19**(7): p. 729-38.
160. Yoon, P.O., et al., *The opposing effects of CCN2 and CCN5 on the development of cardiac hypertrophy and fibrosis*. J Mol Cell Cardiol, 2010. **49**(2): p. 294-303.
161. Gore-Hyer, E., et al., *TGF-beta and CTGF have overlapping and distinct fibrogenic effects on human renal cells*. Am J Physiol Renal Physiol, 2002. **283**(4): p. F707-16.
162. Tank, J., et al., *Single-target RNA interference for the blockade of multiple interacting proinflammatory and profibrotic pathways in cardiac fibroblasts*. J Mol Cell Cardiol, 2014. **66**: p. 141-56.
163. Ahmed, M.S., et al., *Mechanisms of novel cardioprotective functions of CCN2/CTGF in myocardial ischemia-reperfusion injury*. Am J Physiol Heart Circ Physiol, 2011. **300**(4): p. H1291-302.
164. Gravning, J., et al., *Myocardial connective tissue growth factor (CCN2/CTGF) attenuates left ventricular remodeling after myocardial infarction*. PLoS One, 2012. **7**(12): p. e52120.
165. Gravning, J., et al., *CCN2/CTGF attenuates myocardial hypertrophy and cardiac dysfunction upon chronic pressure-overload*. Int J Cardiol, 2013. **168**(3): p. 2049-56.
166. Gravning, J., et al., *Connective tissue growth factor/CCN2 attenuates beta-adrenergic receptor responsiveness and cardiotoxicity by induction of G protein-coupled receptor kinase-5 in cardiomyocytes*. Mol Pharmacol, 2013. **84**(3): p. 372-83.
167. Moe, I.T., et al., *CCN2 exerts direct cytoprotective actions in adult cardiac myocytes by activation of the PI3-kinase/Akt/GSK-3beta signaling pathway*. J Cell Commun Signal, 2013. **7**(1): p. 31-47.
168. Muehlich, S., et al., *Actin-dependent regulation of connective tissue growth factor*. Am J Physiol Cell Physiol, 2007. **292**(5): p. C1732-8.
169. Xu, Y., et al., *Connective tissue growth factor in regulation of RhoA mediated cytoskeletal tension associated osteogenesis of mouse adipose-derived stromal cells*. PLoS One, 2010. **5**(6): p. e11279.
170. Graness, A., I. Cicha, and M. Goppelt-Struebe, *Contribution of Src-FAK signaling to the induction of connective tissue growth factor in renal fibroblasts*. Kidney Int, 2006. **69**(8): p. 1341-9.
171. Simpson, P. and S. Savion, *Differentiation of rat myocytes in single cell cultures with and without proliferating nonmyocardial cells. Cross-striations, ultrastructure, and chronotropic response to isoproterenol*. Circ Res, 1982. **50**(1): p. 101-16.
172. Tullberg-Reinert, H. and G. Jundt, *In situ measurement of collagen synthesis by human bone cells with a sirius red-based colorimetric microassay: effects of transforming growth factor beta2 and ascorbic acid 2-phosphate*. Histochem Cell Biol, 1999. **112**(4): p. 271-6.
173. Brilla, C.G., C. Scheer, and H. Rupp, *Angiotensin II and intracellular calcium of adult cardiac fibroblasts*. J Mol Cell Cardiol, 1998. **30**(6): p. 1237-46.

174. Chen, J.B., et al., *Multiple Ca²⁺ signaling pathways regulate intracellular Ca²⁺ activity in human cardiac fibroblasts*. J Cell Physiol, 2010. **223**(1): p. 68-75.
175. Ikeda, K., et al., *Roles of transient receptor potential canonical (TRPC) channels and reverse-mode Na⁺/Ca²⁺ exchanger on cell proliferation in human cardiac fibroblasts: effects of transforming growth factor beta1*. Cell Calcium, 2013. **54**(3): p. 213-25.
176. Harada, M., et al., *Transient receptor potential canonical-3 channel-dependent fibroblast regulation in atrial fibrillation*. Circulation, 2012. **126**(17): p. 2051-64.
177. Schleifer, H., et al., *Novel pyrazole compounds for pharmacological discrimination between receptor-operated and store-operated Ca(2+) entry pathways*. Br J Pharmacol, 2012. **167**(8): p. 1712-22.
178. Dolmetsch, R.E., K. Xu, and R.S. Lewis, *Calcium oscillations increase the efficiency and specificity of gene expression*. Nature, 1998. **392**(6679): p. 933-6.
179. Colston, J.T., B. Chandrasekar, and G.L. Freeman, *A novel peroxide-induced calcium transient regulates interleukin-6 expression in cardiac-derived fibroblasts*. J Biol Chem, 2002. **277**(26): p. 23477-83.
180. Takahashi, K., K. Sakamoto, and J. Kimura, *Hypoxic stress induces transient receptor potential melastatin 2 (TRPM2) channel expression in adult rat cardiac fibroblasts*. J Pharmacol Sci, 2012. **118**(2): p. 186-97.
181. Pandya, J.D., V.N. Nukala, and P.G. Sullivan, *Concentration dependent effect of calcium on brain mitochondrial bioenergetics and oxidative stress parameters*. Front Neuroenergetics, 2013. **5**: p. 10.
182. Scorziello, A., et al., *NCX3 regulates mitochondrial Ca(2+) handling through the AKAP121-anchored signaling complex and prevents hypoxia-induced neuronal death*. J Cell Sci, 2013. **126**(Pt 24): p. 5566-77.
183. Eisner, V., G. Csordas, and G. Hajnoczky, *Interactions between sarcoplasmic reticulum and mitochondria in cardiac and skeletal muscle - pivotal roles in Ca(2+)(+) and reactive oxygen species signaling*. J Cell Sci, 2013. **126**(Pt 14): p. 2965-78.
184. Kowluru, R.A., et al., *TIAM1-RAC1 signalling axis-mediated activation of NADPH oxidase-2 initiates mitochondrial damage in the development of diabetic retinopathy*. Diabetologia, 2014. **57**(5): p. 1047-56.
185. Velaithan, R., et al., *The small GTPase Rac1 is a novel binding partner of Bcl-2 and stabilizes its antiapoptotic activity*. Blood, 2011. **117**(23): p. 6214-26.
186. Wakatsuki, T., et al., *Effects of cytochalasin D and latrunculin B on mechanical properties of cells*. J Cell Sci, 2001. **114**(Pt 5): p. 1025-36.
187. Kuwahara, M., *Role of [Ca(2+)]_i and F-actin on mesothelial barrier function*. Front Physiol, 2014. **5**: p. 232.
188. Kandabashi, T., et al., *Evidence for protein kinase C-mediated activation of Rho-kinase in a porcine model of coronary artery spasm*. Arterioscler Thromb Vasc Biol, 2003. **23**(12): p. 2209-14.
189. Barandier, C., et al., *PKC is required for activation of ROCK by RhoA in human endothelial cells*. Biochem Biophys Res Commun, 2003. **304**(4): p. 714-9.
190. Dovas, A., A. Yoneda, and J.R. Couchman, *PKCbeta-dependent activation of RhoA by syndecan-4 during focal adhesion formation*. J Cell Sci, 2006. **119**(Pt 13): p. 2837-46.
191. Lammers, M., et al., *Specificity of interactions between mDia isoforms and Rho proteins*. J Biol Chem, 2008. **283**(50): p. 35236-46.
192. Eisenmann, K.M., et al., *Dia-interacting protein modulates formin-mediated actin assembly at the cell cortex*. Curr Biol, 2007. **17**(7): p. 579-91.

193. Kovar, D.R., J.Q. Wu, and T.D. Pollard, *Profilin-mediated competition between capping protein and formin Cdc12p during cytokinesis in fission yeast*. Mol Biol Cell, 2005. **16**(5): p. 2313-24.
194. Tominaga, T., et al., *Diaphanous-related formins bridge Rho GTPase and Src tyrosine kinase signaling*. Mol Cell, 2000. **5**(1): p. 13-25.
195. Lazaro-Dieiguez, F., et al., *Actin filaments are involved in the maintenance of Golgi cisternae morphology and intra-Golgi pH*. Cell Motil Cytoskeleton, 2006. **63**(12): p. 778-91.
196. Fucini, R.V., et al., *Golgi vesicle proteins are linked to the assembly of an actin complex defined by mAbp1*. Mol Biol Cell, 2002. **13**(2): p. 621-31.
197. Chen, Y., et al., *Connective tissue growth factor is secreted through the Golgi and is degraded in the endosome*. Exp Cell Res, 2001. **271**(1): p. 109-17.
198. Miklavc, P., et al., *Actin coating and compression of fused secretory vesicles are essential for surfactant secretion--a role for Rho, formins and myosin II*. J Cell Sci, 2012. **125**(Pt 11): p. 2765-74.
199. Miklavc, P., et al., *Ca²⁺-dependent actin coating of lamellar bodies after exocytotic fusion: a prerequisite for content release or kiss-and-run*. Ann N Y Acad Sci, 2009. **1152**: p. 43-52.
200. Zhang, X.F., et al., *Calcineurin-dependent cofilin activation and increased retrograde actin flow drive 5-HT-dependent neurite outgrowth in Aplysia bag cell neurons*. Mol Biol Cell, 2012. **23**(24): p. 4833-48.
201. Wang, Y., F. Shibasaki, and K. Mizuno, *Calcium signal-induced cofilin dephosphorylation is mediated by Slingshot via calcineurin*. J Biol Chem, 2005. **280**(13): p. 12683-9.
202. Li, X., et al., *Cyclosporine A protects podocytes via stabilization of cofilin-1 expression in the unphosphorylated state*. Exp Biol Med (Maywood), 2014. **239**(8): p. 922-936.
203. Akool el, S., et al., *Molecular mechanisms of TGF beta receptor-triggered signaling cascades rapidly induced by the calcineurin inhibitors cyclosporin A and FK506*. J Immunol, 2008. **181**(4): p. 2831-45.
204. Van Summeren, A., et al., *Proteomics investigations of drug-induced hepatotoxicity in HepG2 cells*. Toxicol Sci, 2011. **120**(1): p. 109-22.
205. Cheng, C.H., et al., *Cyclosporine-induced tubular vacuolization: the role of Bip/Grp78*. Nephron Exp Nephrol, 2012. **122**(1-2): p. 1-12.
206. Zhu, C., F.E. Johansen, and R. Prywes, *Interaction of ATF6 and serum response factor*. Mol Cell Biol, 1997. **17**(9): p. 4957-66.
207. Miller, P.M., et al., *Golgi-derived CLASP-dependent microtubules control Golgi organization and polarized trafficking in motile cells*. Nat Cell Biol, 2009. **11**(9): p. 1069-80.
208. Ott, C., et al., *Modulation of the expression of connective tissue growth factor by alterations of the cytoskeleton*. J Biol Chem, 2003. **278**(45): p. 44305-11.
209. Carlsson, L. and I. Blikstad, *Colchicine treatment of HeLa cells alters the G/F actin ratio*. FEBS Lett, 1981. **124**(2): p. 282-4.
210. Jung, H.I., et al., *Colchicine activates actin polymerization by microtubule depolymerization*. Mol Cells, 1997. **7**(3): p. 431-7.
211. Tsai, M.A., R.E. Waugh, and P.C. Keng, *Passive mechanical behavior of human neutrophils: effects of colchicine and paclitaxel*. Biophys J, 1998. **74**(6): p. 3282-91.
212. Park, S.K., et al., *Hydrogen peroxide is a novel inducer of connective tissue growth factor*. Biochem Biophys Res Commun, 2001. **284**(4): p. 966-71.

213. Adam, O., et al., *Rac1-induced connective tissue growth factor regulates connexin 43 and N-cadherin expression in atrial fibrillation*. J Am Coll Cardiol, 2010. **55**(5): p. 469-80.
214. Drummond, G.R., et al., *Combating oxidative stress in vascular disease: NADPH oxidases as therapeutic targets*. Nat Rev Drug Discov, 2011. **10**(6): p. 453-71.
215. Woods, A., et al., *Rac1 signaling regulates CTGF/CCN2 gene expression via TGFbeta/Smad signaling in chondrocytes*. Osteoarthritis Cartilage, 2009. **17**(3): p. 406-13.

Curriculum Vitae

Personal Information

Name: Naim Kittana
Date of Birth: 11. Jan. 1982
Place of Birth: Nablus, Palestine
Nationality: Palestinian, Jordanian
E-mail: naim.kittana@yahoo.com

Educational level

- 2011-present Ph.D. 'Molecular Medicine program', Institute of Pharmacology, Heart Research Center Goettingen (HRCG), University Medical Center Goettingen (UMG), Georg-August-University Goettingen
- 2006-2008 MSc Pharmacology, Faculty of Medicine, University of Jordan, Amman, Jordan. Average score 3.75 (excellent). Thesis title 'Chemoprevention of meloxicam, grapefruit juice and the combination of both against the formation of colonic aberrant crypt foci induced by 1,2-dimethylhydrazine in rat model'
- 2000-2005 BSc Pharmacy, Faculty of Pharmacy, An-Najah National University, Nablus, Palestine. Average: 89.4% (very good)
- 1999-2000 High School, Qadri Tuqan Secondary School, Nablus, Palestine. Average: 92.7% (excellent)

Scholarships

- 2011-2014 German Academic Exchange Service (DAAD) scholarship for PhD fellowship in Germany
- 2006-2008 DAAD scholarship for MSc degree in pharmacology

Professional Experience

- Lecturer of Pharmacology (fulltime), Faculty of Pharmacy, An-Najah National University, Nablus, Palestine. Aug. 2008- 2010.
- Member of quality control unit at the faculty of Pharmacy, An-Najah National University, Nablus, Palestine. Sep. 2008-Jul. 2010.
- Teaching Assistant (part-time), Faculty of Pharmacy, An-Najah National University, Nablus, Palestine. Sep. 2005- Aug. 2006.
- Pharmacist (fulltime) at a community pharmacy, Nablus, Palestine. Jul. 2005-Aug. 2006.
- Quality Consultant, Doctors of The world-France (short term contract)
- Licensed and registered pharmacist in Palestine.

Conferences, Posters and Talks

- N. Kittana, W. Albrecht, A. Jatho, C. Würtz, K. Schenk, B. Ramba, S. Lutz (2014). Calcium Complexly Regulates Connective Tissue Growth Factor in Cardiac Fibroblasts. Talk at the 80th Annual Meeting of the German Society for Experimental and Clinical Pharmacology and Toxicology (DGPT), Hannover, Germany
- N. Kittana, W. Albrecht, A. Jatho, B. Ramba, S. Lutz (2014). Ang II-Induced Calcium Signaling Complexly Regulates CTGF in Cardiac Fibroblasts. Poster at the 12th Dutch-German Joint Meeting of the Molecular Cardiology Working Groups (DGJM), Groningen, Netherlands (Poster prize)
- N. Kittana, A. Jatho, A. Ongherth, N. Krüger, C. Würtz, K. Schenk, B. Ramba S. Lutz (2013). Multiple Signaling Pathways Regulate Connective Tissue Growth Factor Expression and Secretion in Cardiac Fibroblasts. Poster at the 11th Dutch-German Joint Meeting of the Molecular Cardiology Working Groups (DGJM), Heidelberg, Germany
- N. Kittana, A. Jatho, C. Würtz, K. Schenk, B. Ramba S. Lutz (2012). Role of Tubulin in the Regulation of CTGF Expression and Secretion in Cardiac Fibroblasts: Possible Role in Cardiac Fibrosis. Poster at the 10th Dutch-German Joint Meeting of the Molecular Cardiology Working Groups (DGJM), Kerkrade, Netherlands
- Naim J. Kittana, Maha S. Shomaf, Abdulazim S. Salhab (2008). Chemoprevention of Meloxicam, Grapefruit Juice and Combination Against the Formation of Colonic Aberrant Crypt Foci in Rats Induced by 1,2-

Dimethylhydrazine. Poster at the Annual Meeting of American College of Clinical Pharmacology

Publications

- Zaid AN, Abu Ghosh A, Kittana N. (2010). Weight Uniformity of Scored Tablet Halves Manufactured by Palestinian Pharmaceutical Companies. International Journal of Pharmaceutical Compounding. Issue: May/Jun 2010 - Pain Management
- Naim J. Kittana, Maha S. Shomaf, Abdulazim S. Salhab. (2009). Chemoprevention of Induced Colonic Aberrant Crypt Foci in Rats by the Combination of Meloxicam and Grapefruit Juice. J Med J. 43(4):316- 323